Title

Transcription-Based Molecular Imaging and Gene Therapy for Castration-resistant and Metastatic Prostate Cancer in Translational Models

Author

Jiang, Ziyue

Publication Date

2013

Peer reviewed|Thesis/dissertation

UNIVERSITY OF CALIFORNIA

Los Angeles

Transcription-Based Molecular Imaging and Gene Therapy for Castration-resistant and Metastatic Prostate Cancer in Translational Models

A dissertation submitted in partial satisfaction of the requirements for the degree Doctor of Philosophy in Molecular & Medical Pharmacology

By

Ziyue Jiang

2013

ABSTRACT OF THE DISSERTATION

Transcription-Based Molecular Imaging and Gene Therapy for Castration-resistant and Metastatic Prostate Cancer in Translational Models

By

Ziyue Jiang

Doctor of Philosophy in Molecular & Medical Pharmacology

University of California, Los Angeles, 2013

Professor Lily Wu, Chair

The advanced stage of prostate cancer is the second leading cause of cancer-related death for American men. Novel, effective treatment options and more cancer-specific diagnostic tools are urgently needed to facilitate patient management. Here, we explored the construction and application of an array of gene-based molecular imaging and therapeutic vectors in a variety of clinically relevant settings. These vectors exploit prostate cancer-specific promoters to control the transcription of imaging reporter genes or therapeutic genes, and thus can achieve stringent cancer selectivity. We showed that gene-based imaging vectors can detect prostate cancer

metastasis earlier than conventional imaging modalities; we also developed a dual-reporter imaging system that can specifically interrogate the activation/inhibition status of androgen receptor, and thus monitor the efficacy of androgen deprivation and androgen receptor blockade therapies. Further, we explored the applicability of gene-based vectors in detecting circulating tumor cells and have obtained promising results. Moreover, we employed two strategies to improve the clinical usability of viral vectors in immunocompetent hosts (such as humans). In the first strategy, we used a broad-acting immunosuppressant, rapamycin, to reduce the scale of adenovirus-induced inflammatory responses and also to decrease the eliminating effects of host adaptive immune system on viral vectors and viral-infected, transgene-expressing cells. Rapamycin significantly augmented the magnitude and prolonged the duration of virus-delivered transgene expression, and thus enhanced the diagnostic capability of these imaging vectors. The second approach took advantage of the versatile surface modifying ability of non-viral reagents. We designed a polypeptide coating that can non-covalently bind to adenoviral particles and confer protections against blood components such as neutralizing antibodies and coagulation factors. The coating significantly decreased the inhibitory effects of neutralizing antibodies on adenoviral transduction and markedly abrogated coagulation factors-mediated hepatocyte infection. Furthermore, this polypeptide coating reduced the antigenicity of adenoviral vectors *in vivo*, greatly diminished anti-adenovirus antibody production, and therefore could facilitate repeated administration of viral vectors in immunocompetent hosts. Overall, we herein present a substantial amount of evidence supporting the pre-clinical and translational use of gene-based imaging and therapeutic vectors to assist the management of patients with advanced, treatment-refractory prostate cancer.

The dissertation of Ziyue Jiang is approved.

Johannes Czernin

Donald Kohn

Anna Wu

Lily Wu, Committee Chair

University of California, Los Angeles

2013

TABLE OF CONTENTS

ABSTRACT OF THE DISSERTATION ii
LIST OF ACRONYMS vii
ACKNOWLEDGEMENT ix
VITA x
I. INTRODUCTION 1
Figure 1.1. Three types of prostate specific promoters have different responses to androgen stimulation. 4
Figure 1.2. Dual-reporter system monitors ADT and ARBT. 5
Figure 1.3. Adenovirus induces innate immune responses and inflammation. 7
Figure 1.4. Immunosuppressive effects of rapamycin. 9
II. DETECTING CASTRATION RESISTANT METASTATIC PROSTATE CANCER 12
INTRODUCTION 14
MATERIALS AND METHODS 16
Figure 2.1. Schematic of PSES-TSTA adenoviral vectors 17
RESULTS 21
Figure 2.2. PSES-TSTA activates gene expression under androgen deficient conditions. 22
Figure 2.3. PSES-TSTA is specific to prostate tissue 25
Figure 2.4. PET imaging capacity of PSES-TSTA vector 27
Figure 2.5. PSES-TSTA imaging vector mediated detection of castration-resistant bony prostate cancer metastasis 30
DISCUSSION 31
III. TRANSLATIONAL APPLICATION OF GENE-BASED IMAGING VECTORS 37
INTRODUCTION 38
Figure 3.1. PSA-driven reporters faithfully monitor activation of the AR axis. 39
MATERIALS AND METHODS 43
RESULTS 44
Figure 3.2. PSA-driven reporter monitors efficacy of androgen blockade therapy 45
Figure 3.3. PSME-driven reporters are activated by androgen deprivation and AR blockade treatments. 46

Figure 3.4. The dual-reporter system exhibited simultaneous up- and down-regulation of reporter expression during androgen receptor blockade conditions. 47

Figure 3.5. PSES-TSTA-IFP vector can differentiate prostate cancer cells from white blood cells. 49

Figure 3.6. Ad-PSES-TSTA-IFP exhibited similar, if not higher, CTC detection capability as compared to the EpCAM-based method. 51

DISCUSSION 52

IV. VIRAL VECTOR ADMINISTRATION IN IMMUNOCOMPETENT HOSTS 57

IV-I. Rapamycin Enhances Adenovirus-mediated Cancer Imaging in Pre-Immunized Hosts 57

INTRODUCTION 58

MATERIALS AND METHODS 59

RESULTS 63

Figure 4.1. Rapamycin diminished adenovirus-induced innate immune response. 64

Figure 4.2. Rapamycin mitigated the eliminative effect of adaptive immune system on Ad-mediated transgene expression. 65

Figure 4.3. Rapamycin enhanced Ad-mediated transgene expression in pre-immunized mice. 67

Figure 4.4. Rapamycin suppresses anti-Ad adaptive immune responses. 70

DISCUSSION 72

IV-II. Polypeptide Coatings Shield Adenovirus from Interference of Blood Factors and Reduce Adenoviral Antigenicity 75

INTRODUCTION 76

Figure 4.5. Formation of the hybrid complex. 76

MATERIALS AND METHODS 78

RESULTS 79

Figure 4.6. Effect of polypeptide coating on blood factor interferences and antigenicity of adenovirus. 80

DISCUSSION 82

V. CONCLUSION 84

BIBLIOGRAPHY 86

LIST OF ACRONYMS

AABD	(S)-2-(4-acrylamidobenzyl)-DOTA
Ad	Adenovirus
ADT	androgen deprivation therapy
AR	androgen receptor
ARBT	androgen receptor blockade therapy
ARE	androgen responding element
CAR	coxsackie virus-adenovirus receptor
CMV	cytomegalovirus (promoter)
CRPC	castration resistant prostate cancer
CSF1R	colony-stimulating factor 1 receptor
CTC	circulating tumor cell
DAbR1	DOTA antibody reporter 1
DC	dendritic cells
DHT	dihydrotestosterone
DOTA	1,4,7,10-tetraazacyclododecane-1,4,7,10-tetraacetic acid
Dox	doxycycline
ELISA	Enzyme-linked immunosorbent assay
EpCAM	Epithelial cell adhesion molecule
ERK	extracellular-signal-regulated kinase
FBS	fetal bovine serum
FDG	Fluorodeoxyglucose
FHBG	9-(4-18F-fluoro-3-[hydroxymethyl]butyl)guanine
FKBP12	FK506 binding protein 12
FL	firefly luciferase
FX	coagulation factor X
HIF1α	hypoxia-induced factor α
hK2	human Kallikrein 2
HRE	HIF1a responsive element
HRP	horseradish peroxidase
HSV	herpes simplex virus
i.p.	intraperitoneal
i.v.	intravenous
IFN	interferon
IFP	infra-red fluorescent protein
IκBα	inhibitor of Kappa B-alpha
IL	interleukin

JAK	Janus kinase
kb	kilobase-pair
MAPK	mitogen-activated protein kinase
mKC	mouse Keratinocyte-derived Cytokine
MOI	multiplicity of infection
mTOR	mammalian target of rapamycin
NAb	neutralizing antibody
NCA	α-amino acid-*N*-carboxyanhydride
NFκB	nuclear factor kappa B
NK cells	natural killer cells
p.i.	post infection
PCR	polymerase chain reaction
PEG	poly(ethylene glycol)
PET	positron emission tomography
PFU	plaque forming unit
PI3K	phosphoinositide 3-kinase
PPT	PSA enhancer, PSMA enhancer and TARP promoter
PSA	prostate specific antigen
PSES	prostate specific enhancing sequence
PSMA	prostate specific membrane antigen
PSME	PSMA Enhancer
RANTES	regulated and normal T cell expressed and secreted
RAPA	rapamycin
RL	renilla luciferase
scFv	single chain Fv
SCID	severe combined immunodeficiency
STAT	signal transducers and activators of transcription
TARP	T cell receptor gamma alternate reading frame protein
tk	thymidine kinase
TLR	Toll-like receptor
TNFα	tumor necrosis factor alpha
TORC	TOR complex
TSTA	two step transcriptional amplification
VEGF-C	vascular endothelial growth factor-C
Y	Yttrium

ACKNOWLEDGEMENT

I sincerely thank Drs. Makoto Sato, Steve Hyun, Saul Priceman, Breanne Karanikolas, Mai Johnson, James Sung, Frédéric Pouliot, John David and Yufang Hu for their scientific insights and technical guidance. I also thank Diana Moughon, Jemima Escamilla, Shiruyeh Schokrpur, Jennifer Kuo and Annie Ma for helpful technical assistance.

I thank Sarah Starrett and Aija Gamburg for their tremendous help in administrative matters and Martha Margarita Calderon for keeping the lab running smoothly.

Last but not least, I would like to give my heartfelt gratitude to my parents, Drs. Hongzhi Jiang and Li Zhang, and my loving husband Alvin Yang for their unconditional love, support and inspiration, and for being there for me throughout these years.

VITA

EDUCATION

TSINGHUA UNIVERSITY Beijing, China

Bachelor of Science, Biological Science and Biotechnology July 2007

- *Graduation with the Highest Distinction*

PUBLICATIONS

Ziyue Karen Jiang, Mai Johnson, Diana Moughon, Jennifer Kuo, Makoto Sato, and Lily Wu. Rapamycin Enhances Adenovirus-mediated Cancer Imaging in Pre-Immunized Hosts. *submitted*

Frédéric Pouliot, Makoto Sato, Ziyue Karen Jiang, Steve Huyn, Breanne D.W. Karanikolas, and Lily Wu. A molecular imaging system based on both transcriptional and genomic amplification to detect prostate cancer cells in vivo. **Mol Ther;** 2012 Dec 18. doi: 10.1038/mt.2012.259

Ziyue Karen Jiang*, Sok Boon S. Koh*, Ivo C. Atanasov, Makoto Sato, Mai Johnson, Z. Hong Zhou, Timothy J. Deming and Lily Wu. Engineering Polypeptide Coatings to Augment Gene Transduction and in vivo Stability of Adenoviruses. **Journal of Controlled Release;** 2012 Dec 16;166(1):75-85. *, equal contribution

Ziyue Karen Jiang, Makoto Sato and Lily Wu. The Development of Transcription-regulated Adenoviral Vectors with High Cancer-selective Imaging Capabilities. **Adv Cancer Res**; 2012;115:115-46. **Review**.

Johanna M. Jarchoa, Emeran A. Mayer, Ziyue Karen Jiang, Natasha A. Feierb, and Edythe D. London. Pain, affective symptoms, and cognitive deficits in patients with cerebral dopamine dysfunction. **Pain**; 2012 Apr;153(4):744-54. **Review**.

Ziyue Karen Jiang, Makoto Sato, Wei Liu, Chinghai Kao and Lily Wu. Androgen-independent Molecular Imaging Vectors to Detect Castration-Resistant and Metastatic Prostate Cancer. **Cancer Res**; 2011 Oct 1;71(19):6250-60.

Kuan-Ju Chen, Stephanie M. Wolahan, Hao Wang, Chao-Hsiung Hsu, Hsing-Wei Chang, Lian-

Pin Hwang, Mitch A. Garcia, Ziyue Karen Jiang, Lily Wu, Yung-Ya Lin and Hsian-Rong Tseng. An MRI Contrast Agent Library: Effective Optimization of Gadolinium(III)-Encapsulated Supramolecular Nanoparticles for Improved Relaxivity and Sensitivity. **Biomaterials.** 2011 Mar;32(8):2160-5.

MEETING PROCEEDINGS

2012 World Molecular Imaging Congress. Monitor androgen deprivation and androgen receptor blockade therapy with a functional dual reporter system (award-winning poster)

American Association for Cancer Research Annual Meeting 2012. Monitor androgen blockade therapy with functional androgen receptor reporting system (multi-award-winning poster)

2011 World Molecular Imaging Congress. *In vivo* Gene-based Imaging to Detect Castration Resistant and Metastatic Prostate Cancer (multi-award-winning poster)

35th Annual Western Regional Society of Nuclear Medicine Meeting. Translational investigation of in vivo gene-based imaging to detect castration resistant prostate cancer progression (award-winning oral presentation)

American Society of Gene & Cell Therapy 13th Annual Meeting and Training Course. Characterization of the PSES-TSTA system, an androgen independent prostate specific transcriptional enhancer, in Adenovirus-based gene therapy vectors (poster)

FELLOWSHIP

The Regent of University of California, Los Angeles

Dissertation Year Fellowship. July 2012 – March 2013

UCLA's Jonsson Comprehensive Cancer Center Foundation

Pre-doctoral Research Fellowship. April 2011 – April 2012

I. INTRODUCTION

Prostate cancer is the second leading cause of cancer-related death for American men with estimated 192,280 new cases and around 30,000 mortality every year [1]. The early stage of the disease is largely curable by prostatectomy and radiation therapy. However, approximately 20-40% of patients will develop advanced disease with local invasion or systemic dissemination and the prognosis for this group of patients is unfortunately poor. The current mainstay of systemic treatment for advanced prostate cancer includes hormonal manipulations such as androgen deprivation therapies (ADT) and androgen receptor blockade therapies (ARBT). In ADT, the production of the male hormone androgen (i.e. testosterone and the more potent metabolite dihydrotestosterone (DHT)) is inhibited by surgically removing the testicles (rarely performed nowadays) or by medical interventions that stop testosterone synthesis via neuroendocrine regulation or inhibit the function of enzymes that are important in the synthesis pathway. ARBT, on the other hand, utilizes compounds such as flutamide and bicalutamide to antagonize the action of androgen receptor (AR), the nuclear steroid hormone receptor that executes all the downstream functions of androgen in aspects of cell proliferation, survival and gene transcriptional regulation. Unfortunately, these treatments have been proved to be effective only transiently. The majority of these patients will inevitably progress to a stage called castration resistant prostate cancer (CRPC) manifested by rising serum PSA (prostate specific antigen) and often metastasis (mostly in skeleton bone) within an average of 12-18 months [2-5].

It remains elusive how prostate cancer progresses into the CRPC stage where cancer cells have gained the ability to continue to grow despite the shortage of circulating androgen. However, a growing body of evidence points toward the essential role of AR and the androgen – AR

signaling axis in CRPC. Commonly accepted mechanisms include upregulation of AR co-activators, AR gene amplification, secondary mutations that render a promiscuous receptor and ligand independent activation of AR by other signaling pathways [3, 6-13]. In addition, prostate cancer may evolve compensatory mechanisms to synthesize DHT *de novo* intratumorally [14-15]. Recently, emerging evidence highlights the existence of AR splicing variants that contain truncated or deleted C-terminal ligand binding domain in castrated prostate cancer. Some of these variants possess constitutive activity in transcription and cell proliferation regulation [16-21]. Therefore, albeit in possibly different mutant or variant forms, AR remains a key player in CRPC pathology that underlies disease recurrence and treatment resistance.

Challenged by the disappointing clinical outcome for castration resistant and metastatic prostate cancer, researchers have been intensely pursuing novel therapeutics such as next-generation anti-androgen drugs with improved efficacy and potency, as well as reliable and practical diagnostic markers that are highly specific to prostate cancer. Towards this end, transcription-based gene therapeutic and molecular imaging approaches hold unique potentials and have been actively investigated. As will be discussed further in this thesis, we have exploited a panel of promoters that are specific to advanced prostate cancer to drive the expression of imaging reporter genes as well as cytotoxic suicidal genes and have gathered quite encouraging preliminary results. Three types of prostate cancer-specific promoters are in our arsenal according to their different response towards androgen stimulation: androgen inducible, androgen suppressible and androgen independent promoters (Fig. 1.1). Noteworthily, all these promoters are silenced in AR negative prostate cancer cell lines (e.g. DU145), suggesting the presence of AR is still necessary for their transcriptional regulation, underlying the viability of using these promoters to interrogate androgen signaling in prostate cancer cells. Most traditional prostate promoters fall in the

category of androgen inducible promoters, including PSA, probasin and hK2. Their activity is enhanced by the presence of androgen. On the other hand, PSME, the enhancer region from the PSMA (prostate specific membrane antigen) gene, represents androgen suppressible promoters. The expression of PSMA has been shown to be elevated in castrated prostate cancer samples and PSME activity is down-regulated by addition of synthetic androgen R1881 into culture media [22]. Finally, androgen independent promoters can be created by fusing androgen inducible and suppressible promoters together to form a chimeric transcriptional regulatory element. For example, Lee *et al* pieced together fragments derived from both the PSA and PSME enhancers, and the resultant enhancer PSES (prostate specific enhancing sequence) is able to support prostate cancer specific gene expression irrespectively of the presence or absence of androgen. Specifically, linker-scanning mutations and deletion analyses were conducted across the PSA promoter and the PSMA enhancer regions, respectively, and two strong enhancer regions were identified. The PSA-derived element, namely AREc3, demonstrated stringently androgen-dependent activity, whereas the PSME-derived region, PSME(del2), exhibited higher transcriptional activity in androgen-deficient cultural conditions compared to androgen-supplemented conditions. Interestingly, when tested using reporter essays *in vitro*, PSES manifested transcriptional activity only in prostate cancer cell lines but not in cell lines that are of other tissue origins. Moreover, when injected intraprostatically into male mice, PSES-driven reporter expression was confined in the prostate, whereas a CMV promoter-directed reporter demonstrated leaky expression in the spleen, the lung and the brain [22]. Similar strategies were taken to generate the PPT promoter, a synthetic sequence containing PSA enhancer, PSMA enhancer and TARP promoter [23]. These artificial androgen independent elements serve as constitutive promoters with prostate cancer-confined activity.

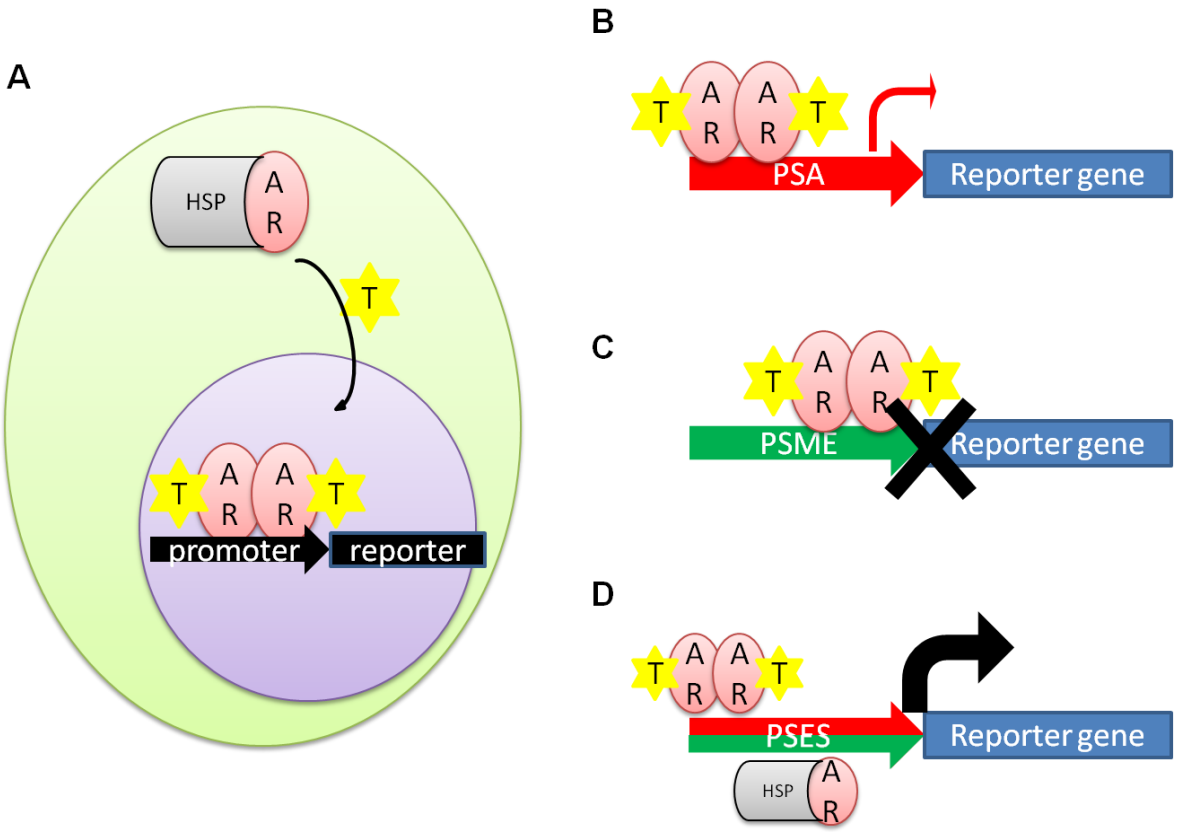

Figure 1.1. Three types of prostate specific promoters have different responses to androgen stimulation. A. Upon androgen (represented by testosterone) stimulation, androgen receptor (AR) gets released from the heat shock protein, dimerizes and translocates into the nucleus, where AR exerts its transcriptional regulatory function. B. Androgen inducible promoters (e.g. PSA) is turned on by androgen liganded AR. C. Androgen suppressible promoter (e.g. PSME) is silenced when AR is active. D. Chimeric PSES promoter is constitutively active regardless of AR activation status.

The unique advantages of gene-based vectors lie in the employment of these cancer-specific promoters that enable selective expression of imaging reporters and therapeutic genes (ideally) only in cancer cells. For example, the chemotherapy agent docetaxel exerts its cytotoxicity by binding to microtubules, stabilizing microtubule assembly, hence preventing mitotic cell division. However, despite some uneven distribution among different cell types, docetaxel still affects

normal cells and thus will inhibit cell division in all rapidly proliferating cells, resulting in side effects of chemotherapy such as hair loss, fatigue, nausea and more seriously, immune suppression. In gene therapy, in contrast, we used prostate cancer-specific promoters to drive a therapeutic gene, (e.g. HSV-sr39tk, a more potent variant form of the herpes simplex virus-thymidine kinase gene), and the restricted activity of the promoters assured confined cytotoxicity within prostate cancer cells, reducing systemic toxic side effects. For another example, the clinical gold standard cancer imaging modality is ^{18}F-FDG PET imaging based on the assumption that cancer cells uptake and utilize more glucose due to their fast proliferation rate and the Warburg's effect of high glycolysis. However, in reality, FDG scans may suffer from high background from heavily glucose-using organs and limited sensitivity because not all tumors are actively taking up and consuming glucose. Reporter genes-based approaches, on the other hand, target transcriptional activities that are uniquely present in cancer cells by controlling reporter expression under prostate cancer promoters, and thus offering a superior specificity. More discussion regarding this aspect will be covered in Chapter II.

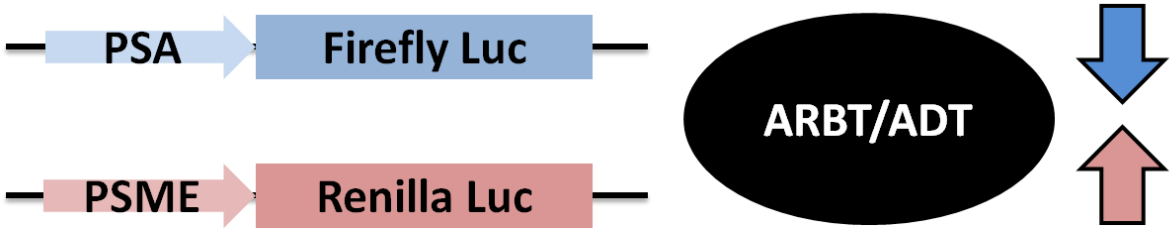

Figure 1.2. Dual-reporter system monitors ADT and ARBT. AR activity is monitored by simultaneously examining the androgen inducible PSA-FL and the androgen suppressible PSME-RL signals. An effective ARBT/ADT will diminish FL but raise RL expression by inhibiting AR signaling.

Chapter III of this thesis demonstrates other benefits of implementing transcription-based

imaging vectors in two highly-clinically relevant experimental trials. The first trial explores the idea of using transcription-based imaging to interrogate the activity of particular signaling pathways by placing reporters under the regulation of the downstream effecter transcriptional factors of that pathway. For instance, to monitor hypoxia, a common condition in tumor environment due to poor oxygen perfusion, one can link a reporter gene (e.g. luciferase) expression cassette to HIF1α responsive element (HRE). As HIF1α (hypoxia-induced factor α) is a transcriptional factor activated under low oxygen tension, hypoxic cells will be visualized according to the heightened level of luciferase expression and emission of bioluminescent signal. Similarly, we here adopted the androgen inducible PSA and the androgen suppressible PSME promoters to drive two reporter genes and used this dual reporter system to monitor the activation status of AR signaling axis. Specifically, in the presence of an effective ADT/ARBT regimen, the expression of the PSA-Firefly luciferase (FL) cassette will be decreased because of castration level of androgen or inhibited AR function; meanwhile, the expression of the PSME-Renilla luciferase (RL) will oppositely increase (Fig. 1.2). This simultaneous down- and up-pattern of imaging signals provides not only information regarding the presence, size and location of a malignant lesion, but also a functional readout of the state of AR signaling axis that is critical for prostate cancer progression.

In the second experiment, we adopted the androgen independent PSES promoter to drive the expression of an infra-red fluorescent protein (IFP) through the TSTA amplification system. We proposed to use this Ad-PSES-TSTA-IFP vector to infect cells that are isolated from the blood of metastatic prostate cancer patients in order to detect and quantify circulating tumor cells and thus predict the outcome of these patients. However, before implementing this vector to patient samples, pilot studies need to be performed to determine the optimal conditions for infection, IFP

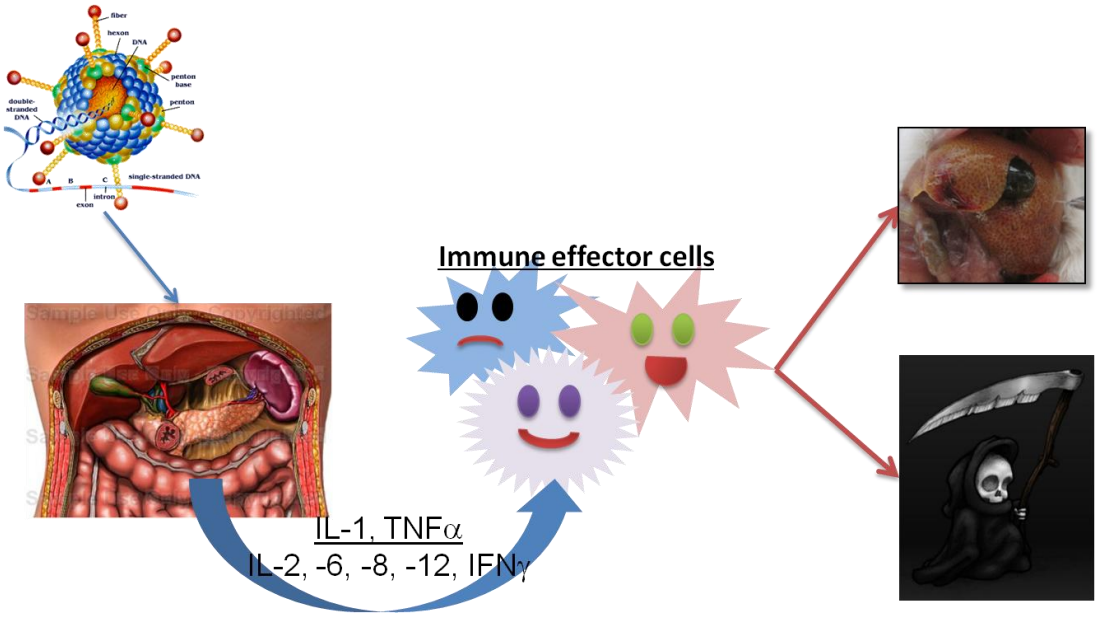

Figure 1.3. Adenovirus induces innate immune responses and inflammation. Systemically administered adenovirus predominantly infects liver-resident macrophages (Kupffer cells), hepatocytes and endothelial cells as well as splenic dendritic cells. This infection leads to secretion of inflammatory chemokines and cytokines, which in turn could trigger the activation and infiltration of systemic immune effector cells, potentially causing tissue damages and, in some severe cases, death.

gene expression and the final analytical assays as well as to evaluate the specificity and sensitivity of this method. Therefore, we took blood cells from healthy donors and purified white blood cells, which were then mixed with C4-2 prostate cancer cells and then subjected to vector transduction and fluorescent microscopy. Our preliminary observations encouragingly validated the feasibility and accuracy of this approach to visualize circulating tumor cells.

Chapter IV of this thesis is focused on the efforts and progress that we have made towards the clinical translation of gene-based imaging and therapeutic vectors, especially in the form of adenoviral vehicles. Historically, adenoviral vectors (Ad) have been one of the most widely used *in vivo* gene-delivery agents in preclinical and clinical cancer trials [29] because of its high

efficiency of transduction in a broad spectrum of cells, the ease of preparation of high-titer stocks, as well as the low pathogenicity and minimal oncogenic potential. Moreover, the spacious 38-kb Ad genome enables manipulations that incorporate lengthy promoter sequences and multiple transgenes. However, several hurdles need to be overcome before it is realistic to consider using these viral vectors to image and treat cancer in human patients as illustrated below.

(1) Restricted biodistribution of systemically injected Ad. Systemically administered Ad exhibits predominant liver tropism largely due to the presence of the liver-resident macrophages (Kupffer cells) that can entrap and sequentially destroy >90% of the virus load rapidly post injection [24]. In addition, coagulation factors IX and X and certain complement proteins can bind to the hexon protein on Ad capsid; this interaction efficiently mediates Ad tropism toward hepatocytes via cell surface heparin sulfate proteoglycans or low-density lipoprotein receptor-related proteins [24]. These effects markedly perturb the distribution of Ad and greatly reduce the amount of virus effectively delivered to the target tissue.

(2) Adenovirus-induced acute inflammation and toxicity. Systemically administered adenovirus will primarily hit Kupffer cells, hepatocytes and endothelial cells in the liver, as well as cells in the splenic compartment. Infection of these cells results in activation of inflammatory signaling cascades at low viral doses and causes necrotic cell death at high viral loads; both of these events can trigger the secretion of a series of pro-inflammatory chemokines and cytokines, which in turn will signal and recruit immune effector cells such as neutrophils to infected organs and cause severe tissue damage, systemic aseptic shock or even death depending on the extent of inflammation [25-29] (Fig. 1.3).

(3) Adaptive immune system-mediated inhibition of adenoviral transgene expression. Both

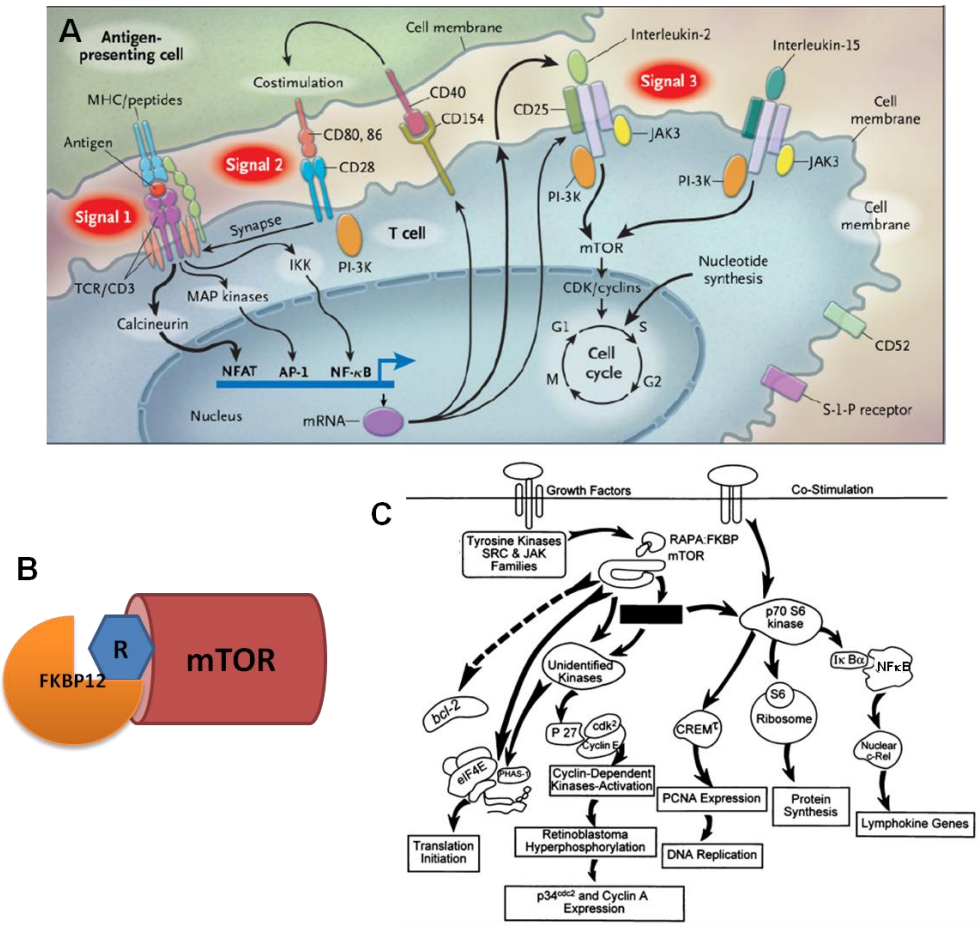

Figure 1.4. Immunosuppressive effects of rapamycin. A. Activation of T lymphocytes entails 3 signals. Signal 1: an antigen presented by antigen-presenting cells (e.g. dendritic cells) triggers cognate T-cell receptor and CD3 complex; signal 2: costimulatory signal delivered by CD80 and CD86 by engaging CD28 in T cells. These 2 signals will induce a cascade of signaling including calcineurin activation, MAP kinase activity and release of the inhibition of NF-κB from IκB, which leads to transcription of CD25, CD154, IL-2 and IL-15. The cytokines will in turn activate PI-3K and mTOR pathway, which constitutes the "signal 3" for T cell proliferation (adopted from *Halloran P, New England Journal of Medicine, 2004*). B. Mechanism of rapamycin's action. Rapamycin (R) binds to the immunophilin FKBP12, and this complex engages mTOR to inhibit the formation of TORC1. C. Cellular events that involve mTOR and thus can be inhibited by rapamycin (adopted from *Sehgal S, Clinical Biochemistry, 1998*)

humoral and cellular immune responses participate in the reduction of the effectiveness of Ad-mediated gene expression [30-32]. The majority of human population has anti-Ad neutralizing antibodies due to previous exposure to this pathogen. Administration of Ad for gene therapy or imaging purposes would prime the secondary activation of Ad-specific memory B cells, leading to their differentiation into robustly anti-Ad antibody-producing cells [31]. On the other hand, NK cells, CD4+ and CD8+ T cells are involved in abrogation of virally infected, foreign transgene-expressing cells through cytotoxic and noncytotoxic mechanisms [32].

As will be discussed further in Chapter IV, we here explored two strategies to address these challenges. The first strategy entails the use of an FDA-approved immunosuppressant, rapamycin, to transiently dampen the activation of both innate and adaptive immune responses induced by Ad infection. Specifically, rapamycin is FDA-approved for organ transplantation patients. It is conventionally believed to inhibit the activity of mTOR kinase and TOR complex 1 (TORC1), which is a critical signaling hub for a number of cell survival functions such as transcription, translation initiation, protein synthesis, cell cycle progression, nutrition sensor and autophagy (Fig. 1.4.). Suppression of mTOR kinase by rapamycin directly halters cell cycle progression in fast-proliferating immune cells and decreases their ability to differentiate/activate upon inflammatory stimulations [33]. Incorporation of rapamycin into Ad gene therapy and cancer imaging procedures successfully reduced Ad-triggered acute inflammation and significantly enhanced transgene expression even in the presence of pre-existing anti-Ad host immunity. In the second strategy, we developed a polypeptide coating procedure that can shield antigenic epitopes on the surface of Ad capsid from being recognized by neutralizing antibodies present in human sera; this coating also reduced the antigenicity of Ad in immunocompetent hosts by lowering the titer and delaying the onset of anti-Ad antibody production. Furthermore,

polypeptide coating decreased coagulation factor X-mediated Ad transduction of mouse liver cells *in vitro*, suggesting that it could be a potentially valuable approach to circumvent Ad's liver tropism.

Overall, in this thesis, we demonstrated the value of gene-based vectors in the setting of prostate cancer molecular imaging and therapy. We explored the potential use of these vectors in detecting metastasis, evaluating circulating tumor cells, and monitoring AR signaling axis activation in castration resistant prostate cancer. Moreover, we investigated several strategies to translate these viral vectors into clinically relevant immunocompetent hosts with pre-existing anti-Ad immunity.

II. DETECTING CASTRATION RESISTANT METASTATIC PROSTATE CANCER

Androgen Independent Transcription-Based Molecular Imaging Vectors Detect Castration Resistant Prostate Cancer and Metastasis

Abstract

Prostate specific promoters are frequently employed in gene mediated molecular imaging and therapeutic vectors to diagnose and treat CRPC that emerges from hormone ablation therapy. Many of the conventional prostate specific promoters rely on the androgen axis to drive gene expression. However, considering the cancer heterogeneity and varying androgen receptor status, we herein evaluated the utility of PSES, an androgen-independent transcriptional regulatory element, in CRPC. The PSES is a fused enhancer derived from the PSA promoter and PSMA enhancer. We augmented the activity of PSES by the two-step transcriptional amplification (TSTA) system to drive the expression of imaging reporter genes for either bioluminescent or positron emission tomography (PET) imaging. The engineered PSES-TSTA system exhibits greatly elevated transcriptional activity, androgen-independency and strong prostate specificity, verified in cell culture and preclinical animal experimentations. These advantageous features of PSES-TSTA elicit superior gene expression capability for CRPC in comparison to the androgen-dependent PSA promoter driven system. In preclinical settings, we demonstrated robust PET imaging capacity of PSES-TSTA in a castrated prostate xenograft model. Moreover, intravenous administrated PSES-TSTA bioluminescent vector correctly identified tibial bone marrow

metastases in 9 out of 9 animals while NaF- and FDG-PET were unable to detect the lesions. Taken together, this study demonstrated that the promising utility of a potent, androgen-independent and prostate cancer-specific expression system in directing gene-based molecular imaging in CRPC even in the context of androgen deprivation therapy.

INTRODUCTION

Prostate cancer is the most common cancer for males in America. The disseminated disease remains a major cause of cancer-related morbidity and mortality [34]. Hormone therapies such as ADT and ARBT are the most effective systemic treatments for patients with metastasis [35]. However, despite initial response to androgen withdrawal, CRPC progression will occur within an average of 12-18 months in the majority of the cases [34]. Due to the unfortunate lack of cure for CRPC, the search for more effective treatment and diagnostic regimen deserves urgent attention.

Ad mediated molecular imaging and gene therapy vectors have been intensely studied to diagnose and treat CRPC for the past decade ([36] and reviewed by [37]). In these Ad vectors, prostate specific promoters or enhancers such as the ones derived from PSA, probasin, and human glandular kallikrein 2 (hK2) have been broadly used to drive tissue restricted transgene expression so as to ensure the minimum toxicity to normal and non-targeted organs [36]. Many of these promoters rely on the presence of testosterone and activated AR for transcription. A large volume of evidence has shown that AR remains active in CRPC via mechanisms such as AR amplification, mutation or intragenic rearrangement, upregulation of co-activators, ligand independent activation of AR, as well as emergence of hyper-active AR splicing variants [7-8, 19, 38], theoretically supporting the use of AR driven promoters in castrated patients. However, prostate cancer exhibits great heterogeneity [39] and the functional status of AR vary amongst different metastatic lesions and primary tumors [40]. Moreover, under acute maximal ADT transcriptional activity of AR is expected to be strongly inhibited. A prostate cancer selective but less androgen- or AR-dependent promoter would likely be more active under this setting. Interestingly, the transcriptional regulation of the PSMA gene differs dramatically from the PSA

gene in that it is negatively regulated by androgen (i.e. androgen suppressive) [41-42]. In addition to its proximal 1.2 kb promoter of PSMA, the prostate specificity and androgen suppressive activity is highly regulated by its enhancer element (PSME), located in the third intron of the FOLH1 gene [43]. The expression of PSMA was found to be elevated in more malignant prostate cancer, CRPC, as well as tumor associated vasculature [44]. Although the transcriptional regulatory mechanism of PSME is still not well understood, several groups have exploited the strong prostate cancer selectivity of PSMA promoter/enhancer ($PSMA_{P/E}$) to direct gene therapy against advanced prostate cancer [45-46]. Kao and colleagues have further advanced the prostate cancer-selective gene expression strategy by creating a chimeric prostate specific enhancing sequence (PSES) [22] that is comprised of gene regulatory elements from both the androgen inducible PSA enhancer and the androgen suppressive PSMA enhancer. Consequently, PSES can activate gene expression irrespectively of androgen status, making it a promising promoter for gene therapy in subjects with CRPC, especially considering the scenario of combining gene therapy under maximal ADT. The activity of PSES, however, is relatively limited compared to constitutive promoters, such as the CMV promoter. When injected intraprostatically into male mice, PSES enabled prostate-selective expression of reporter gene but the magnitude was only ~40% of the CMV-directed reporter [22].

In this study we took advantage of the two step transcriptional amplification (TSTA) system to boost the transgene expression level of PSES. The principle of TSTA system is shown in Fig. 2.1.A. In the first step, PSES drives the expression of the chimeric activator GAL4-VP16 [47] (GAL4 is the DNA binding domain while VP16 domain activates transcription), which then augments the transcription of the reporter genes upon recruitment to five GAL4 binding sites (G5). Two Ad vectors were generated with PSES-TSTA system regulating the expression of FL

or HSV-sr39tk as bioluminescent and PET imaging reporter gene, respectively. Here, we demonstrated the benefits of prostate specificity and androgen independency of the PSES-TSTA vectors to achieve sensitive and specific imaging in the challenging clinical scenario of metastatic CRPC.

MATERIALS AND METHODS

Adenoviral generation. Adenoviral vectors were constructed based on a modified AdEasy system – the AdNUEZ system, in which transgenes can be placed into the E3 region by multiple cloning sites (Fig. 2.1.B). In Ad-PSES-TSTA-FL, the PSES-GAL4VP16 was constructed by replacing PSEBC with PSES in pBCnewVP2BS. PSES-GAL4VP16 was then cloned into pAdNUEZ vector to generate pAd-PSES-VP2EZ. pShuttleG5-FL was then used for recombination with pAd-PSES-VP2EZ. In Ad-PSES-TSTA-DAbR1-sr39tk, the E3 region was constructed by subcloning G5-sr39tk into pNEB193, followed by insertion of PSES-GAL4VP16 in tail-to-tail configuration. The two cassettes were then cut out by *SpeI* and placed into pAdNUEZ to generate pAd-G5sr39tkPSESVP2EZ. pShuttleG5-DAbR1 was constructed by replacing FL with DAbR1 in pShuttleG5-FL. Homologous recombination of pAdEZ and pShuttle was realized in *E. Coli* BJ5183 competent cells. Viral clones were screened, propagated, purified and titrated as previously described [48].

Cell lines and cell culture experiments. All cell lines were cultured in medium containing 10% fetal bovine serum and 1% penicillin/streptomycin. The CWR22Rv1, LNCaP, HeLa and A549

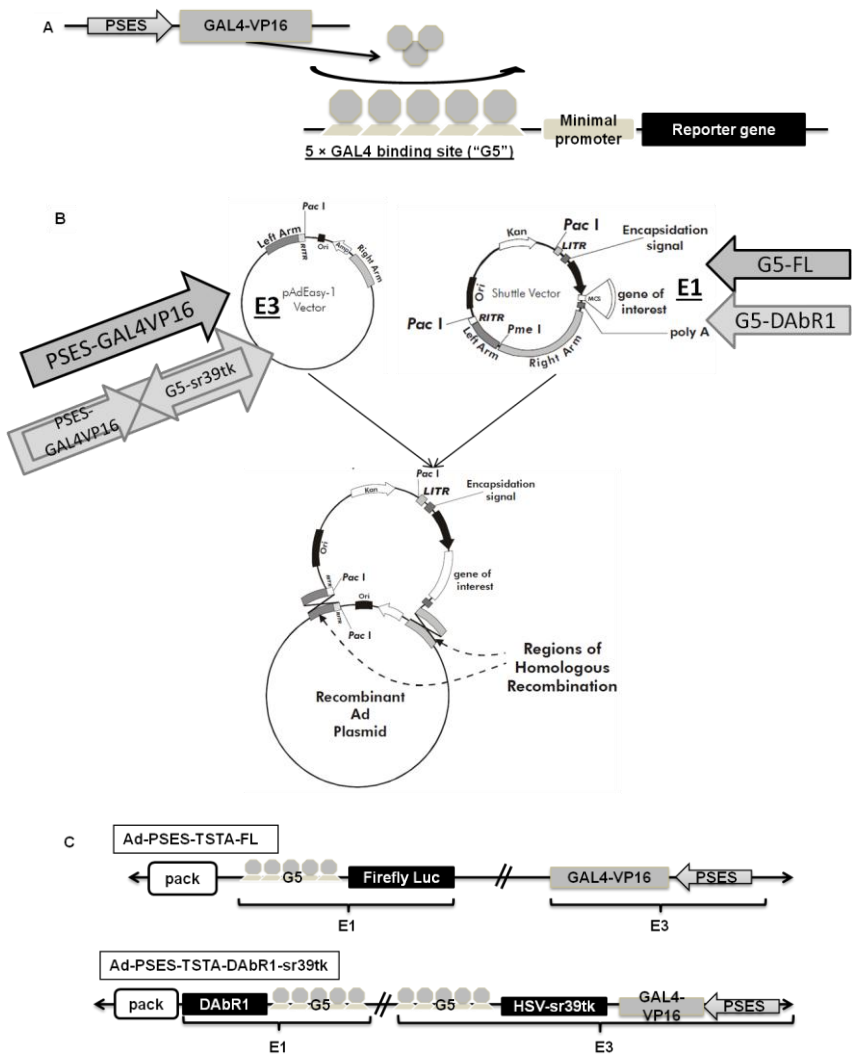

Figure 2.1. Schematic of PSES-TSTA adenoviral vectors. A. The AdNUEZ system. The E3 region of Ad genome was modified by direct means of molecular cloning on the AdEasy vector; whereas the E1 transgenes were placed into the genome by homologous recombination mediated by the left and right arms present in both the AdEazy and the Shuttle Vector plasmids. Transgenes of different vectors were respectively color-coded. Panel modified from The AdEasy™ Technology manual. B. The PSES-TSTA system (see the text). C. Configuration of Ad vectors: the Ad-PSES-TSTA-FL contains PSES-GAL4VP16 in the E3 and G5-FL in the E1 region of adenoviral genome. The Ad-PSES-TSTA-DAbR1-sr39tk contains PSES-GAL4VP16 and G5-sr39tk (tail-to-tail configuration) in the E3 and G5-DAbR1 in the E1 region.

cells were maintained in RPMI. EMEM was used for DU145 cells. The 293, MIA PaCa2 and MDA-MB-231 cells were grown in DMEM. Synthetic androgen methylenetrienolone (R1881; NEN Life Science Products, Boston, MA) was used at 10 nmol/L. Androgen receptor antagonist bicalutamide and MDV3100 was added to media as indicated at 10 μmol/L.

For *in vitro* luciferase assay, cells were seeded onto 24-well plates at 5×10^4 cells/well and infected with corresponding multiplicity of infection (MOI)s the next day. At 72 hrs post infection, the cells were harvested and lysed in passive lysis buffer. FL luciferase activity was measured according to the manufacturer's instructions (Promega, Madison, WI) using a luminometer (Berthold Detection Systems, Pforzheim, Germany). Each value was normalized to cell number or protein amount and calculated as the average of triplicate samples. Due to the similarity of infectivity among human cell lines, activity results were not adjusted.

For Western blot, 5×10^5 CWR22Rv1 and LNCaP cells were seeded into each well in 6-well plates, and infected with indicated virus at MOI=1 the next day. 72 hrs post infection, cells were collected and lysed in passive lysis buffer, and cell lysates were fractionated on 4% to 12% gradient acrylamide gels (Invitrogen, Carlsbad, CA) and subjected to immunoblot analysis using polyclonal anti-HSV-sr39tk antibody (Santa Cruz Biotechnology) and monoclonal anti β-actin A5316 antibody (Sigma). Visualization was performed by BM Chemiluminescence (Roche Diagnostics, Indianapolis, IN) with HRP-conjugated respective antibodies (GE healthcare, UK).

Subcutaneous tumor xenograft experiments. Animal experiments were performed in accordance with the University of California Animal Research Committee guidelines. 5×10^5 CWR22Rv1 cells that were marked with lentivirus expressing CMV driven Renilla Luciferase were implanted subcutaneously onto both flanks of 4- to 6-week-old female SCID mice (Taconic

Farms, Germantown, NY) in matrigel (1:1 v/v). 1×10^7 Plaque forming units (PFU) viruses were intratumorally injected in a volume of 10 μL PBS (with calcium and magnesium). Luciferase expression was monitored using a cooled IVIS CCD camera (Xenogen). Images were analyzed with IGOR-PRO Living Image Software (Xenogen). In the LAPC-9 androgen independent (AI) model, subcutaneous tumor explants were serially passaged *in vivo* in castrated male SCID-Beige mice (Taconic Farms). 1×10^7 PFU indicated virus were injected intratumorally in 10 μL PBS (with calcium and magnesium) followed by the same imaging and analysis procedure.

Orthotopic viral injection experiments. 8 to 10-week-old male SCID (Taconic Farms) mice were used. 2×10^7 PFU respective Ad was injected into dorsal lobe of the prostate in 10 μL PBS (with calcium and magnesium) using a 30-gauge insulin needle while the animals were anesthetized. Bioluminescent imaging (BLI) was performed at 7 days and 14 days post injection. *Ex vivo* imaging was done after sacrificing the animals and dissecting the indicated organs. Luciferase imaging and analysis were performed as described above.

PET imaging experiment. For all orchiectomy procedures, bilateral testicles of male mice were exposed and surgically removed by making a small incision from the center line of their scrotal sacks. Blood vessels leading to the testicles were sealed by cauterization. The skin was then glued together using Vetbond Tissue Adhesive (3M Animal Care Products, St. Paul, MN). The animals were allowed two weeks for recovery and also for systemic level of androgen to decrease. Subcutaneous LAPC-4 AI was serial-passaged in castrated SCID-Beige mice (Taconic Farms). Tumor chunks at the size of $(3\ mm)^3$ were cut and implanted subcutaneously onto the right shoulder of castrated SCID-Beige mice. 5 weeks later, a total of $1\text{-}2\times10^9$ PFU Ad-PSES-TSTA-sr39tk-DAbR1 was injected intratumorally in 4 consecutive days. 7 days after the initial

infection, ^{18}F-FHBG PET imaging was performed according to previously described procedures [48]. Animals were sacrificed after imaging.

Intra-tibial tumor experiment. 4-6 weeks old male SCID-Beige mice (Taconic Farms) were castrated according to UCLA ARC procedure. 2 weeks later, 1×10^5 LAPC-4 AI [49] tumor cells were injected into the right tibial bone marrow. Specifically, tumor cells were suspended in a mixture of PBS and matrigel (1:1 v/v) and injected in a volume of 10 μL using a 28-gauge needle to avoid cells shearing. The injection site was the dent on top of the tibial bone which can be accessed from underneath the knee cap. 6 weeks later, the animals received 1×10^8 PFU of Ad-CMV-GFP and 4×10^8 PFU Ad-PSES-TSTA-FL virus through tail vein with a 4-hr interval in between. The purpose of pre-dosing with irrelevant CMV-GFP virus is to blunt the Kupffer cells in the liver to improve transduction efficiency [50]. FL-mediated BLI was performed 4 days post viral administration. ^{18}F-NaF and ^{18}F-FDG PET imaging was done 6 and 11 days post infection, respectively. Briefly, for both ^{18}F-NaF and ^{18}F-FDG PET imaging, 70 μCi of probe was injected through the tail vein or i.p., respectively, and the animals were allowed to move around and excrete during 1-hr probe uptake. Afterwards, animals were given inhalation isoflurane anesthesia, placed in a prone position and imaged for 10 min in the microPET scanner. A 10-min CAT imaging session followed to provide structural information. All animals were sacrificed after the last imaging session, and tibial bone from both sides were removed and subjected to immunohistological staining with anti-pan-cytokeratin antibody purchased from Bio Genex, CA.

Statistical analysis. Statistical analyses were performed using the one-tailed Mann Whitney Test. For all analyses, $p<0.05$ was considered statistically significant.

RESULTS

PSES-TSTA activates gene expression under androgen deprivation or AR blockade

To examine the cell-targeted transcriptional activity of the PSES-TSTA system, we constructed two recombinant adenoviral vectors (Ads) that control the expression of the imaging reporter gene FL or HSV-sr39tk, respectively (Fig. 2.1.C). Recapitulating extensive prior experiences ([23, 47, 51]), the incorporation of TSTA amplification system dramatically boosted the promoter activity of PSES at least three orders of magnitude compared to the parental PSES straight vector (data not shown). Another advantageous feature of the TSTA system is its ability to drive the expression of multiple functional transgenes in the same vector simultaneously, exemplified by the Ad-PSES-TSTA-DAbR1-sr39tk vector (Fig. 2.1.C). The DAbR1 gene (DOTA Antibody Reporter 1) encodes a membrane-anchored engineered antibody that can irreversibly bind to radiometal chelates [52]. Therefore, similar to HSV-sr39tk, it possesses both imaging and cytotoxic therapeutic capability. We have confirmed the expression of DAbR1 in Ad-PSES-TSTA-DAbR1-sr39tk (data not shown). However, we did not explore the utility of DAbR1 here as we are actively investigating the multi-modal imaging, suicide and radioimmune therapeutic capability of Ad-PSES-TSTA-DAbR1-sr39tk in a comprehensive treatment study of CRPC.

Next, we thoroughly evaluated the androgen responsiveness of Ad-PSES-TSTA-FL in comparison to the enhanced PSA promoter driven Ad-PSA-TSTA-FL (previously denoted as AdTSTA-FL, [47]) in androgen-dependent (AD) cell line LNCaP (Fig. 2.2.A), AR-expressing yet androgen-independent (AI) CWR22Rv1, VCaP and C4-2 (Fig. 2.2.B), as well as AR-

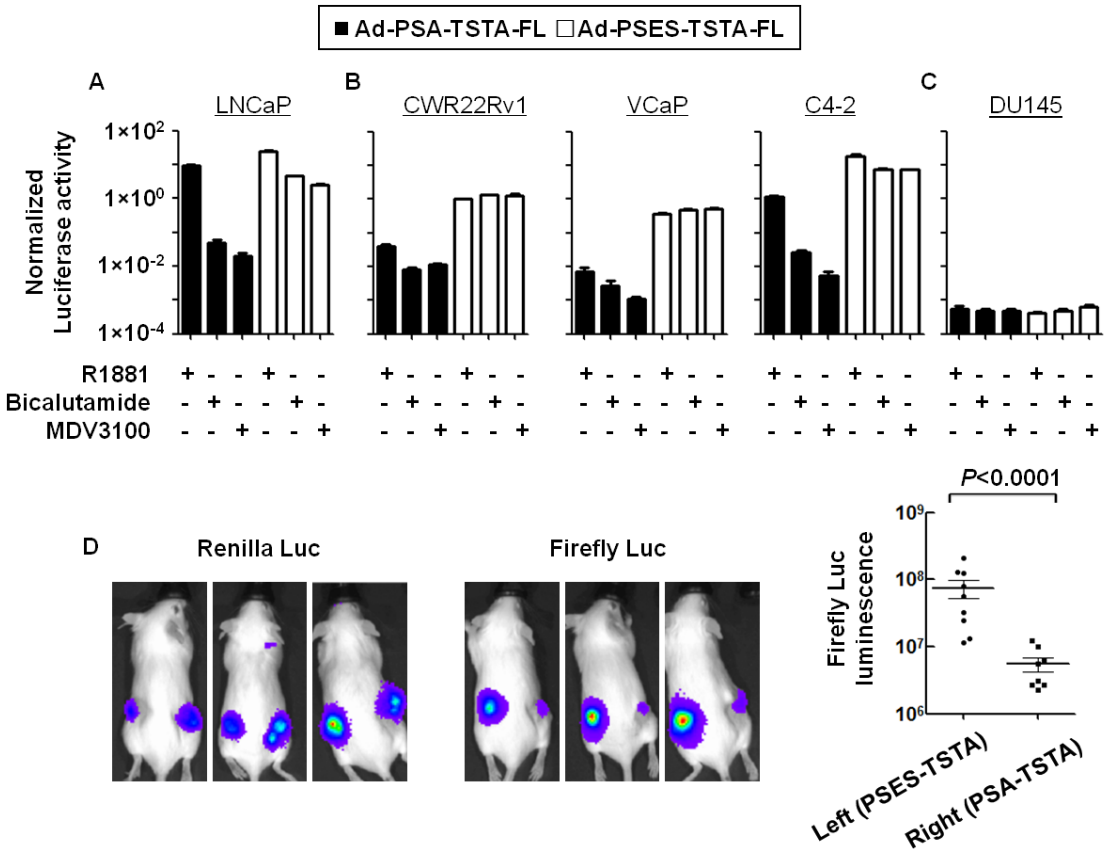

Figure 2.2. PSES-TSTA activates gene expression under androgen deficient conditions. AR positive AD cell line LNCaP (A), AR positive AI cell lines CWR22Rv1, VCaP, and C4-2 (B) and AR negative cell line DU145 (C) were infected by indicated virus at MOI of 1. The cell lines were cultured in media containing either R1881 (at 10 nM) or indicated AR antagonist (bicalutamide or MDV3100 at 10 μM). FL activity was examined 72 hrs afterwards. The activity of Ad-PSES-TSTA-FL in CWR22Rv1 with R1881 was set to 1 (absolute value = 4.64×10^{11} Relative Luminescence Units/mg) and the activity of all other cell lines is presented in reference to this level. D. 1×10^7 PFU Ad-PSA-TSTA-FL and Ad-PSES-TSTA-FL respectively were injected into the right and left CWR22Rv1 tumors on female SCID mice. Renilla luciferase imaging verified the establishment and similar volume of the two tumors. FL activity was monitored 4 days post viral injection. The absolute luminescence was plotted. Shown are three representative animals. One-tail *t* test was used.

negative prostate cancer cell line DU145 (Fig. 2.2.C). To investigate the magnitude of androgen

induction, the vector infected cells were cultured in media supplemented with either the synthetic androgen R1881 or AR antagonists. Both the first generation agent bicalutamide and the more potent second generation antagonist MDV3100 [3] were examined. In the highly AR-dependent, AD cell line LNCaP, bicalutamide and MDV3100 treatment substantially reduced PSA-TSTA-driven FL expression to 0.6% and 0.2%, respectively, compared to the R1881 condition, whereas the PSES-TSTA-driven FL only dropped down to 13% and 10%. In contrast, in the AI cell line CWR22Rv1, the presence of bicalutamide and MDV3100 decreased PSA-TSTA-FL activity to 28% and 32% of the R1881 condition, but the PSES-TSTA-driven FL expression was upregulated to 134% and 136%, respectively. Consistent results were observed in VCaP and C4-2 cells as well. In the DU145 cells that lack AR, both PSA-TSTA and PSES-TSTA vector were inactive (Fig. 2.2.C). Remarkably, the absolute FL activity from the PSES-TSTA promoter was higher than that from PSA-TSTA in all the conditions tested in the AR-expressing tumor cells. The results in the DU145 cell line support that AR is necessary for the androgen-suppressible activity of PSME.

Next, the gene expression capabilities of our vectors were examined in tumor-bearing animals. In our initial experiment, we implanted two CWR22Rv1 xenografts, stably expressing Renilla luciferase (RL), onto both flanks of female severe combined immunodeficiency (SCID) mice (n=9), using the low androgen level in female animals to mimic an androgen-deprived condition. The RL-mediated BLI verified the establishment of both tumors that grew to similar volume (Fig. 2.2.D, left panel). Subsequently, equivalent doses of Ad-PSA-TSTA-FL and Ad-PSES-TSTA-FL vector were injected into the right and left tumor, respectively. *In vivo* FL imaging verified the PSES-TSTA vector is about 10-fold more potent than the PSA-TSTA vector in CWR22Rv1 tumors in androgen deficient conditions (Fig. 2.2.D). To further substantiate the superior activity

of PSES vector in an androgen deprived setting, we injected Ad-PSES-TSTA-FL or Ad-PSA-TSTA-FL into solitary LAPC-9 AI (androgen-independent subline of LAPC-9) tumors established in castrated male SCID-Beige mice [20]. The intratumoral FL signal directed by the PSES-driven vector was nearly 100-fold higher than the PSA-driven vector (data not shown). In summary, these results demonstrated that PSES-TSTA remained transcriptionally active regardless of androgen status. The Ad-PSES-TSTA-FL was able to achieve 10-100 fold higher gene expression level than the androgen dependent PSA-TSTA-driven vector in several CRPC models.

PSES-TSTA retains stringent prostate tissue selectivity

The prostate specificity of PSES has been documented in previous reports [22]. However, it is necessary to evaluate the specificity of the amplified PSES-TSTA system, considering the introduction of the strong GAL4-VP16 transcriptional activator. First, a panel of cancer cell lines from various tissue origins was transduced with Ad-PSES-TSTA-FL. Robust expression was detected only in the prostate cancer cell line CWR22Rv1, while PSES-TSTA remained silent in non-prostatic cancer cell lines (Fig. 2.3.A).

To confirm the tissue specificity *in vivo*, we injected Ad-PSES-TSTA-FL into the prostate of male SCID mice (n=5). The control cohort received the universal CMV promoter-driven vector.

In vivo BLI was performed 7 and 14 days afterwards (Fig. 2.3.B-C). Similar to our previous studies [53], we observed the systemic vector leakage despite the orthotopic injection manifested

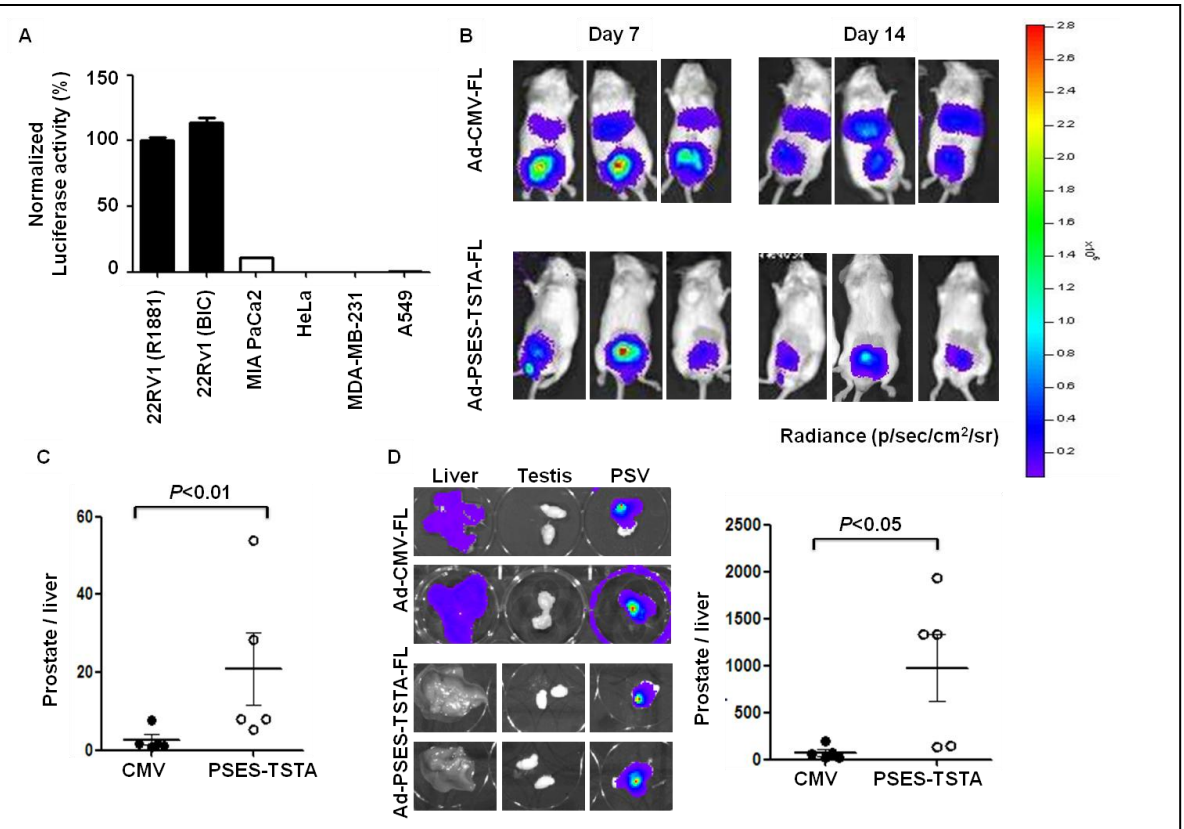

***Figure 2.3. PSES-TSTA is specific to prostate tissue*.** A. Ad-PSES-TSTA-FL was used to transduce prostate (CWR22Rv1), pancreatic (MIA PaCa-2), cervical (HeLa), breast (MDA-MB-231) and lung (A549) cancer cell lines at MOI=1. FL activity was tested 72 hrs post infection. CWR22Rv1 cells were cultured in media containing 10 nM R1881 or 10 μM bicalutamide (BIC) as indicated. The activity of Ad-PSES-TSTA-FL in CWR22Rv1 with R1881 was set at 100%. B-D: 2×10^7 PFU indicated virus was injected into the dorsal lobes of prostate of male SCID mice. B. *In vivo* BLI image of three representative animals at 7 and 14 days post viral injection. C. The ratio of signal from the prostate region of interest (ROI) to liver ROI on day 14. D. *Ex vivo* image of liver, testis and prostate-seminal vesicle (PSV) in two representative animals and quantification of prostate-to-liver ROI ratio. One-tail *t* test was used.

by the strong liver signal displayed from the CMV group. In contrast, Ad-PSES-TSTA-FL activated gene expression selectively in the prostate gland while inhibiting expression in the liver.

Ex vivo imaging of harvested liver, testicles and prostate-seminal vesicles (PSV) again confirmed the prostate specificity of PSES-TSTA seen *in vivo* (Fig. 2.3.D). Collectively, our results demonstrated that the PSES-TSTA system activated gene expression only in prostate cancer cell lines, and that the *in vivo* transcriptional activity was restricted to the prostate.

Directing PET imaging in castration resistant prostate cancer

Bioluminescent imaging (BLI) has very limited application as a whole body imaging modality in clinical settings due to its poor tissue penetration and inability to provide quantitative signal *in vivo*. Previous experience with PET reporter genes such as HSV-sr39tk indicated it is less sensitive than bioluminescent reporter genes and therefore demands a very high level of gene expression [48]. Encouraged by the amplified activity of PSES-TSTA, we explored its ability to direct PET imaging in CRPC tumors. We first examined the magnitude of HSV-sr39tk gene product expressed by Ad-PSES-TSTA-DAbR1-sr39tk (Fig. 2.1.C) in the LNCaP and CWR22Rv1 prostate cancer cell lines (Fig. 2.4.A). Corroborating the previous result of the Ad-PSES-TSTA-FL vector (Fig. 2.2.A-B), we observed that the PSES-TSTA is capable of achieving not only androgen independent expression compared to PSA-TSTA, but also very robust expression of reporter gene, exceeding even the level achieved by the strong universal CMV vector.

Next, we examined the *in vivo* PET imaging capability of Ad-PSES-TSTA-DAbR1-sr39tk with the use of the PET reporter probe 9-(4-[^{18}F]-fluoro-3-hydroxymethylbutyl) guanine (^{18}F-FHBG)

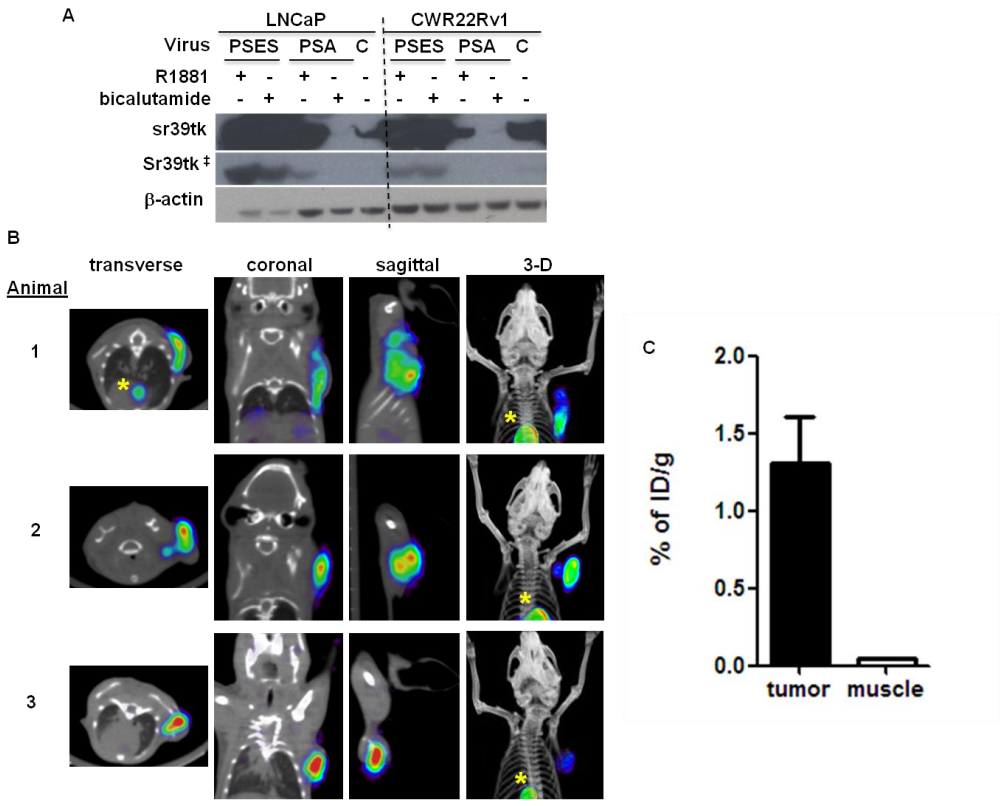

Figure 2.4. PET imaging capacity of PSES-TSTA vector. A. LNCaP and CWR22Rv1 cells were infected with Ad-PSES-TSTA -DAbR1-sr39tk (PSES), Ad-PSA-TSTA-sr39tk (PSA) or Ad-CMV-sr39tk (C) vectors and cultured in R1881 or bicalutamide supplemented media or regular media for CMV virus. Cells were lysed 72 hrs post infection and subjected to western blot. ‡, a shorter exposure time revealed the similar expression level of sr39tk by PSES-TSTA virus in androgen + and - conditions. B. Subcutaneous LAPC-4 tumor explants were passaged *in vivo* in castrated male SCID-Beige mice. A total of 1×10^9 PFU (animal 1 and 2) or 1.5×10^9 PFU (animal 3) of the Ad-PSES-TSTA-DAbR1-sr39tk vector was administered intratumorally via 4 sequential daily injections. ^{18}F-FHBG PET imaging was performed 7 days after the first viral injection. *, accumulation of circulating probe ^{18}F-FHBG in the heart. C. The %ID/g calculated from the tumor ROI or the muscle (background) ROI.

in an androgen-independent subline of LAPC-4 prostate cancer cells (LAPC-4 AI) xenografts [20]. As shown in Fig. 2.4.B-C, intratumoral delivery of Ad-PSES-TSTA-DAbR1-sr39tk was

able to produce distinct tumor signal in all 3 castrated animals that were tested. The asterisk indicated accumulation of circulating probe in the cardiac blood pool and it is not attributed to non-specific gene expression from the PSES-TSTA system. Overall, these results support the feasibility of PSES-TSTA to direct tumor-specific PET imaging in CRPC patients, even in the setting of ADT.

Image bony prostate cancer metastasis with systemic vector administration

Bone is the major site for prostate cancer metastasis [54-55]. Osseous involvement of this disease severely worsens the prognosis and quality of life. A reliable diagnostic tool to detect emergence of bony metastasis would be, therefore, highly valuable. To investigate the applicability of the PSES-TSTA in detecting bone metastasis, we injected LAPC-4 AI cells directly into the right tibia of nine castrated SCID-Beige mice, to develop osseous lesions [56]. As shown in the timeline of this study (Fig. 2.5.A), Ad-PSES-TSTA-FL was administered through the tail vein 6 weeks after tumor cell implantation. This time point was chosen based on our previous experience showing that, although there is some variability in the rate of tumor establishment with this model, a majority of osseous lesions will be established in this time frame. *In vivo* BLI detected positive FL signals in the right tibia in 7 out of the 9 animals (Fig. 2.5.B). Remarkably, immunohistochemistry staining with a prostate cancer marker, pan-cytokeratin, demonstrated that the 2 negative animals indeed failed to establish any tumor in the bone (Fig. 2.5.C). On the other hand, the presence of prostate cancer in the 7 "positive" animals was confirmed by either pan-cytokeratin staining or gross observation of the bone (Fig. 2.5.C and data not shown). Furthermore, this imaging approach can qualitatively reflect the volume of

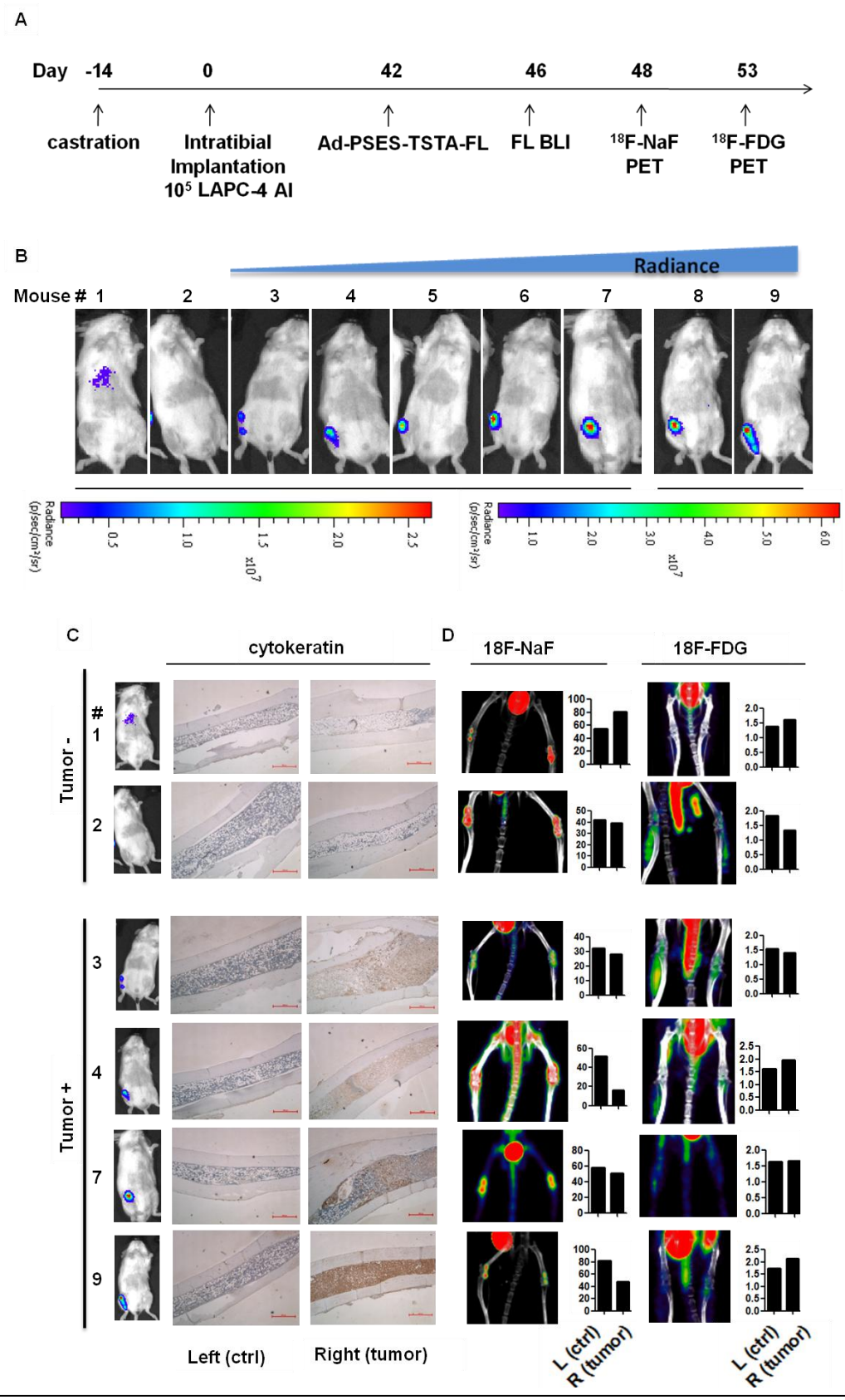
A
Day -14
0
42
46
48
53
castration
Intratibial Implantation 10^5 LAPC-4 AI
Ad-PSES-TSTA-FL
FL BLI
18F-NaF PET
18F-FDG PET
B
Radiance
Mouse # 1 2 3 4 5 6 7 8 9
Radiance (p/sec/cm²/sr)
x10^7
C
cytokeratin
Tumor -
Tumor +
1
2
3
4
7
9
Left (ctrl)
Right (tumor)
D
18F-NaF
18F-FDG
L (ctrl)
R (tumor)

Figure 2.5. PSES-TSTA imaging vector mediated detection of castration-resistant bony prostate cancer metastasis. A. Time frame: 4-5-wk-old male SCID-Beige mice were castrated. 1×10^5 LAPC-4 AI tumor cells were injected into the right tibiae. Forty two days later, the animals received 1×10^8 PFU of Ad-CMV-GFP (to blunt the vector uptake by Kupffer cells), followed by 4×10^8 PFU Ad-PSES-TSTA-FL through tail vein 4 hrs later. FL BLI, ^{18}F-NaF and ^{18}F-FDG PET-CT imaging was performed at indicated times. B. Ad-PSES-TSTA directed FL BLI. Mice are displayed according to radiance intensity emitted from the right tibiae. The 2 mice on the left were negative while the other 7 mice were positive for tumor. Note the difference in intensity scales for mice 1-7 versus mice 8-9. C. Immunohistochemistry staining of the right tibiae of six representative animals using a human-specific pan-cytokeratin antibody. D. ^{18}F-NaF and ^{18}F-FDG PET signals from tumor bearing mice. The quantification represents % Injection Dose/g from left (control) and right (tumor injected) tibial ROI. Bar, 500 μm.

tumor mass because the magnitude of FL luminescence roughly correlated with the intensity of cytokeratin staining of the tumor mass (Fig. 2.5.C). Importantly, we observed no emission at any other site, albeit a negligible level in the liver of 1 animal, demonstrating the high prostate cancer specificity of PSES-TSTA (Fig. 2.5.B).

To determine if the PSES-TSTA approach was superior to other PET based imaging technologies, we assessed the diagnostic ability of two conventional PET tracers ^{18}F-NaF (sodium fluoride) and ^{18}F-FDG to image these animals bearing osseous lesions 2 and 7 days after the BLI (Fig. 2.5.A). The fluoride ion tends to deposit at active bone remodeling sites, such as cancer osseous metastatic lesions, where intertwined interactions of cancer cells, osteoblasts and osteoclasts dynamically occur. Thus, there is an increased interest to use ^{18}F-NaF as a tracer to assess metastatic bone lesions for prostate and other cancerous malignancies [56-57]. However,

as shown in the left panel of Fig. 2.5.D, ^{18}F-NaF PET-CT failed to identify the tumor-bearing tibia in the 6 animals examined. On the other hand, due to the well known Warburg effect of heightened glucose metabolism in most cancer, ^{18}F-FDG has been used as the standard PET imaging tracer in oncology [56, 58]. Hence, we also assessed the detection capability of ^{18}F-FDG PET-CT for bone metastases (Fig. 2.5.D, right panel). Out of the 6 animals examined, ^{18}F-FDG PET imaging was unable to distinguish between animals with histologically proven lesions from those without lesions. Nor could ^{18}F-FDG distinguish between the lesion-positive (right) and -negative (left) tibia within the same animal.

We conclude that that systemically injected Ad-PSES-TSTA-FL and subsequent bioluminescent imaging can detect an experimental prostate cancer osseous metastasis model with high degree of accuracy (9 out of 9 animals). This transcription-based imaging is more specific and sensitive than ^{18}F-FDG and ^{18}F-NaF PET-CT, two standard methods currently used in clinics.

DISCUSSION

In the battle against advanced prostate cancer, there is an urgent and unmet need for a selective imaging modality. The transcription-based molecular imaging approach is particularly advantageous in its ability to be tailored to the molecular and genetic alterations in cancer [59-60]. Recent pre-clinical and clinical evidence demonstrate that AR signaling is required to sustain the growth of prostate cancer, even in CRPC [7-8, 19, 38-39, 61]. Based on this property, we and others employed the AR-dependent PSA promoter to drive reporter gene-based imaging

and demonstrated the feasibility of this approach to monitor dynamic AR transcription function *in vivo*, to image castration resistant tumors and metastatic diseases [60, 62-64]. Although the TSTA amplification system can boost the activity of the PSA promoter and facilitate imaging of CRPC tumors, we speculate that the incorporation of an androgen-independent and cancer-selective gene regulatory element could be more efficacious in driving the imaging reporter, especially in the context of maximal androgen blockade therapy. To this end, the enhancer element of the PSMA gene (PSME) appeared to be particularly promising due to its prostate cancer-specificity and its unique androgen suppressible transcriptional activity [42]. In this study we applied the TSTA amplification method to the PSES promoter, which fused the PSMA enhancer element (PSME) with the PSA enhancer element. The resulting PSES-TSTA vectors were able to achieve dramatically elevated transcriptional potency compared to the parental PSES promoter alone. Moreover, they were capable of directing androgen independent and prostate cancer-specific expression. As a consequence of their augmented capabilities, we observed that the utility of the PSES-TSTA vectors in imaging application for CRPC was also expanded. For instance, we demonstrated that the PSES-TSTA vector expressing the HSV-sr39tk gene elicits robust PET signals in CRPC tumors. Moreover, systemic delivery of Ad-PSES-TSTA-FL was capable of detecting bony CRPC metastases in a manner more sensitive and specific than current, conventional PET imaging modalities. The ability of the PSES-TSTA vector to accomplish this challenging task of detecting metastatic lesions within the systemic circulation further affirms the CRPC-selective expression capability of the PSES-TSTA vector.

At this current juncture, the mechanism of the intriguing androgen suppressible activity of PSME is not well understood. It is clear that linkage of PSME to the PSA enhancer countered the highly androgen/AR induced activity of the PSA enhancer, especially in the context of acute AR

blockade (Fig. 2.2). In response to treatment with AR antagonists, the activity of the PSA enhancer driven reporter (Ad-PSA-TSTA-FL) was drastically inhibited in both AD LNCaP cell line and the castration resistant AR-positive CWR22Rv1 cell line. Moreover, the magnitude of PSA-TSTA activity suppression correlated with the potency of AR antagonists (Fig. 2.2.A), as the second generation antagonist MDV3100 was reported to be nearly 10-fold more active than bicalutamide, the first generation agent [3]. In contrast, the PSES-TSTA mediated luciferase signal was not sensitive to AR blockade, even under the more efficacious MDV3100 treatment. The activity of the PSA enhancer component of PSES can be appreciated in highly androgen- and AR-dependent settings. For instance, in LNCaP cells in the presence of androgen, the activity of PSA-TSTA vector is almost equivalent to the PSES-TSTA vector. However, in the CWR22Rv1 CRPC model, despite ample level of androgen, the expression level of PSA-TSTA remains significantly reduced (by over 100-fold) when compared to PSES-TSTA. This result again highlights that, in the context of suppressed AR function, the contribution of PSME driven transcriptional activity will play a dominant role. Interestingly, the inability of PSES-TSTA to function in AR-negative DU145 (Fig. 2.2.C) and PC-3 cell line (data not shown) reaffirms previous reports that the androgen suppressible activity of PSME is likely mediated through AR by an indirect mechanism [44]. Further investigation of the transcriptional regulation of PSME is needed to resolve the interesting androgen-suppressive and prostate cancer-selective activity of this enhancer element.

In the clinical management of prostate cancer, a molecular imaging modality that could distinguish between indolent and aggressive disease will be of great value, especially if it can be applied in the active surveillance of prostate cancer patients, as a great majority of them present with low grade disease. The transcription-based imaging reported here is particularly amendable

to monitor the molecular and genetic alterations of cancer progression. For instance, heightened PSMA expression and androgen-independent gene regulatory program are features known to occur in advanced disease. Consequently, the use of a PSME-driven PET reporter imaging approach might be expected to produce stronger, more robust signal after the transition to aggressive disease, when compared to expression in more indolent disease. PET has distinct advantages of producing quantitative signals with three-dimensional spatial resolution and it is a clinical imaging modality widely used in oncology. Hence, the paired HSV-sr39tk/^{18}F-FHBG PET reporter gene/PET reporter probe system described here can be adapted to the clinic without difficulty. Moreover, we recently reported that this form of reporter-based PET imaging (using PSA-TSTA) can be specifically applied to monitor a transcription program in orthotopically grafted prostate tumor in mouse and in canine prostate tissues (Pouliot et al JNM, in press). Hence, translation to the clinic of transcription-based PET imaging to detect prostate cancer progression could be implemented in the near future.

The advanced lethal stage of prostate cancer has a particular propensity to metastasize to bone, severely impacting the patient's quality of life [54-55, 65]. The affinity for bone is likely due to pro-tumorigenic growth factors and a favorable environment produced as a result of the reciprocal interactions between prostate cancer and bone cells [66]. ADT can induce factors that promote the process of prostate cancer bone metastasis [67]. The current established clinical standard for imaging bone metastasis is whole body planar bone scan with ^{99m}Tc-MDP. Due to the low spatial resolution of bone scans, there is a favorable trend towards using ^{18}F-NaF PET/CT with the hope of improving the sensitivity and resolution of bone metastasis detection [68]. Several drawbacks of these two imaging modalities result from the fact that uptake of ^{99m}Tc-MDP and ^{18}F-NaF are reliant on bone remodeling, a later event in the bone metastatic

process [69]. For instance, both ^{99m}Tc-MDP bone scan and ^{18}F-NaF PET/CT will be unable to directly assess tumor volume especially in the early stage of metastasis or to detect concomitant visceral metastatic lesions. These reasons could explain why specific detection of prostate cancer metastases in the tibial bone marrow was feasible via intravenous Ad-PSES-TSTA-FL injection but not with ^{18}F-NaF PET/CT. Our data suggest that our model represents an early stage of CRPC osseous metastasis, since we were unable to detect any bony deformity by inspection or CT scan (data not shown). In addition, the animals did not exhibit any abnormality in ambulation. The histological analyses of the metastatic lesions also revealed the involvement of cancer cells in the bone marrow, but not the cortex of the bone. The clinical experience with FDG PET in detecting prostate cancer is equivocal [70-71]. Our experience indicates that human prostate cancer xenografts are not particularly avid in uptake of ^{18}F-FDG (data not shown). The current study further demonstrated this point in bone marrow metastases of CRPC LAPC-4 tumor.

Several challenges are anticipated in the clinical translation of adenoviral-based reporter gene imaging described here. Significant hurdles to overcome will include the immunogenicity of the adenoviral vector. In particular, the pre-existing immunity in a large proportion of the human population against the Ad5 serotype used here will likely induce rapid clearance of the vector. In addition, interaction of virus with blood borne factors in the circulation could result in liver sequestration and thus hinder its biodistribution in human patients [72-73]. Recent advances shed light on promising strategies to overcome these challenges. For instances, based on the recent reported ultra-high resolution of viral capsid structure [74], one could mutate the virion capsule residues to ablate immunogenic epitopes, disrupt the interactions with circulating factors, or insert targeting ligands. The use of bi-specific molecule has been successful in not only de-

targeting the native tropism of adenovirus *in vivo* but also re-targeting the vector to tumor cell surface antigens [75]. We and others have obtained promising results by applying advanced polymer technologies to coat the virus to blunt its immunogenicity as well as to enhance cell-targeted entry [76]. The use of transient immunosuppression regimen has established traction in overcoming the immunogenicity issues of Ad gene therapy to facilitate long term administration [31]. In a very recent study, Bhang and colleagues demonstrated that a non-viral cationic polymer vector can achieve efficient gene delivery and imaging to detect systemic metastasis in melanoma and breast cancer models [59]. Their results also reaffirm the great specificity of transcription-based molecular imaging.

In summary, we report here the development of PSES-TSTA as an androgen-independent and prostate cancer-specific gene expression system. The transcriptional amplification strategy undertaken boosted the expression of both a bioluminescent reporter gene and a PET reporter gene, to achieve sensitive and prostate cancer specific molecular imaging in pre-clinical models of CRPC. The potency, cell-selectivity and diagnostic potential of PSES-TSTA vectors was illustrated by the ability of a PSES-TSTA imaging vector to detect early CRPC bone marrow metastases following systemic vector administration. The PSES-TSTA vectors can be modified to simultaneously express imaging reporter genes and cytotoxic therapeutic genes. Hence, the implementation of multipronged therapeutic strategy such as combined ADT with image-guided gene therapy to treat advanced and even metastatic CRPC may be feasible, using the PSES-TSTA system described in this study.

III. TRANSLATIONAL APPLICATION OF GENE-BASED IMAGING VECTORS

Application of Prostate Cancer-Specific Reporters in Monitoring Androgen Receptor Blockade Therapy and Detecting Circulating Tumor Cells

Abstract

In this chapter, we explored the applicability of transcription-based imaging reporters in monitoring the efficacy of androgen deprivation and androgen receptor blockade therapies, as well as functionally detecting and enumerating circulating tumor cells. Specifically, a variety of prostate cancer-selective promoters, including the prostate specific antigen (PSA) promoter, the prostate specific membrane antigen gene enhancer (PSME) and the prostate specific enhancing sequence (PSES), was employed to regulate reporter expression in these vectors. PSA- and PSME-driven reporters exhibited opposing responses towards androgen deprivation and androgen receptor blockade, underlying our rationale to utilize these reporters simultaneously to interrogate the activation/inhibition status of androgen receptor signaling axis during anti-androgen treatments. On the other hand, in order to differentiate circulating tumor cells from other cellular components in the blood, as well as to assess their origin from prostate and their viability, we adopted a PSES-directed reporter to identify transcriptionally active prostate cancer cells in combination with fluorescent microscopy based on a microfluidic capturing platform.

INTRODUCTION

Androgen deprivation therapy (ADT) that inhibits androgen biosynthetic pathways and androgen receptor blockade therapy (ARBT) that antagonizes the function of the nuclear steroid receptor of androgen (AR) remain the first line of treatments for advanced prostate cancer. Unfortunately, the majority of patients who receive such treatment will develop castration resistant prostate cancer (CRPC) marked by rising serum prostate specific antigen (PSA) and ~85% of these patients will eventually develop distant metastasis, most of times in the skeletal bone, which severely impairs their quality of life and worsens the survival [2, 4].

Ample evidence has pointed out that even at the CRPC stage, prostate cancer cells still rely on androgen and the AR signaling axis for proliferation and survival [7-8, 10]. Numerous mechanisms, such as AR amplification, mutation or intragenic rearrangement, upregulation of co-activators, ligand independent activation of AR, as well as emergence of hyper-active AR splicing variants [3, 6, 19], have been proposed to explain how CRPC circumvents the shortage of circulating testosterone and thrives. Hence, the development of novel generations of AR antagonists (e.g. MDV3100) and androgen synthesis inhibitors (such as abiraterone acetate) has been intensely pursued [2-3, 6]. Given the promising efficacy of these new reagents, a practical and reliable reporting system that reflects the functional status of the AR axis will be valuable. Such a system will enable the real-time assessment of the efficacy of ADT/ARBT at the molecular level, in living subjects.

Previously, we reported the utilization of a series of gene-based molecular imaging vectors to selectively visualize CRPC in mice that were surgically castrated [77]. These vectors employed a chimeric androgen independent prostate specific promoter, PSES (prostate specific enhancing

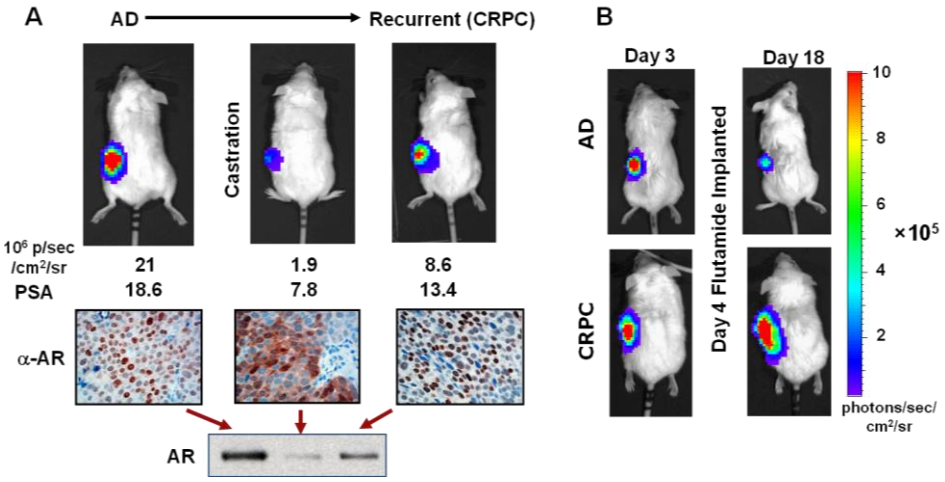

Figure 3.1. PSA-driven reporters faithfully monitor activation of the AR axis. A. The PSA-reporter monitored the progression of prostate cancer into castration resistant stage. S.c. LAPC-9 prostate cancer xenograft was established in intact male SCID mice and 1×10^7 PFU adenoviral vector carrying PSA-driven FL was injected intratumorally when tumor was palpable. Bioluminescent imaging was performed 3 days later and animals were castrated and followed up by imaging at 4 and 10 days post castration. Maximum luminescent intensity and corresponding serum level of PSA were indicated; AR cellular/nuclear localization and AR protein level were also shown. B. PSA-reporters can differentiate hormone sensitive versus castration resistant prostate cancer. SCID mice bearing either androgen dependent (AD) or castration resistant (CRPC) s.c. LAPC-9 tumors were injected with the PSA-driven FL-expressing adenoviral vector and imaged 3 days later. Then animals received s.c. implantation of flutamide on day 4 and were imaged on day 18. [Figure modified from Zhang *et al*, Cancer Res. 2003]

sequence), to direct the expression of imaging reporter genes firefly luciferase (FL) and the mutant form of herpes simplex virus-thymidine kinase (HSV1-sr39tk) for bioluminescent imaging and positron emission tomography (Fig. 2.1-2.5). The unique androgen independency of PSES is attributed to its composition of transcriptional elements derived from both the androgen inducible PSA promoter and the androgen suppressible PSME enhancer [22]. Specifically, the

PSA promoter represents those prostate-specific promoters that are activated by androgen-liganded AR. As shown in Fig. 3.1, PSA-driven imaging reporters enabled faithful monitoring of the efficacy of ADT and ARBT in treatment-responsive tumors, as well as the progression of androgen dependent prostate cancer to the CRPC phenotype [62]. PSME, on the other hand, was isolated from the enhancer region of the prostate specific membrane antigen (PSMA) gene, which is well documented in the literature to be negatively regulated by androgen [42]; its expression increases as prostate cancer progresses to the more malignant and castration resistant stage [44, 78-84].

In this study, we separated the two components of PSES by molecular cloning and constructed a dual-imaging reporter system that can be adopted to examine the activation status of androgen/AR axis. The dual-reporter system contains expression cassettes of both PSA-regulated FL and PSME-driven Renilla luciferase (RL); and both lentiviral and adenoviral vectors were established. In particular, the two-step transcriptional amplification (TSTA) system was incorporated into the adenoviral vectors to generate Ad-PSA-TSTA-FL and Ad-PSME-TSTA-RL; but, due to the size restriction in the lentiviral genome, only direct PSA-FL and PSME-RL expression cassettes were cloned in lenti vectors, without the TSTA system. We here explored the implementation of the dual-reporter system in ADT/ARBT regimens and demonstrated that, during an effective anti-androgen treatment, PSA-directed reporters are silenced while PSME-regulated vectors are activated (Fig. 1.2). Of note, the simultaneous up- and down- regulations of reporter expression in this system are more advantageous than using only one reporter for several reasons: (1) if only PSA reporters were used, an efficacious therapy would be indicated by a negative change in the imaging signal, which could also be the outcome of an unsuccessful imaging procedure. (2) Simple reduction of the tumor mass could result in a down-regulation of

PSA-directed signal, hence deceptively reporting the efficacy of an anti-androgen treatment; the utilization of dual reporters permits a more definite interrogation of the direct target of ADT and ARBT – the AR signaling axis. (3) The two reporters in this dual system could serve as each other's transduction control. The implementation of this dual imaging system has significant impact for two reasons: first, it could serve as a practical and biologically relevant drug screening platform for novel anti-androgen compounds. Second, it can be applied to biopsy samples or circulating tumor cells isolated from a patient in combination with *ex vivo* treatments; the readout from this system could provide insights regarding if a specific therapeutic regimen will be effective for that individual patient – embodying the concept of personalized medicine.

In the second section of this chapter, we further expanded the application of gene-based reporters and explored the utilization of Ad-PSES-TSTA-IFP, an adenoviral vector that carries the infra-red fluorescent protein (IFP) under the regulation of the androgen independent PSES promoter, to detect circulating tumor cells (CTCs) from prostate cancer patient blood. The enumeration and characterization of CTCs have recently emerged as potential independent prognostic parameters for many types of cancers, including melanoma, colorectal, breast, prostate and non-small cell lung cancer [85-90]. In prostate cancer, specifically, an increase in CTC number after treatment coincides with biochemical recurrence marked by a rising level of serum PSA (personal communication with Dr. Hsian-Rong Tseng). Moreover, CTCs can reflect a patient's response to therapy in that CTCs from docetaxel-resistant patients did not manifest any changes in microtubule bundling after *in vitro* on-chip drug treatment [88]. Therefore, there has been a growing interest in pursuing strategies that can identify and count CTCs in an accurate and time-efficient manner.

In our experiment, blood samples are obtained when prostate cancer patients come in for follow-up visits and cells are isolated by disrupting red blood cells and subsequent centrifugation (conducted in Tseng's laboratory). The cells are then infected by Ad-PSES-TSTA-IFP and 48 hrs later, subjected to a silicon nanowire microfluidic chip, which enables highly efficient cell capturing (performed by collaborator Mitch Garcia). Then, blood cells are identified by positive FITC-conjugated anti-CD45 staining (performed by Mitch Garcia) whereas viable circulating prostate cancer cells are identified by IFP expression visualized in the Cy5 channel. This method of CTC detection is advantageous over conventional approaches that are largely mediated by EpCAM antibody staining [91] because the incorporation of the PSES-driven IFP expression allows us not only to distinguish cells that are functionally active (hence viable and potentially metastatic), but also to examine the transcriptional profile of target cells. Contaminating epithelial cells that usually constitute false positive in EpCAM staining will appear negative in this procedure due to the lack of an androgen/AR signature that is uniquely present in cells of the prostate origin. Cancer cells that undergo epithelial-to-mesenchymal transition (and therefore lose the expression of epithelial marker EpCAM) usually constitute false negative in EpCAM based detections; but in this PSES-TSTA based approach, they will demonstrate positive IFP expression due to their prostate-specific transcriptional activity. Moreover, since PSES possesses constitutive yet prostate-specific transactivity, the cancer cells will be detected regardless of the patient's anti-androgen treatment status.

MATERIALS AND METHODS

Cell culture experiments. LNCaP, C4-2 and CWR22Rv1 cells were obtained from ATCC and cultured in RPMI medium containing 10% normal or charcoal-stripped fetal bovine serum and 1% penicillin/streptomycin. R1881 was used at final concentration of 10 nM, Casodex and MDV3100 at 10 μM or as specifically indicated. For transfection experiment, cells were seeded and transfected by Lipofectamine 2000 as instructed by the manual. Lentiviral infection (pCCL backbone) was performed 24 hours after the cells were seeded at multiplicity of infection (MOI) of 1-2 in the presence of 8 μg/mL polybrene. Medium was changed after 6-8 hrs. For adenoviral infection, cells were also seeded 24 hrs prior and adenovirus (serotype 5) was added into medium at indicated MOI. Luciferase activity was assayed 48-72 hrs post infection according to the manufacturer's instructions (Promega, Madison, WI) using a luminometer (Berthold Detection Systems, Pforzheim, Germany).

Endogenous PSMA expression. LNCaP and C4-2 cells were stably transfected with a scrambled sequence or a short-hairpin that inhibits the expression of androgen receptor. The expression of the short-hairpin is controlled by doxycycline-responsive elements. The cells were cultured in RPMI medium containing 10% fetal bovine serum, 1% penicillin/streptomycin, 1 μg/mL puromycin and 1.25 μg/mL Blasticidine to maintain the stable transfection. To induce AR knockdown, 1 μg/mL doxycycline was added to the culture medium. Total RNA was isolated using TRIzol reagent (Life Technologies Coorporation) according to manufacturer's instruction. cDNA was synthesized using the iScript cDNA Synthesis Kit (Bio-Rad). PSMA expression was determined by quantitative real-time PCR (forward primer: GTGGCATG CCCAGGATAAGCAAAT; reverse primer: TATACCGTGCTCTGCCTGAAGCAA;

ValueGene, San Diego, CA)

C4-2 and blood cells co-infection experiment. White blood cells were obtained from a healthy donor and isolated by centrifugation after lysing red blood cells. 2.5×10^4 white blood cells and the same amount of C4-2 prostate cancer cells were mixed and seeded in a well of a 24-well plate. 24 hrs later, Ad-PSES-TSTA-IFP virus was used to infect the cells at MOI of 10. 3 days later, the cells were examined by fluorescent microscopy following 1 hr of incubation with IFP substrate biliverdin (Toronto Research Chemicals Inc. North York, ON, Canada; 1:500) and anti-CD45 staining.

Circulating tumor cell detection experiment. Blood sample was obtained from a metastatic prostate cancer patient (approved protocol under Hsian-Rong Tseng) and then subjected to red blood cell lysis and centrifugation. The sample was then split into two aliquots. The first portion was infected by Ad-PSES-TSTA-IFP at MOI of 10 in suspension culture, and 48 hours later, subjected to microfluidic chip capturing and IFP fluorescent microscopy. The second aliquot was immediately subjected to microfluidic chip capturing and anti-cytokeratin antibody staining. DAPI staining was applied to both aliquots at the end of the procedure.

RESULTS

PSA-directed reporters are silenced by androgen antagonists

We sought to thoroughly evaluate the responsiveness of PSA-driven reporters to anti-androgen treatments. We infected androgen sensitive prostate cancer cell line LNCaP with Ad-PSA-TSTA-FL vector and then incubated them with an escalating dose of androgen antagonists (both

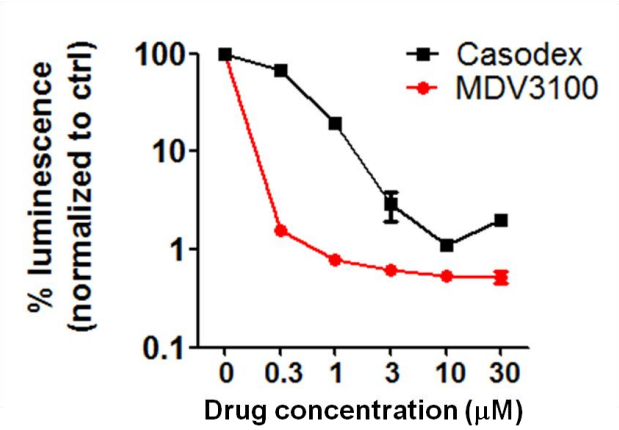

***Figure 3.2. PSA-driven reporter monitors efficacy of androgen blockade therapy*.** LNCaP cells were infected with Ad-PSA-TSTA-FL vector at multiplicity of infection (MOI) of 1 and at the same time treated with indicated doses of androgen receptor antagonist Casodex or the more potent compound MDV3100. FL expression was tested 72 hrs post treatment by *in vitro* luciferase assay, and then normalized to corresponding control condition (zero drug concentration as 100%).

the first generation compound Casodex and the second generation, more potent drug MDV3100). Consistent with previous results [62], *in vitro* luciferase assay revealed that the PSA reporter was silenced by these reagents. More importantly, this response was highly sensitive to the dose and potency of the anti-androgen. Casodex induced a dose dependent suppression of PSA promoter activity, with the maximum inhibition occurred at 10 μM. At 30 μM, however, FL expression was increased by Casodex, echoing the well-documented partial agonist activity of this drug at higher concentration [3]. In contrast, the more potent second-generation molecule MDV3100 exhibited strong inhibition on PSA-regulated FL expression even at the lowest dose tested. So, PSA-driven reporters can monitor the effects of anti-androgen treatments in a very faithful and sensitive manner.

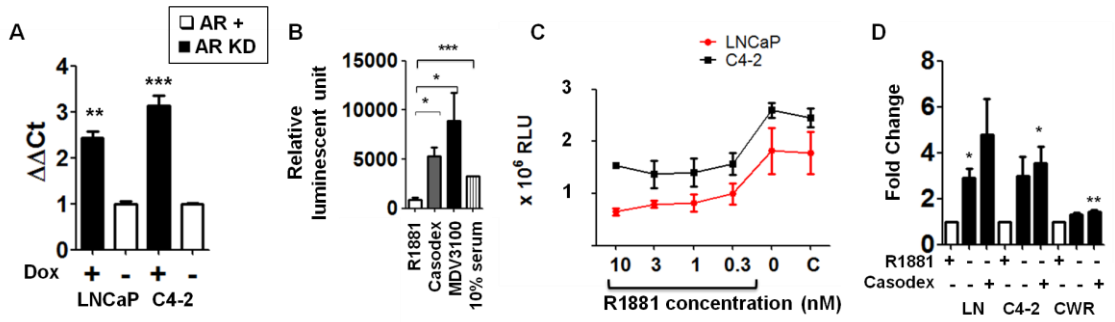

Figure 3.3. PSME-driven reporters are activated by androgen deprivation and AR blockade treatments. A. LNCaP and C4-2 cells were stably transfected with doxycycline (Dox)-turned-on anti-AR short hairpin. These cells were then incubated with diluent or 1μg/mL Dox and with 10 nM R1881 for 72 hours. Total mRNA was then isolated and cDNA synthesized. Quantitative real-time PCR was performed to measure the endogenous expression level of PSMA gene using PSMA-specific primers. Data are then normalized to β-actin level and then normalized to corresponding AR + condition. B. LNCaP cells were cultured in medium containing 10% FBS and then transfected with PSME-RL plasmid using Lipofectamine according to manufacturer's protocol. Cells were then treated with 10 nM R1881, 10 μM Casodex or 10 μM MDV3100. Luciferase activity was measured 48 hours later. C. LNCaP and C4-2 cells were cultured in media containing 10% FBS. The cells were then infected by lenti-PSME-RL at MOI of 1 and treated by indicated concentration of R1881 or 10 μM Casodex (C). RL activity was measured 48 hours later. D. LNCaP (LN), C4-2 and CWR22Rv1 (CWR) cells were infected by Ad-PSME-TSTA-RL at MOI of 1-2 and then cultured in media containing 10% charcoal-stripped serum (hormone free) plus indicated drugs. R1881 was used at 10 nM and Casodex 10 μM. RL activity was measured 48 hours post treatment and normalized to corresponding R1881 condition. Shown are means from 3 independent trials. For all experiments, *, P<0.05; **, P<0.01 and ***, P<0.001.Two-tailed paired *t* test was used for D and unpaired *t* test used for other panels.

PSME-directed reporter expression is suppressed by androgen-liganded AR

First, we asked if the expression of PSMA gene is indeed negatively regulated by the activation

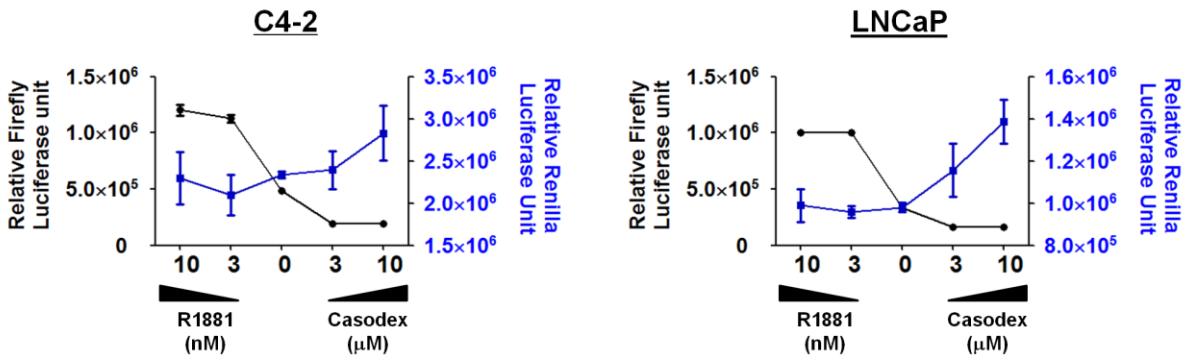

Figure 3.4. The dual-reporter system exhibited simultaneous up- and down-regulation of reporter expression during androgen receptor blockade conditions. C4-2 and LNCaP cells were co-infected with Lenti-PSA-FL and Lenti-PSME-RL. The cells were then treated with indicated dose of synthetic androgen, R1881, or anti-androgen, Casodex, for 48 hours and FL (left axis, black) and RL (right axis, blue) activities were determined *in vitro* using respective substrates.

of the androgen/AR signaling axis. We examined PSMA mRNA level in androgen-treated control or AR-knockdown LNCaP and C4-2 cells. As shown in Fig. 3.3.A, in both cell lines, the knockdown of AR protein expression by short hairpin RNA significantly increased endogenous PSMA gene expression, indicating that PSMA is truly an androgen-suppressible gene. These results also suggested that PSME-driven RL reporters should be turned on by ADT and ARBT treatments.

We then transfected LNCaP cells with a plasmid DNA that expressed RL under the direct regulation of the PSME enhancer. As shown in Fig. 3.3.B, compared to the no treatment, normal serum containing-medium control, the addition of synthetic androgen R1881 significantly reduced RL expression whereas androgen antagonists Casodex and MDV3100 increased RL level in a drug potency-dependent manner. Similarly, when we infected LNCaP and C4-2 cells with lenti-PSME-RL vector followed by treatment with Casodex or an escalating dose of

synthetic androgen R1881, we observed a suppression of RL expression with androgen (Fig. 3.3.C). Consistently, when Ad-PSME-TSTA-RL vector was employed to infect LNCaP and C4-2 cells, RL expression was markedly heightened in androgen free conditions and in the presence of Casodex (Fig. 3.3.D). Interestingly, when CWR22Rv1 (an androgen insensitive CRPC cell line) was used to conduct this experiment, we observed a similar trend of regulation but the magnitude of PSME-RL activation by anti-androgen was drastically lower than that in androgen responsive LNCaP and C4-2 cells (Fig. 3.3.D). These data support the note that PSME activity is inhibited by androgen-liganded AR and thus PSME-driven reporters are activated by ADT and ARBT. Further, the magnitude of the change in PSME signal might indicate the androgen responsiveness of the cells being tested. Therefore, while PSA-regulated reporters are silenced by anti-androgen drugs, PSME reporters can provide a positively changing readout during effective androgen deprivation and AR blockade.

Furthermore, when we applied the dual-reporter system on prostate cancer cells by double-infecting LNCaP and C4-2 cells with Lenti-PSA-FL and Lenti-PSME-RL, we found that in the presence of escalating doses of synthetic androgen and anti-androgen, the dual reporter system exhibited concomitant up- and down- regulation pattern (the X-shaped plot as shown in Fig. 3.4), confirming the regulation mechanism of the dual reporter and substantiating the applicability of this system in interrogating AR activity. However, it is noteworthy that the difference in responsiveness of PSME reporter towards the androgen dose escalation was not as pronounced as that of the PSA reporter against androgen antagonists (note the different scales of the two Y axes in Fig. 3.4). This could be attributed to the indirect nature of AR's regulation on PSME transcriptional activity ([44, 92]; unpublished data; personal communication with Dr. Pikarsky from Rambam Health Care Campus in Israel). Nonetheless, we here showed the proof-of-

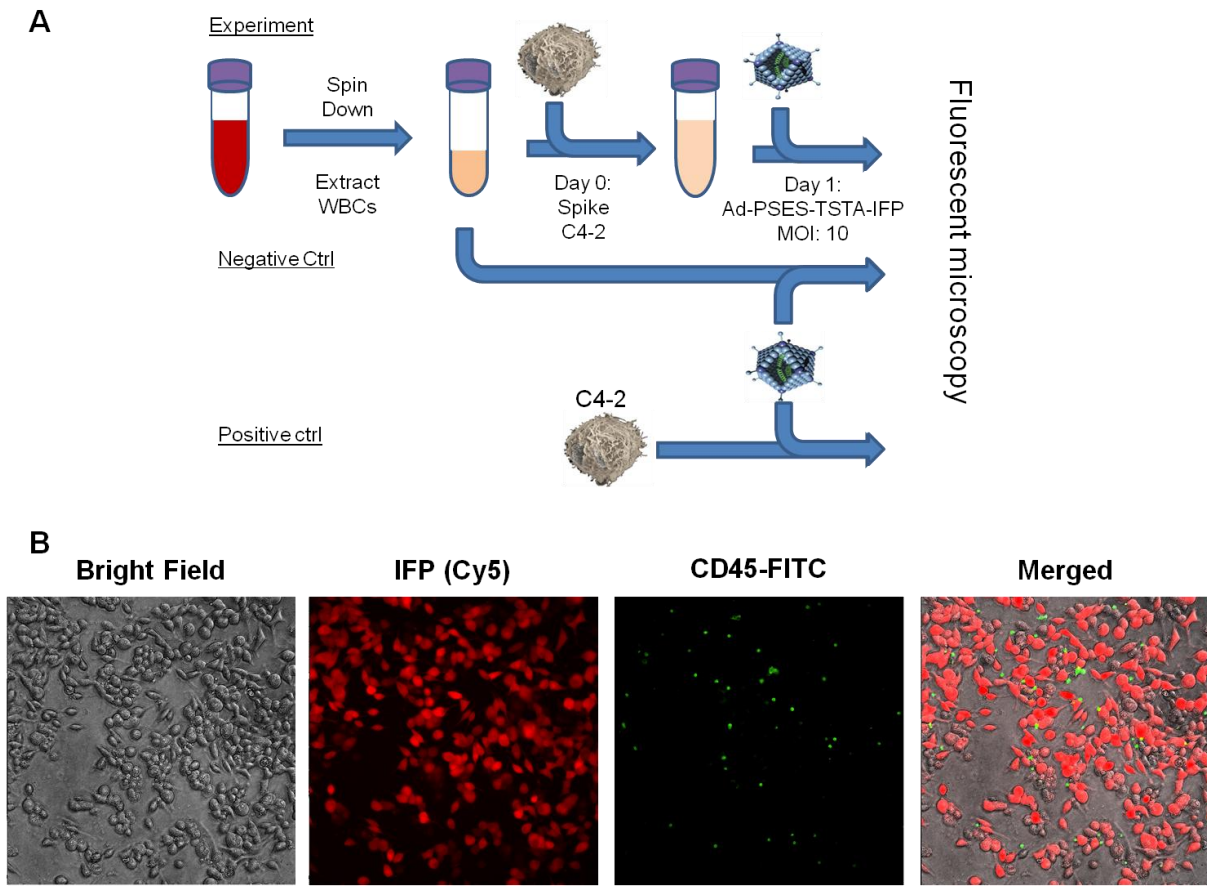

Figure 3.5. PSES-TSTA-IFP vector can differentiate prostate cancer cells from white blood cells. A. Experimental design. Blood of a healthy donor was obtained and centrifuged after bursting red blood cells to isolate white blood cells (WBC). C4-2 cells were mixed with white blood cells at a 1:1 ratio and seeded into a 24-well plate. 24 hours later, the cells were infected by Ad-PSES-TSTA-IFP at MOI of 10. 3 days later, cells were incubated with IFP substrate, biliverdin, for 1 hour at 37 ℃ and stained for CD45 (green) and then subjected to fluorescent microscopy. Positive control contained C4-2 cells only and negative control contained white blood cells only (data not shown). B. Representative images of the experiment group in indicated channels. Red: IFP expression; green: CD45 staining. Magnification: 200 ×.

principle that the PSA- and PSME-driven reporters in the dual imaging system can provide a simultaneous up- and down-regulation of signals, thus offering a more definite interpretation of

the androgen/AR signaling activity compared to a unidirectional readout.

PSES-TSTA-IFP vector directs detection of circulating tumor cells

Before evaluating the applicability of Ad-PSES-TSTA-IFP to identify CTCs in patient blood samples, a pilot trial was performed to search for the optimal experimental conditions, whereby a healthy donor's white blood cells were mixed with C4-2 cancer cells. As laid out in Fig. 3.5.A, C4-2 cells were spiked in a 1:1 ratio with white blood cells and then infected with Ad-PSES-TSTA-IFP vector at MOI of 10. Positive and negative controls were also established with C4-2 cells and white blood cells alone, respectively. The C4-2 cells were anticipated to support IFP expression due to their prostate origin whereas white blood cells should appear negative despite viral infection.

Indeed, as shown in Fig. 3.5.B, while the majority of C4-2 cells demonstrated IFP positivity, no white blood cells (stained by FITC-conjugated anti-CD45 antibody by collaborator Mitch Garcia in Hsian-Rong Tseng's laboratory) exhibited leaky expression of this reporter. These results proved the feasibility to differentiate prostate cancer cells versus white blood cells based on their expression of PSES-TSTA-driven IFP under these experimental conditions. Of note, the apparently higher number of C4-2 cells compared to blood cells is speculated as a result from the continuous proliferation of cancer cells in culture. The number of CTCs in real patient samples, however, is more likely to be lower than white blood cells, raising the possibility of a less efficient viral infection. Toward this end, experiments with a cancer-to-white blood cells ratio of

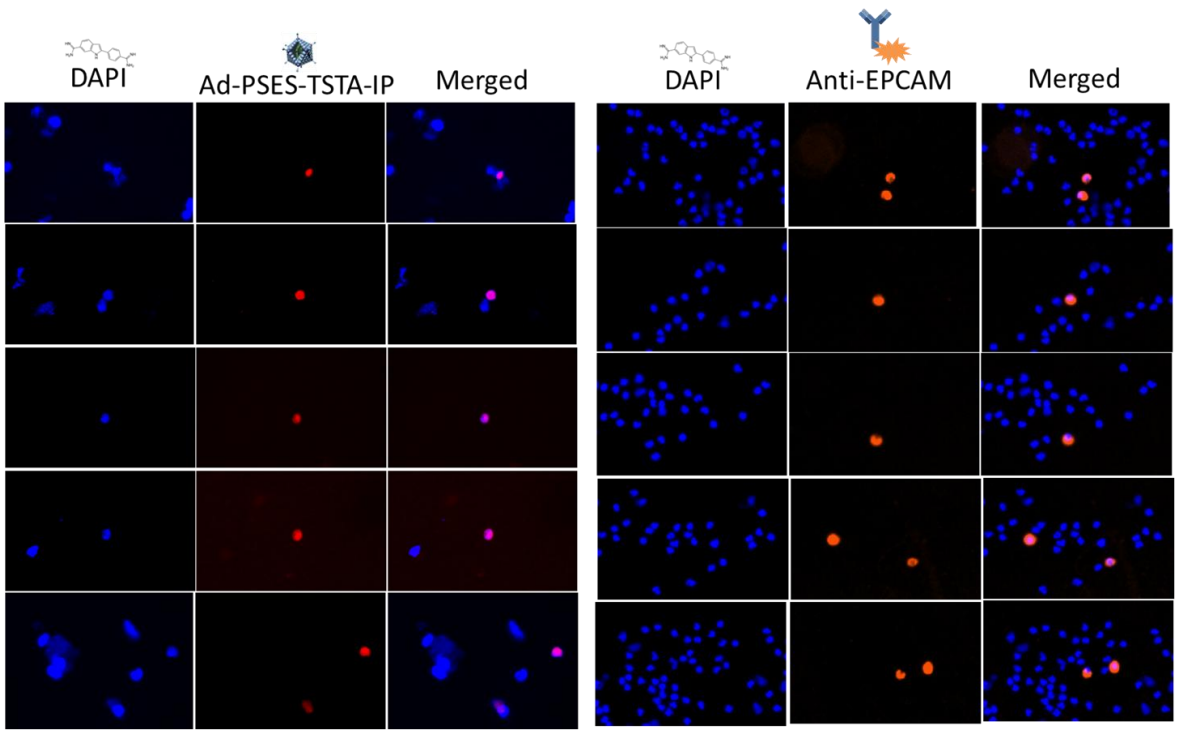

Figure 3.6. Ad-PSES-TSTA-IFP exhibited similar, if not higher, CTC detection capability as compared to the EpCAM-based method. Blood sample from a metastatic prostate cancer patient was subjected to red blood cell lysis and centrifugation, and was then either infected by Ad-PSES-TSTA-IFP at MOI of 10 or kept untreated. 48 hours later, due to biosafety concerns, residual virus from the first sample was removed by centrifugation and then both samples were subjected to microfluidic chip capturing and fluorescent microscopy. Virus infected cells were examined for IFP expression (left panels) while the untreated sample was stained for EpCAM (right panels). DAPI was applied to both samples at the end of the procedure. Shown are DAPI, IFP or EpCAM, and overlap images of selected representative CTC-containing fields.

1:100 were conducted; but at this condition, massive killing of cancer cells was observed due to histoincompatibility (data not shown).

Further, Tseng and Garcia obtained blood sample from a metastatic prostate cancer patient. After

red blood cells lysis and processing performed in their laboratory, the cells were split into two samples – one infected with Ad-PSES-TSTA-IFP for 48 hours and the other subjected to epithelial marker-based detection immediately. Both samples were applied to microfluidic chips (also coated with EpCAM antibody to enrich CTCs) and subsequent fluorescent microscopy. The virus infected sample was examined for IFP expression while the other sample was stained for cytokeratin expression. Both samples were stained with DAPI to mark nucleus. As shown in Fig. 3.6, the virus-based approach demonstrated similar, if not higher, CTC detection rate as compared to the cytokeratin staining procedure, verifying the viability of gene-based imaging vectors in facilitating the detection and functional evaluation of prostate cancer CTCs.

DISCUSSION

In this chapter, we investigated the application of gene-based prostate cancer-specific reporters in interrogating the activation status of androgen/AR signaling as well as detecting circulating tumor cells. Even though the data presented in these exploratory experiments are mainly preliminary, we see great promise in the utilization of these vectors.

The dual AR reporting system consisting of both the PSA- and the PSME-driven vectors holds unique practical potential in this era when numerous anti-androgen reagents are rapidly being developed. Superior to a unidirectional single vector, the simultaneous up- and down-regulation of PSME and PSA reporters offers an all-around examination of AR activity, minimizing possible confounding effects such as failed imaging sessions or a simple reduction of tumor mass. This system is readily translatable to animal xenograft models and syngeneic cancer models to screen for more potent and more effective androgen antagonists and androgen synthesis

inhibitors. It could also serve as an apt readout for therapeutic regiments that exploit the combinational usage of multiple drugs that hit different steps of the androgen/AR signaling cascade. Furthermore, in addition to aiding drug development, this dual system can be widely used in a number of clinically relevant scenarios to facilitate individual decision making and improve patient management in the implementation of personalized medicine. For example, cells from patient biopsy samples can be dissociated and transiently cultured *in vitro* to be transduced with this dual reporter system. Candidate treatment plans can then be tested on these cells before implementing in the patient to predict which plans are most likely to be efficacious. Similarly, this system can be applied to the samples from a panel of patients and predict who would be the best responder to a particular therapeutic strategy.

Importantly, several recent studies have reported the use of radioactively labeled PSA and PSMA antibodies as PET imaging reagents to measure androgen receptor signaling [93-95]. However, all these studies only presented a disappointingly small power to distinguish AR activation and inhibition. For instance, the free PSA-targeting radiotracer used by Ulmert *et al* only demonstrated a 15-fold decrease during MDV3100 treatment as compared to the testosterone condition [95]; the PSMA antibody-based probe used by Evans *et al* only manifested a 1.5-fold increase in MDV3100 treated LNCaP xenograft-bearing mice, and showed no response in mice that are surgically castrated compared to the control cohort [93]. We here exploited reporter systems that are transcription-based, and thus much more sensitive than antibody-based approaches. Since the PSA promoter is a direct AR target and thus more sensitive to AR regulation, we could readily achieve over 100-fold difference *in vitro* (Fig. 3.2) and over 10-fold difference *in vivo* (Fig. 3.1) when AR signaling was abrogated. Even the PSME-driven reporter, which is not a direct AR target, demonstrated a consistent 4 to 6-fold increase during

ADT/ARBT (Fig. 3.3). These results implicated that transcription- and gene-mediated imaging vectors present a more sensitive and hence reproducible readout for AR inhibition; they are therefore superior to antibody-based tracers and more suitable for this molecular imaging purpose. Even though translating viral-based imaging vectors into clinics may face a tremendous amount of difficulties considering the biodistribution issue and virus-induced host immune reactions (as will be discussed in Chapter IV), the dual-imaging reporter system is highly amenable for *ex vivo* applications. It can be used to transduce cancer cells that are collected from biopsy samples or circulating tumor cells and provide an expedient readout of drug efficacy after a short-term *ex vivo* anti-androgen treatment. This will help circumvent the time-consuming and expensive *in vivo* PET imaging procedures, and thus is more convenient and economical compared to antibody-based PET probes. Furthermore, the Firefly and Renilla luciferase genes in this system can be readily replaced by PET or SPECT imaging reporters, enabling the *in vivo* application of this dual-reporter system.

One very intriguing question regarding the dual reporting system is the molecular mechanism underlying the transcriptional control of the PSME promoter. Despite the presence of a half consensus ARE site in this element, recent discoveries from several groups around the globe using microarray analysis and deep sequencing to study the transcriptional signature of AR and its cofactors seem to point out that there is unlikely a direct interaction of AR with this segment of DNA [92]. Hence, the suppressed activity of PSME in the presence of androgen-liganded AR might be a secondary effect of AR signaling; and this may explain why the PSME-reporter was only marginally activated during ADT/ARBT whereas a PSA (a known AR binding target)-directed reporter was very sensitive to AR inhibition. The detailed molecular regulation from PSME warrants further investigation.

Another exploration on the applicability of gene-based reporters is to use Ad-PSES-TSTA-IFP to detect circulating tumor cells. The prognostic value of CTCs has been increasingly acknowledged in the field of cancer research [96-97]. Conventional methods of capturing CTCs mostly rely on the expression and recognition of surface epithelial markers on these cells; but unfortunately, the false negative rate is high due to the loss of epithelial markers in cells that undergo epithelial-to-mesenchymal transition [96]. Recently, Miyamoto *et al* employed antibodies against PSA and the extracellular domain of PSMA to visualize circulating prostate cancer cells [97]. Moreover, these authors found a correlation between the expression level of PSA and PSMA on patients' CTCs and their responsiveness to respective ongoing anti-androgen therapies; therefore, they were able to stratify patients according their CTC phenotypes and predict therapeutic outcome. The idea implemented in that study was highly valuable and more advanced than other detective means that are solely reliant on surface expression of epithelial markers. However, antibodies-mediated identification inevitably suffers from high background noise and the necessity of long, finicky staining procedures. The present study is advantageous in that we exploit prostate cancer specific promoters to drive restricted reporter expression only in viable and functionally active cancer cells. The usage of microfluidic chips provides additional benefits to CTC capturing owing to the unique surface characteristics of nanostructures; therefore, the specificity of the microfluidic chip-based, transcription-mediated CTC detection system is superior.

In summary, by investigating gene-based cancer specific reporters in two pre-clinical applications, we demonstrated in this chapter that 1) the PSA and PSME dual promoter-driven reporter system is very suitable to functionally interrogate the activation/inhibition status of the AR signaling axis in prostate cancer cells during ADT and ARBT; 2) Ad-PSES-TSTA-IFP holds

great potentials in selectively detecting and functionally evaluating circulating tumor cells in prostate cancer patients. The ongoing work and future directions include performing downstream experiments to elucidate the molecular mechanism underlying the transcriptional control over the PSME promoter to further substantiate the applicability of the dual-reporter system. Moreover, we are actively collaborating with Hsian-Rong Tseng's group in the biomedical engineering department to establish a reproducible CTC detection protocol and evaluate its accuracy in patient samples.

IV. VIRAL VECTOR ADMINISTRATION IN IMMUNOCOMPETENT HOSTS

IV-I. Rapamycin Enhances Adenovirus-mediated Cancer Imaging in Pre-Immunized Hosts

Abstract

Tumor-specific adenoviral vectors comprise a fruitful gene-based diagnostic imaging research area for advanced stage of cancer, including metastatic disease. However, clinical translation of viral vectors has encountered considerable obstacles, largely due to host immune responses against the adenovirus. Here, we explored the utilization of the immunosuppressant rapamycin to circumvent host immunity in immunocompetent murine prostate cancer models. Rapamycin diminished viral-induced acute immune response by inhibiting NF-κB activation; it also reduced the scale and delayed the onset of inflammatory cytokine secretion. We also found that rapamycin prolonged and enhanced adenovirus-delivered transgene expression *in vivo*, and thus augmented the imaging capability of adenoviral vectors using both bioluminescent and positron emission tomography modalities. Furthermore, rapamycin significantly abrogated anti-adenovirus antibody production and strongly retarded the function of myeloid cells and lymphocytes activated upon viral administration in pre-immunized hosts. Overall, transient immunosuppression by rapamycin was able to boost the diagnostic utility of adenoviral vector-mediated cancer imaging.

INTRODUCTION

Adenoviral vectors (Ads) are widely used as *in vivo* gene-delivery agents in preclinical and clinical settings, for both cancer diagnostic and therapeutic purposes [63, 98]. Recently, our group has demonstrated Ad's ability to sensitively detect cancer metastasis following lymphatic-directed or systemic viral administration [63, 77]. Despite these encouraging results in animal models, several hurdles need to be overcome before the implementation of Ads in clinical applications; the most formidable obstacle being the host immune responses against Ad (reviewed by [99]). Previous studies with rodents and non-human primates have shown that systemically injected Ad (serotype 5) predominantly localized to the liver and infected Kupffer cells, endothelial cells and hepatocytes [25-27]. Ad infection of these cells and splenic dendritic cells (DCs) initiates an avalanche of inflammatory cytokines and chemokines characterized by early induction of interleukin (IL)-1 and tumor necrosis factor (TNF)-α [28-29], followed by IL-2, IL-6, macrophage inflammatory protein-2 (IL-8), regulated and normal T cell expressed and secreted (RANTES), IL-12 and interferon (IFN)-γ [100-105]. These factors in turn recruit and activate effector cells including neutrophils, monocytes, polymorphonucleocytes and $V_{\alpha}14$ invariant natural killer (NK) cells, which can lead to tissue (mainly hepatic) damages, aseptic shock and even death [106-108].

While Ad casts inflammatory insults against hosts by triggering innate immune system [25, 27, 109], the adaptive immune system also posts strong clearance for virally transduced cells, impairing the effectiveness and applicability of Ad-based therapeutic approaches [31, 108, 110]. Furthermore, the majority of human population possesses anti-Ad antibodies due to natural exposure to this pathogen; consequently, repeated administration of Ad vectors would prime the

expansion of Ad-specific plasma cells, leading to vigorous secondary antibody secretion and subsequent viral clearance, reducing vector bioavailability and potentiating host toxicity [31, 102]. In addition, transgene-expressing cells will encounter cell-mediated immune clearance [111-113]. Notably, such elimination is not limited to Ad directed immunity but can be also associated with the introduced foreign transgene, if the gene product is immunogenic [109]. Since most imaging and therapeutic genes are exogenous to the host, this immunogenicity issue constitutes a significant challenge for achieving successful outcome of Ad-based gene therapy.

In this study, we adopted an FDA-approved immunosuppressant, rapamycin (RAPA), to assess the value of transient immunosuppression in reconciling these conflicts between Ad and the host immune system. RAPA binds to FKBP12 (FK binding protein 12) and inhibits the activity of mTOR kinase complex 1; an enzyme complex vital to a wide range of cellular functions required for rapidly proliferating cells [114-115]. RAPA hampers cell cycle progression (G1/S), proliferation, activation and differentiation of T and B lymphocytes elicited in response to a variety of stimulants as well as the response of DCs and other innate immune cells to inflammatory cues [116-119]. Furthermore, RAPA exhibits appreciable anti-angiogenesis and anti-cancer properties [31, 120]. In this study, we report that rapamycin successfully diminished Ad-associated innate and adaptive immune responses in immunocompetent hosts in two pre-immunized mouse models. The strategy taken here could serve as a platform to improve the safety profile, transgene expression and therapeutic efficacy of Ad mediated gene therapy.

MATERIALS AND METHODS

Cell culture and drugs. Murine prostate cancer cell lines RM-9 (kind gift from Dr. Timothy C.

Thompson, Baylor College of Medicine) and MycCaP (kind gift from Dr. Charles Sawyers, Memorial Sloan Kettering Cancer Center) were cultured in DMEM medium containing 10% fetal bovine serum and 1% penicillin/streptomycin. i.p. dose of rapamycin (LC Laboratories, Woburn, MA) was dissolved in sterile DMSO and used at indicated concentrations. Orally applied Rapamune was purchased from Wyeth Pharmaceuticals Inc, Philadelphia, PA.

Innate immune response experiments. All animal experiments were performed in accordance with the University of California Animal Research Committee guidelines. 4-5-week-old BALB/c mice (Taconic Farms, Germantown, NY) were given daily oral treatment of Rapamune (30 mg/kg; Wyeth, Madison, NJ) 3 days prior to viral injection and continued until the end of the study. At indicated time points, mice were sacrificed, serum samples collected and cytokine ELISA performed according to manufacturer's instructions (Mouse cytokine ELISA Kit, BD Biosciences). Mice liver tissues were lysed and subjected to western blot. Rabbit anti-IκB-α (Santa Cruz Biotechnology, Santa Cruz, CA), anti-β actin (Sigma, St. Louis, MO), horseradish peroxidase-conjugated anti-rabbit and anti-mouse secondary antibodies (Santa Cruz) were used.

SCID and immunocompetent animal comparison experiment. 5-6-week-old male SCID and BALB/c129 mice (Taconic Farms) were treated with daily oral Rapamune for 3 days and then intraprostatically injected with 2×10^8 PFU of FL-expressing Ad. Luciferase expression was monitored using an IVIS cooled CCD camera (Xenogen, Alameda, CA). Images were analyzed with IGOR-PRO LivingImage Software (Xenogen).

PET imaging experiment. RM-9 cells were implanted subcutaneously on the right shoulder of male C57BL/6 mice (Taconic Farms), which, 7 days later, received oral saline or Rapamune treatment for 4 days. 5×10^8 PFU sr39tk-expressing Ad was then intratumorally injected and 6

days later mice were subjected to PET imaging with ^{18}F-FHBG as previously described [77]. A 10-min Computed Axial Tomography imaging session followed to provide structural information.

Imaging experiments in pre-immunized models. 4- to 5-week-old C57BL/6 and FVB mice (Taconic Farms) were implanted with RM-9 or MycCaP tumors, respectively. In both models, animals were pre-exposed to Ad by i.p. injection of 1×10^8 PFU of irrelevant adenovirus (serotype 5). Three weeks after the primary viral exposure, 2.5×10^5 RM-9 cells or 3×10^6 MycCaP cells were then implanted subcutaneously onto the right flank of animals in matrigel (1:1 v/v; BD Biosciences). Indicated dose (for C57BL/6) and 5 mg/kg (for FVB) daily i.p. RAPA or diluents treatment started when tumor were palpable (~$(5mm)^3$) and 3 days later, animals received intratumoral injection of 1×10^8 PFU (for C57BL/6) or 5.42×10^8 PFU (for FVB) FL-expressing adenovirus. Animals received continued daily RAPA or diluents treatment until the end of the study. Bioluminescent imaging was performed at indicated time points as described above.

Immunofluorescent staining. Subcutaneous tumors were dissected and fixed in histology cassette in 3% paraformaldehyde at 4 ℃ overnight. Paraffin embedded tumor sections (5 μm) were made at the pathology lab at UCLA. Anti-F4/80 (1:500; Serotec, Raleigh, NC) and anti-CD31 (1:300; BD Biosciences, Bedford, MA) antibodies were used to stain the tumor sections. Pictures were taken using Eclipse 90i microscope from Nikon.

Flow cytometry of tumors. Subcutaneous tumors were dissected and dissociated by physically chopping and collagenase treatment (Invitrogen, Carlsbad, CA; 80 unit/mL in DMEM media containing 10% FBS) at 37 ℃ for 1.5 hours. Myeloid cells are defined by CD11b and CSF1R staining while lymphocytes are defined as CD11b- CD4+ or CD11b- CD8+. To make the

"stimulation" medium used in the T cell reactivity experiment, 7.6×10^6 MycCaP cells were infected with 3.8×10^7 PFU FL-expressing Ad; 36 hours later, cells were harvested in 200 μL passive lysis buffer (Promega, Madison, WI), subjected to three cycles of freeze-and-thaw and centrifuged. The stimulation medium contained 120 μg/mL cell lysate and 3×10^7 PFU/mL empty virus (replication-deficient Ad carrying no transgenes). Cell suspensions from dissociated tumors were then incubated with plain or this stimulation medium at 37 ℃ for 3.5 hours. All flow cytometry antibodies were purchased from BD Biosciences.

Anti-adenovirus antibody titration. Mouse serum was obtained before viral administration and at the end point of the study by retro-orbital bleeding followed by centrifugation in a table-top centrifuge at 8000 rounds per minute for 10 min. 96-well plates were coated with 1.5×10^7 PFU/well adenovirus in 100 μL of sodium carbonate buffer (0.1 mol/L, pH 8.8) and incubated at 4 ℃ overnight. At the time of assay, the viral solution was removed and the plate was incubated with 6% blocking reagent (Roche, Indianapolis, IN) in 0.05% PBS-Tween at 37 ℃ for 1 hour. Serial dilutions of mouse serum were made in duplicate and incubated at 37 ℃ for 2 hours, followed by 5 × washes with 0.5% PBS-Tween. Biotinylated goat anti-mouse IgG (Vector Laboratories, Inc, Burlingame, CA) was used to incubate the plate at room temperature for 1 hour followed by 5 × washes. Streptavidin-HRP (PerkinElmer, Boston, MA) was then used to incubate the plate at room temperature for 30 min, followed by 5 × washes and development with TMB substrate (Thermo scientific, Rockford, IL). The optical density of the plate was then read at 450 nm wavelength. The anti-adenovirus antibody titer was determined as the highest dilution at which the post-viral serum has a reading of 0.05 greater than the corresponding pre-viral serum.

Statistical analysis. Statistical analyses were performed using unpaired or paired two-tailed *t* test. For all analyses, $P<0.05$ was considered statistically significant.

RESULTS

Rapamycin diminished Ad-elicited innate immune responses

Depending on target cell type and cell entry mechanism, Ad infection can trigger a diverse repertoire of signaling molecules, including lipid kinase PI3K, mitogen-activated protein kinase (MAPK), focal adhesion kinase-ERK1/2, and JAK-STAT pathways [25, 28, 99, 101]. Nuclear factor (NF)-κB is a common downstream effector for activation of multiple signaling pathways [28]. We first asked, by interrogating the degradation of its inhibitor IκB, if RAPA could diminish Ad-induced NF-κB activation. Saline or 1×10^9 PFU (plaque forming unit) of Ad were injected i.v. into control or RAPA-treated BALB/c mice, and liver tissues were harvested at indicated time points and subjected to western blot (experiments performed by Dr. Mai Johnson in Lily Wu's laboratory). As shown in Fig. 4.1.A, Ad caused pronounced IκB degradation (and thus NF-κB activation) at 6 and 12 hrs post infection (p.i.); RAPA appreciably abrogated this effect.

Since NF-κB activity is linked to the transcription of many inflammatory factors, the results in Fig. 4.1.A suggested that RAPA could effectively mitigate the Ad-elicited cytokine storm. Therefore, the serum levels of a panel of cytokines and chemokines from these mice were

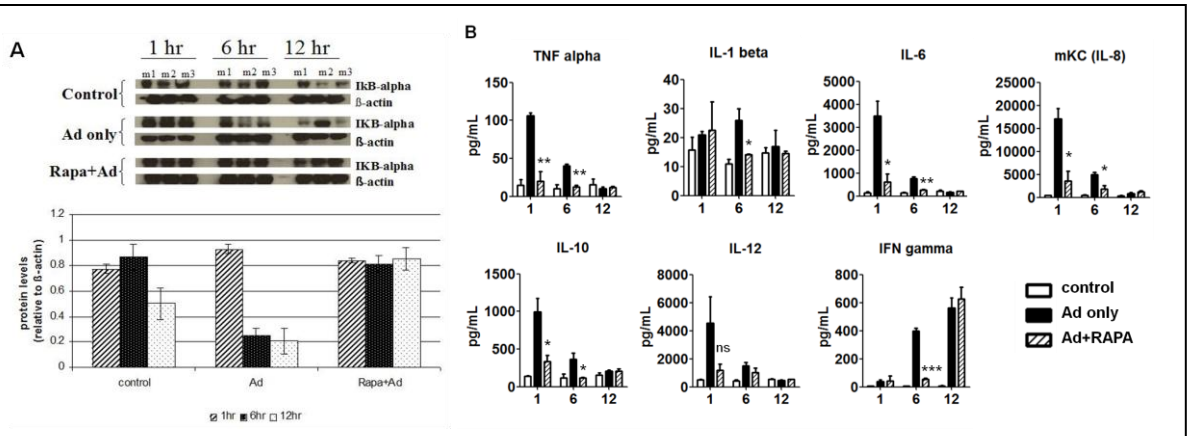

Figure 4.1. Rapamycin diminished adenovirus-induced innate immune response. A. BALB/c mice were given daily oral rapamycin (30 mg/kg) or saline treatment 3 days prior to i.v. injection of 1×10^9 PFU Ad-CMV-FL or saline. Liver tissues from these mice were harvested at indicated time points, lysed and subjected to western blot to examine IκB degradation. B. Sera from these mice were collected at 1, 6 or 12 hours and cytokine levels were assayed by ELISA. ns, not significant; *, P<0.05; **, P<0.01; ***, P<0.001 by two-tailed *t* test compared to Ad only group.

examined by ELISA (experiment performed by Johnson). IL-1 and TNF-α are among the first cytokines that are activated by Ad; they lead to expression of other downstream factors and also relay signals to the adaptive immune system [113]. IL-6 and IL-8 play essential roles in the recruitment of effector cells, such as neutrophils, to liver and are linked directly to Ad-related hepatic injuries; IL-10 is a key regulator in development of humoral immunity [100-101, 103, 121]. As shown in Fig. 4.1.B, Ad markedly increased TNF-α, IL-6, mKC (mouse Keratinocyte-derived Cytokine, analog to human IL-8), IL-10 and IL-12p70 secretion at 1- and 6-hour and IL-1β level 6 hours p.i.; RAPA significantly blocked these inductions. Additionally, the onset of IFN-γ production was delayed by RAPA from 6 to 12 hours p.i. (since RAPA was administered before virus infection, note the possibility that the secretion of IFN-γ at 12 hours in the RAPA group might be a result of losing effective dose of the drug in those animals). Thus, these results

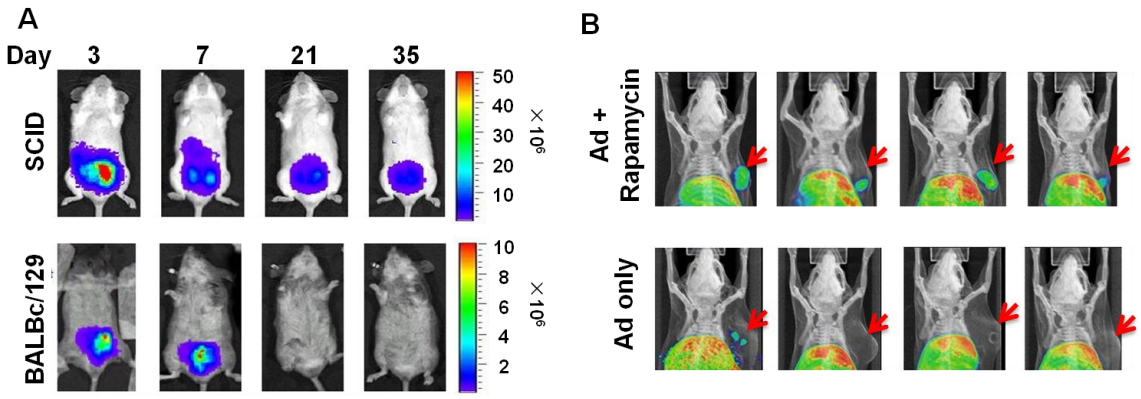

Figure 4.2. Rapamycin mitigated the eliminative effect of adaptive immune system on Ad-mediated transgene expression. A. 2×10^8 PFU prostate-specific FL-expressing Ad was orthotopically injected into the prostate of immunocompetent BALBc/129 or immunodeficient SCID mice. FL imaging was performed at indicated time points post viral administration. Color bar: photons/second/cm^2/sr. B. Male C57BL/6 mice carrying subcutaneous RM9 tumors were given saline or RAPA treatment for 4 days starting at 7 days post tumor implantation. Then, 5×10^8 PFU sr39tk-expressing Ad was injected intratumorally. PET imaging was performed 6 days later with ^{18}F-FHBG. Subcutaneous tumors were marked by red arrows.

suggest that RAPA treatment can reduce the magnitude or delay the onset of components of the Ad-induced cytokine storm.

Rapamycin potentiated Ad-delivered transgene expression

Robust and persistent transgene expression is crucial to ensure diagnostic and therapeutic efficacy of Ads. Therefore, we first set out to determine the impact of the host immune system on Ad-conveyed transgene expression. Firefly luciferase (FL)-expressing Ad was injected into the prostate of immunocompetent BALBc/129 or severe combined immunodeficiency (SCID)

mice and *in vivo* bioluminescent imaging was used to monitor FL expression over 5 weeks (experiments performed by Johnson). As shown in Fig. 4.2.A, both the duration and magnitude of transgene expression was severely reduced in BALBc/129 mice that possessed intact immune functions. Next, we asked if RAPA could relieve the host immune clearance effect. As the ultimate goal of our study is the facilitation of the clinical application of Ads, we examined if RAPA could augment Ad-mediated cancer imaging by positron emission tomography (PET), a clinically–relevant imaging modality. The imaging reporter gene used in this experiment is the HSV1-sr39tk, an enhanced variant form of herpes simplex virus thymidine kinase gene, and the probe for this gene is its substrate ^{18}F-FHBG [122]. Syngeneic RM-9 tumor-bearing, immunocompetent C57BL/6 mice were treated with vehicle or RAPA prior to intratumoral Ad-CMV-sr39tk injection (experiments performed by Johnson). PET analysis six days after viral injection revealed distinctly heightened sr39tk-specific ^{18}F-FHBG tumoral signal in all four mice in the RAPA-treated cohort; in contrast, only one mouse in the control group exhibited weak signal (Fig. 4.2.B). These results indicated that RAPA can potentiate Ad-mediated transgene expression in immunocompetent hosts, boding well for the utility of combining this form of transient immunosuppression with Ad diagnostic imaging approaches in clinical context.

To further assess this combined drug and molecular imaging approach in a clinically relevant scenario, we asked if the enhancing effect of RAPA can be extended to animals with pre-existing anti-Ad immunity. We employed two strains of immunocompetent mice, C57BL/6 and FVB, and immunized them with an intraperitoneal (i.p.) dose of Ad (1×10^8 PFU, non FL-expressing virus; experimental time line shown in Fig. 4.3.A). This viral immunization scheme led to the development of robust anti-Ad humoral immune response in these mice (data not shown). Syngeneic prostate tumors (RM-9 or MycCaP [123]) were then established subcutaneously 3

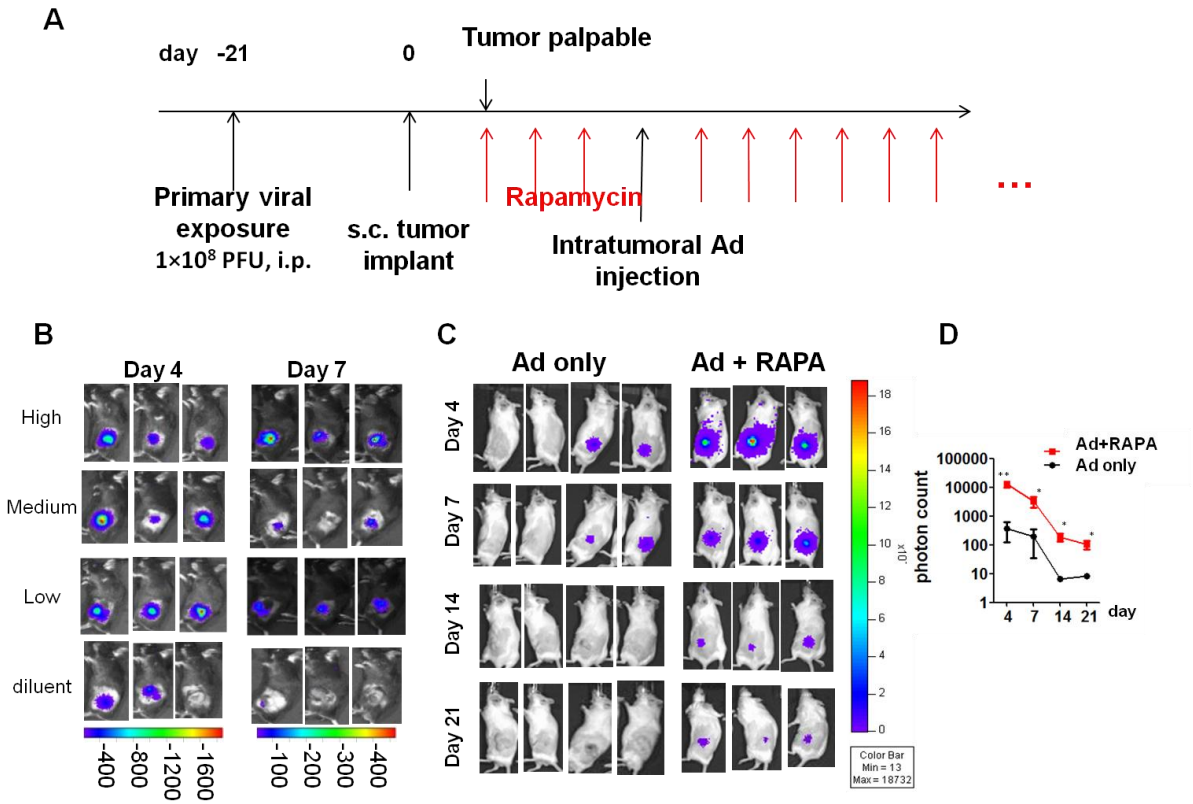

Figure 4.3. Rapamycin enhanced Ad-mediated transgene expression in pre-immunized mice. A. Time line of pre-immunity models. Animals were primed with an intraperitoneal dose of 1×10^8 PFU irrelevant Ad and, 3 weeks later, subcutaneous tumors were inoculated. RM9 tumors became palpable 4-5 days post implantation; MycCaP tumors became palpable 5-7 days post implantation. At this point, rapamycin or control treatment initiated and intratumoral Ad imaging vectors were administered 4 days later. FL bioluminescent imaging was conducted at 4, 7, 14 and 21 days post viral injection as indicated in B and C. B. FL bioluminescent imaging of RM-9 bearing C57BL/6 mice on day 4 and 7. High: 5 mg/kg/d rapamycin; Medium: 1.5 mg/kg/d; Low: 0.5 mg/kg/d. n=3. C. FL bioluminescent imaging of MycCaP bearing FVB mice (n=3 or 4) at indicated time points. D. Quantification of imaging signal from C. Color bar of bioluminescent imaging: photon count. * $P<0.05$, ** $P<0.01$ by two-tailed *t* test.

weeks after the primary viral immunization. When tumors became palpable (4-5 days for RM9;

5-7 days for MycCaP), daily i.p. injection of RAPA or diluent was administered 3 days prior to the secondary intratumoral injection of FL-expressing Ad (1×10^8 PFU for RM9; 5×10^8 PFU for MycCaP) (Fig. 4.3.A). Bioluminescent imaging was performed, to monitor FL expression. In the RM-9 tumor model, high (5 mg/kg), medium (1.5 mg/kg) and low (0.5 mg/kg) doses of RAPA were tested; all dosages enhanced FL expression on day 4 relative to mice that received the diluent control. Tumor transgene expression was still detectable at day seven in RAPA treated mice (Fig. 4.3.B).

In the FVB compatible MycCaP tumor model, only 5 mg/kg RAPA was used; mice were followed by imaging for 21 days. As shown in Fig. 4.3.C-D, RAPA increased FL expression level on day four, and significantly extended detectable transgene persistence at all time points tested. Taken together, these results demonstrate that, even with the challenge of pre-existing immunity, the incorporation of immunosuppressant RAPA into the adenovirus imaging protocol can augment the Ad-mediated transgene imaging signal and prolong the diagnostic time window. These data also support that the facilitating effects of RAPA are not tumor model- or mouse strain-specific.

Rapamycin suppression of anti-Ad adaptive immune responses

To further investigate the mechanism underlying the promoting effects of RAPA on Ad transgene expression in pre-immunized hosts, we first examined the titer of anti-Ad antibodies in mice sera at the end of the previous studies. In the RM-9 model, both medium and high RAPA doses, but not the low RAPA dose, prevented secondary production of anti-Ad IgG in pre-

immunized C57BL/6 mice (unpublished data). A trial with larger cohort size revealed that high dose RAPA reduced IgG titer from $1.36 \pm 0.33 \times 10^5$ to $9.88 \pm 2.02 \times 10^3$ (P=0.0021, two-tailed *t* test; n=8) (Fig. 4.4.A). Similarly, RAPA reduced end-point IgG titer by nearly 3-fold in pre-immunized FVB mice (P=0.0368, two-tailed paired *t* test; n=3 to 4) (Fig. 4.4.A). These data are consistent with prior studies showing RAPA's inhibition of Ad-elicited B cell activation and IgG production [31]. Of note, we focused on titers of IgG over IgM because IgM secretion preceded that of IgG and was of a lower magnitude in these pre-immunized animals (unpublished data). In addition, we would expect that secondary viral exposure would induce isotype switching to IgG [124].

Next, we explored RAPA's role in modulating cell-based anti-Ad immunity [115, 117]. Specifically, we assessed both infiltration and activation of immune cells in Ad-infused tumors. In the RM-9 model, immunofluorescent staining uncovered greater infiltration of F4/80 positive macrophages triggered by Ad injection. However, the macrophage infiltration was markedly suppressed by RAPA (Fig. 4.4.B). We then used flow cytometry to achieve better quantification of intratumoral myeloid cell populations. Consistent with the immunostaining results, RAPA treatment significantly decreased myeloid infiltration in the tumors (Fig 4.4.C, first panel). Particularly, cells expressing colony-stimulating factor-1 receptor, a crucial molecule for the differentiation of the macrophages, dendritic cells, and other myeloid-derived monocytes [125], were almost completely eliminated by RAPA (Fig. 4.4..C, second panel) in these tumor infiltrating myeloid cells. Furthermore, both mature (CD69+) and immature (CD62L+) phenotypes of CD4+ T cells were decreased by RAPA (Fig. 4.4.C, third panel), implying that both the recruitment and activation of CD4+ T cells were impeded. CD8+ cytotoxic T cells also appeared to be reduced by RAPA (Fig. 4.4.C, last panel) although the CD8+ content of RM-9

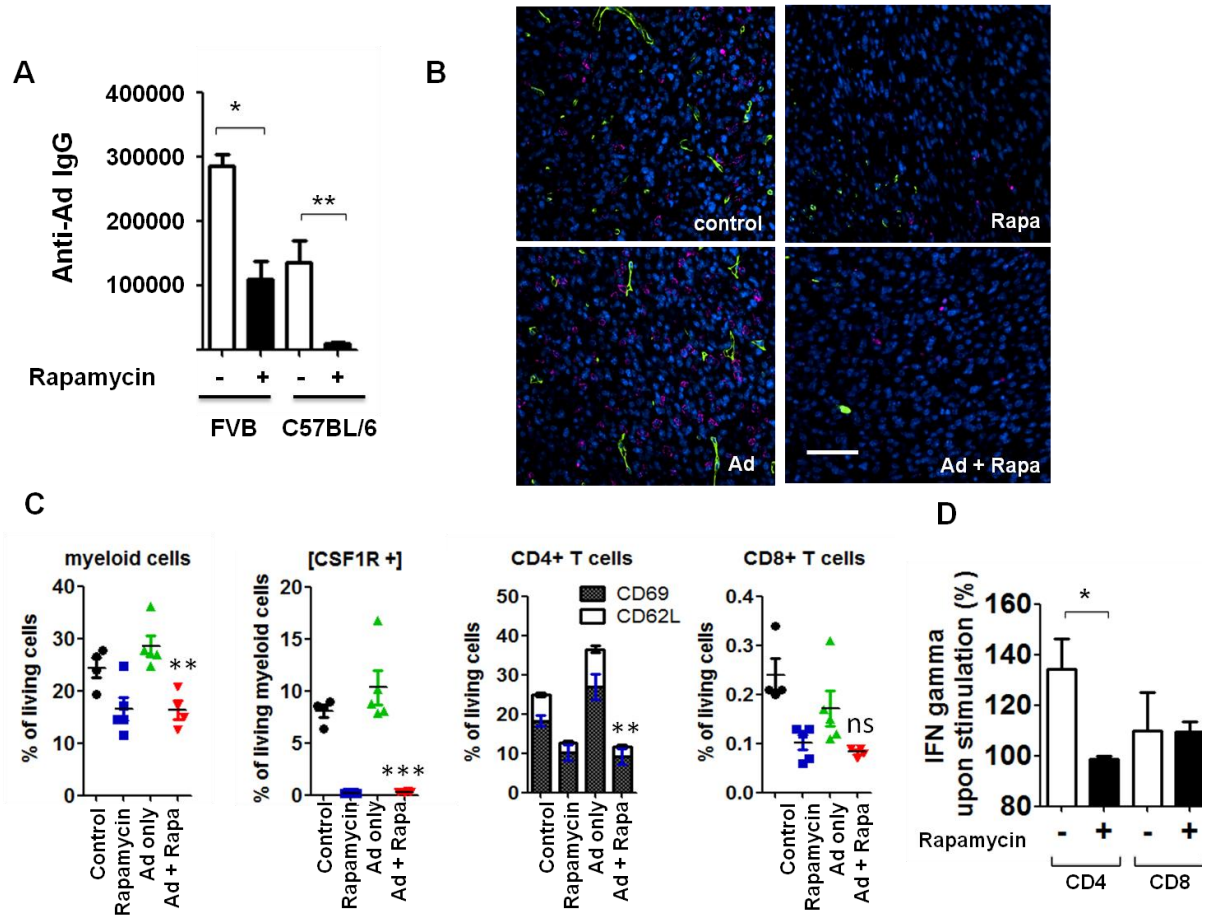

Figure 4.4. Rapamycin suppresses anti-Ad adaptive immune responses. A. FVB and C57BL/6 mice were treated according to the protocol shown in Fig. 4.3.A. Mouse serum samples were collected at the end of study and subjected to ELISA for anti-Ad antibody titration (FVB: means from 3 independent trials; *, P=0.0368 by two-tailed paired *t* test. C57BL/6: representative data from 2 independent trials; **, P=0.0021 by two-tailed *t* test). B. Representative immunofluorescent staining of thin sections from RM-9 tumors with indicated treatment. Cyanine, macrophage marker F4/80; green, blood vessel marker CD31; blue: DAPI. Bar, 200 μm. C. RM-9 tumor from indicated treatment groups were dissociated and subjected to flow cytometry analysis for myeloid and T cells populations. Myeloid cell lineage was defined by CD11b staining. **, P<0.01; ***, P<0.001 compared to Ad only group by two-tailed unpaired *t* test. **Figure legend continues on next page.**

tumors was very low, and thus difficult to accurately measure. Interestingly, consistent with

(Fig. 4.4. Continued) D. MycCaP tumors from control or rapamycin-treated animals (n=3) were harvested at 1.5 cm diameter, dissociated, and then incubated with plain media or media containing adenovirus and Ad-infected MycCaP cell lysate for 3.5 hours at 37 ℃, stained with intracellular IFNγ antibodies and subjected to flow cytometry. IFNγ expression with stimulation was then normalized to corresponding non-stimulated control (n=3). T cell subsets were delineated by CD4 and CD8 staining. *, P=0.0431 by two-tailed unpaired *t* test.

other reports [31], RAPA decreased tumor angiogenesis, as reflected by reduced staining of the vasculature CD31 marker (Fig. 4.4.B), offering another possible mechanism underlying RAPA's inhibition of immune cell infiltration and activation observed in this model.

Next, we sought to determine if RAPA could impact the reactivity of tumor infiltrating immune cells towards Ad and Ad-infected cancer cells. IFNγ, a key regulatory cytokine for T cell development and activation, was chosen as a readout for immune cell functionality. MycCaP tumors, established in Ad pre-immunity conditions noted in Fig. 4.3.A and 4.4, were harvested at 1.5 cm diameter, and dissociated to single cells. The dissociated cells were then incubated with medium or with a "stimulation" cocktail composed of adenoviral particles and cell lysate from MycCaP cells infected with FL-expressing virus. IFNγ production from T cells upon stimulation was then assessed by intracellular staining and flow cytometry. As shown in Fig. 4.4.D, in the cohort without RAPA treatment (-, control), Ad-mediated stimulation resulted in a 40% increase in IFNγ expression from CD4+ T cells over non-stimulated (plain media) baseline; however, T cells from RAPA treated tumors were not responsive to these stimuli. The reactivity of the rare CD8+ T cells in MycCaP tumors appeared to be unaltered by RAPA. Collectively, the addition of RAPA to the Ad-mediated tumor gene transfer protocol decreased the infiltration of myeloid

and T immune cells in the tumor environment; it also blunted T cell reactivity towards virus-related stimuli.

DISCUSSION

The combined use of rapamycin with oncolytic Ad was explored in one previous study to treat colon cancer [31]; RAPA decreased anti-Ad antibodies and enhances intratumoral viral retention by inhibiting angiogenesis, and consequently improved therapeutic outcome. The present study, however, is the first to provide a comprehensive evaluation of RAPA's effects on moderating Ad-related immune responses (including innate, humoral and cellular adaptive responses) in pre-immunized hosts. These results are of significant relevance to clinical translation of Ad in that they shed light on issues such as drug safety, fast vector clearance, inadequate transgene expression and difficulty of repeated vector administration due to antibody induction.

Short-term pretreatment with RAPA markedly attenuated Ad-induced NF-κB activation and the cytokine storm response, and thus improving the safety profile of Ad vectors (Fig.4.1). Of note, these benefits are readily applicable to trials involving second and third generations (helper-dependent) Ad vectors, because the innate immune response is provoked solely by Ad capsid proteins [109]. Also, unlike prior studies that targeted single inflammatory pathways [28-29, 101], RAPA inhibits expression of a broad panel of cytokines/chemokines and activation of a diverse repertoire of immune cells (Fig. 4.1 and 4.4), reducing the risk of upregulation of alternative compensating factors. Because mTOR function is involved in nearly all cell types, RAPA usage may raise the concern of side effects. However, we did not observe any standard

signs of morbidity (e.g., hunched back, sunken eyes, dehydration or lethargy) in RAPA cohorts although an expected reduction of 15-18% of body weight did occur due to RAPA's suppression on cell size and metabolic rate [119].

PET imaging, a modality that enables functional non-invasive interrogation of cancer cells with high spatial resolution, is widely used in clinics. However, due to its low sensitivity, Ad-directed reporter gene-based PET diagnostic trials usually demand the administration of a high dose of vector. We show here that RAPA incorporation allowed us to achieve unambiguous tumor detection with as low as 5×10^8 Ad PFU (Fig. 4.2.B), an Ad level well below the lethal dose in mice ($5\text{-}10\times10^9$ PFU). These data illustrate the viability of incorporating RAPA into Ad-mediated imaging regimens, so that a lower and thus safer viral dose is sufficient to achieve cancer detection.

Of note, other non-immunosuppressive measures have been undertaken to tackle host immune reactions against Ad. For example, serotypes of less prevalent Ad have been exploited to reduce recognition and neutralization by anti-Ad5 antibodies [126]. Fiber and hexon manipulations have also been attempted to modulate viral interaction with target cells, seeking reduction of immune response and hepatic injury [27, 103, 127]. Moreover, even though host immune systems present the most formidable obstacle for Ad vectors, there are other factors contributing to the impediment in their clinical application. For instance, over 90% of i.v. Ad dose will be sequestered in the mouse liver due to Kupffer cells entrapment, RGD-integrin bridged endothelial cell infection and coagulation factors-mediated hepatocyte transduction [24, 128-132], which unfavorably diverts the biodistribution of Ad vectors and restrains access to cancer sites. This problem can be partially evaded by eliminating Kupffer cells with a pre-dose of virus

[24, 50, 77], chemical compounds [27, 133-134], or inhibiting coagulation factors' activity by warfarin treatment. Additionally, various non-viral polymer- and nanoparticle-based strategies have been investigated to mitigate immune reactions against the viral vector [135-136]. Another daunting challenge specific to humans is that human erythrocytes express the major receptor for Ad – Coxsackie virus-adenovirus receptor (CAR). This can lead to trapping and inactivation of the majority of i.v. delivered Ad5 [73]. The complement receptor on human erythrocytes also contributes to the elimination of Ad vectors [73]. Overall, these questions deserve further investigations by alternative approaches that include Ad surface modification, development of hybrid serotypes and liver de-targeting tactics. Meanwhile, more human-related experimental models need to be established to mimic these challenging situations.

In summary, we report that rapamycin alleviated Ad-induced inflammation and toxicity, strengthened Ad gene expression, diminished anti-Ad antibody production, repressed Ad-elicited myeloid and T cell infiltration and activation, and improved the efficacy of Ad gene therapy in immunocompetent and pre-immuned hosts. This study offers a viable strategy to integrate transient immunosuppression into Ad-mediated cancer diagnostic and therapeutic applications and presents evidence towards their successful clinical translation.

IV-II. Polypeptide Coatings Shield Adenovirus from Interference of Blood Factors and Reduce Adenoviral Antigenicity

Abstract

In this section of the thesis, some advantageous characteristics of non-viral gene delivery vehicles were incorporated to complement the property of adenoviral vectors. Specifically, Shuwen Sok (a previous graduate student jointly mentored by Drs. Lily Wu and Timothy Deming) used α-Amino acid-N-carboxyanhydride chemistry to synthesize homopolypeptides and diblock copolypeptides that possess well-defined secondary structures to coat the surfaces of adenoviral particles in a non-covalent manner and modify their transduction efficiencies. Sok showed that our polypeptide coating was able to shield viral particles from the neutralizing effect of antibodies and mitigate their binding to blood coagulation factor X *in vitro*. Furthermore, I performed *in vivo* experiments and showed that the coating also reduced the antigenicity of adenovirus in immunocompetent mice. These results offer a valuable alternative strategy utilizing polypeptide coating to circumvent the inhibitory effects of host blood components and the humoral immune system on adenovirus.

INTRODUCTION

Polymeric materials have been used previously to modify and confer complementary surface functionalities to adenoviral vectors (Ad) for gene therapy. Among them, poly(ethylene glycol) (PEG) is often used as a protective coat and as a tether for targeting ligands in surface modification due to its biocompatibility and ability to impart "stealth-like" properties [137-139].

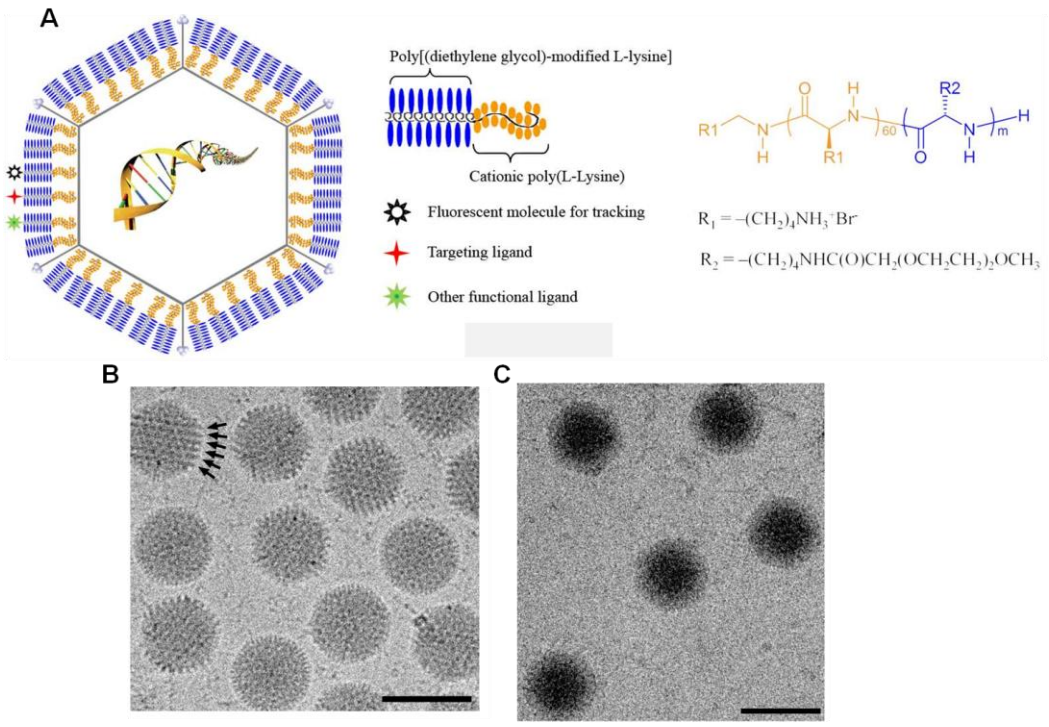

Figure 4.5. Formation of the hybrid complex. A. Schematics of the hybrid complex. The diblock copolypeptide self-assembles around the negatively charged adenoviral capsid. A variety of potential functionalities can be introduced through the incorporation of ligands. B-C, CryoEM images of uncoated Ad (B) and Ad incubated with $K_{60}K^{P}_{370}$ (C). As indicated by the arrows in B, characteristic six-spikes can be seen along each edge of the uncoated Ad particle whereas coated Ad had smooth surfaces (C). Scale bar, 100 nm.

In this project, however, we undertook an alternative approach of binding polypeptides to Ad capsids using polyion complexation to form physical hybrid complexes. This approach circumvents the need for multiple buffer changes and careful optimization of reaction conditions required to obtain high conjugation yields in the PEGylation of Ad particles [140]. Importantly, our method can also avoid reduced infectivity observed when Ad capsid proteins are covalently modified [141]. Ad vectors, bearing a net negative surface charge, have previously been complexed with cationic lipids, poly(L-lysine) as well as polyethylenimine [141-145]. Ad particles modified this way possess a net positive surface charge, which has been shown to enhance the transduction of negatively charged cells and augment gene transfer *in vitro*. However, these vectors interact and form aggregates with oppositely charged biopolymers and serum proteins *in vivo*, complicating *in vivo* applications. Here, we use block copolypeptides to provide strong virus complexation while simultaneously minimizing their net surface charges.

As shown in Fig. 4.5, we employed the well-established α-amino acid-*N*-carboxyanhydride (NCA) polymerization procedure and synthesized diblock copolymers with controlled molecular weights and size distributions and then coated the surface of Ad particles (experiments performed by Sok; [146-147]). In particular, $K_{60}K^{P}_{370}$, a polymer coating composed of poly(L-lysine) with an average length of 60 residues (K_{60}) and a nonionic ethylene glycol-modified lysine domain (K^{P}_{370}), demonstrated the most desirable characteristics in terms of preserving viral viability and structural integrity *in vitro* and *in vivo*. All subsequent experiments were performed using this coating moiety.

MATERIALS AND METHODS

General Chemical and Polypeptide Synthesis. The synthesis of polypeptide diblocks was described in [148].

Preparation of polypeptide-adenovirus complexes. The polypeptide was dissolved in Millipore water and passed through a 0.45 μm PTFE filter to remove any particulates before the stock solution was autoclaved. Subsequent dilutions were made using PBS. The polypeptide-to-Ad ratio was calculated based on the total number of Ad particles (viral particles/mL). We assumed that the cationic polypeptides used have 100% of K residues protonated at physiological pH based on their pK_a values. The number of lysine molecules was hence calculated based on the mass of polypeptide and molecular weight of the poly(L-lysine) segments. Equal volumes of each component were mixed by gentle pipette tip aspiration and incubated for 15-30 minutes at room temperature before application.

Cryo-Electron Microscopy and Fluorescence Microscopy. For cryoEM, an aliquot (5 μL) of the particle suspension (Ad alone or Ad mixed with K_{60}), prepared as described below, was placed on each Quantifoil R 2/1 holey carbon grid (Quantifoil GmbH), blotted for 5 seconds on Whatman type 1 filter paper and vitrified in liquid ethane. The grid was placed in a Gatan 626 cryo-sample holder and transferred to a Tecnai G^2 TF20 electron microscope (FEI Co., Hillsboro, OR) for CryoEM imaging. CryoEM images were recorded on a 16 megapixel CCD camera (TVIPS) using 200 keV electrons at an electron dosage of 20 electrons/$Å^2$/image.

Transduction studies with blood components. The experiment was conducted in 24-well plates. The total inoculation volume of all transduction studies was 200 μL and the inoculant was removed after 2 hours of incubation. 800 μL of fresh complete media was added to each well and

infection was allowed to proceed for 48 hours. Then the cells were harvested and lysed in passive lysis buffer. FL luciferase activity was measured according to the manufacturer's instructions (Promega, Madison, WI) using a luminometer (Berthold Detection Systems, Pforzheim, Germany). Ad or Ad-$K_{60}K^{P}_{370}$ was incubated with 1% human serum in PBS for 30 minutes at room temperature before being applied to A549 cells. Human serum (pooled from 10 donors) was purchased from Innovative Research, Inc., Novi, MI. Ad or Ad-$K_{60}K^{P}_{370}$ was applied to AML-12 cells in serum-free media or serum-free media containing blood clotting factor, Factor X (FX), at physiological concentration (8 μg/mL). FX was purchased from Haematologic Technologies, Inc., Essex Junction, VT.

***In vivo* immunity experiment**. 6-week-old male BALB/c mice were purchased from Taconic Farms and intravenously injected with 1×10^{7} PFU of either naked or polymer-coated AdCMV-FL. Mouse serum was obtained before and after viral administration at indicated time points by retro-orbital bleeding followed by centrifugation in a table-top centrifuge at 8000 RPM for 10 minutes. The serum sample was then stored at -80 ℃ for future assays. Antibody titer was determined as previously described.

RESULTS

Polypeptide coating of adenovirus reduced the interference of blood components

A great proportion of human population is exposed to naturally presented Ad thus possesses anti-Ad cellular and humoral immunities, which obstruct distribution and bioavailability of Ad vectors. Therefore, here we first examined the ability of the coating to protect Ad from pre-

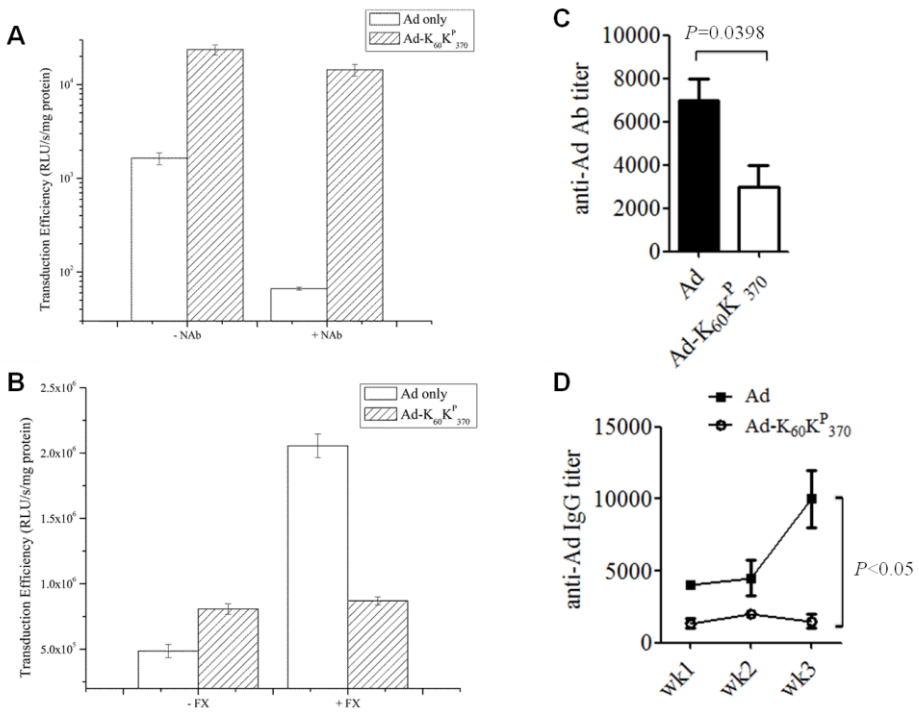

Figure 4.6. Effect of polypeptide coating on blood factor interferences and antigenicity of adenovirus. A. FL-expressing Ad or Ad-$K_{60}K^{P}_{370}$ was incubated with 1 vol. % of human serum in PBS for 30 minutes at room temperature. The complexes were then applied to A549 cells at an MOI of 5 in 200 µL of serum-containing RPMI. Transduction efficiency was determined by luciferase assays. B. Ad or Ad-$K_{60}K^{P}_{370}$ was applied to AML-12 cells at an MOI of 5 in 200 µL of serum-free media or serum-free media containing FX at physiological concentration (8 µg/mL). The inoculant was removed by aspiration and replaced with fresh media after 2 hours. FL activity was assayed 48 hours later. Cells transduced in the absence of any serum served as control. Each point represents mean ±SE (n=3). C-D. Immunocompetent BALB/c mice were injected with naked or $K_{60}K^{P}_{370}$ complexed adenovirus, and serum titer of anti-Ad antibody was tested 7 days post viral administration by ELISA (C; P=0.0398). D. Serum antibody titer was determined at indicated time points. The polymer coated virus did not induce strong antibody production ($p<0.05$). For both experiments, two-tailed unpaired *t* test was used.

existing neutralizing antibodies (NAbs). Ad or Ad-$K_{60}K^{P}_{370}$ complexes were incubated with

human serum that contained NAbs and the capability of the coating to lessen the inactivating effect of NAbs was assayed by measuring the transduction efficiency of the Ad-$K_{60}K^{P}_{370}$ complexes compared to unmodified Ad (experiments performed by Sok). In the presence of 1 vol. % human serum, the transduction efficiency of Ad-$K_{60}K^{P}_{370}$ was about 216-fold of the value obtained for unmodified Ad under the same conditions (Fig. 4.6.A), which suggests the protective ability of the polypeptide coating against NAbs. The ability of FX to mediate the binding of Ad to AML-12 cells, a mouse liver cell line, was also tested because FX has been shown to be responsible for the liver-tropism of Ad in mouse models [149] (experiments performed by Sok). We found that a physiological concentration of FX (8 μg/mL) was able to increase the binding of Ad particles to the mouse liver cells and enhanced the transduction more than 4-fold (Fig. 4.6.B) compared to controls in the absence of FX. Conversely, the transduction efficiency of Ad-$K_{60}K^{P}_{370}$ was essentially unchanged in AML-12 cells upon addition of FX (Fig. 4.6.B). This is likely due to the polypeptide masking the Ad capsid and preventing FX from mediating cell binding.

Polypeptide coating diminished the antigenicity of adenovirus in immunocompetent mice

Next, laboratory mice were used to examine the related issue of vector antigenicity to gain a broader understanding on the utility of the polypeptide coating. If the polypeptide coating could reduce Ad immunogenicity and blunt anti-Ad antibody production *in vivo*, this could allow repeated vector administration to achieve more effective gene delivery. 1×10^{7} PFU of Ad (n=4) or Ad-$K_{60}K^{P}_{370}$ (n=3) was injected into immunocompetent BALB/c mice and assayed for anti-adenovirus IgG production triggered by viral administration. Mouse serum was obtained 7 days

after viral injection and titrated for anti-Ad antibody compared to the serum drawn prior to viral exposure. As shown in Fig. 4.6.C, the polymer coating significantly decreased anti-Ad antibody production (p=0.0398). Moreover, in a longitudinal study, we found that the polymer coating's suppressive effects on antibody production last at least up to 3 weeks post viral infection, when the antibody titer in the naked virus cohort reached the highest point (p<0.05; Fig. 4.6.D). These kinetics agreed with other studies showing that anti-Ad IgG production peaks at 3-4 weeks post infection [30] when the IgM to IgG isotype switch takes place [150].

DISCUSSION

In this project, we explored the utilization of polymer coating in modifying the surface characteristics of adenoviral vectors in order to circumvent the interaction between viral particles and blood components such coagulation factor X and neutralizing antibodies. We showed that the coating successfully shielded Ad from binding to FX, and thus reduced the *in vitro* transduction of mouse liver cell line AML-12 (Fig. 4.6.B). Furthermore, the polymer coating significantly reduced the inhibitory effects of neutralizing Abs on Ad and therefore increased the transduction efficiency of Ad vector in the presence of human sera (Fig. 4.6.A). Moreover, *in vivo*, Ad-$K_{60}K^{P}_{370}$ complexes appeared to be less antigenic than uncoated virus in that they elicited a significantly lower amount of anti-Ad antibody production in immunocompetent mice (Fig. 4.6.C). This effect was even more dramatic at later time points when IgG production induced by uncoated virus peaked (Fig. 4.6.D). These phenomena were likely because the coating formed a protective barrier around the Ad capsid and prevented access to neutralizing

antibodies as well as antigen presenting cells. More importantly, based on these data, we are optimistic that the $K_{60}K^{P}_{370}$ coating could aid adenovirus to evade pre-existing antibodies in a pre-exposed immunocompetent host.

Although we showed that the polymer coating could attenuated FX-facilitated Ad transduction of mouse liver cells (Fig. 4.6.B), this *in vitro* shielding effect did not influence liver transduction in mice (data not shown, [148]). Several reasons can account for this finding. First, our study only examined the impact of FX. Other Vitamin K dependent coagulation factors (such as FIX, FVII and protein C [131]) have also been reported to be involved in bridging Ad toward hepatocytes, which could be at play in our animal study. Second, the cell surface characteristics of hepatocytes in their endogenous environment, especially regarding heparin sulfate proteoglycan expression, could differ from the AML-12 cell line. Hence, the *in vivo* infectivity of hepatocytes by coated or uncoated Ad would be difficult to predict based on cell culture conditions. Furthermore, $K_{60}K^{P}_{370}$ coated Ad exhibited enhanced transduction capability on both CAR + and – cells [148]; therefore the polymer coating could be boosting the transduction of liver cells *in vivo,* despite inhibition of FX-Ad interactions. The net result of these two counteracting effects is the maintenance of prominent liver transduction observed.

In conclusion, we here report that our synthetic polypeptides were able to coat Ad particles, yielding complexes that conferred protection against neutralizing antibodies and FX interactions *in vitro*. Pilot studies using immunocompetent mice showed both reduced and delayed peak production of anti-Ad antibodies provoked by coated Ad, suggesting that Ad-$K_{60}K^{P}_{m}$ behaved differently from unmodified Ad *in vivo*. The focus of future studies will be to explore the potentially versatile targeting capability by incorporating ligands onto the polypeptides.

V. CONCLUSION

In this thesis, we investigated the application of gene-based imaging and therapeutic vectors in the context of diagnosis and treatment for advanced stage of prostate cancer. We approached this topic from perspectives of cancer detection, therapy monitoring and clinical translation of these vectors. First, we took advantage of an androgen independent promoter, PSES, in corporation with the transcriptional amplification system, TSTA, to direct the expression of molecular imaging reporter genes and successfully detected castration resistant prostate cancer in subcutaneous and intratibially metastatic models. Our findings indicated that transcription-based imaging strategies may have the capability to identify metastatic lesions at an earlier stage than conventional PET tracers such as metabolic probe FDG and bone imaging probe NaF. We also employed the simultaneous utilization of androgen induced and androgen suppressed reporters to functionally interrogate the activation status of androgen receptor, which remains an essential player in cell viability and proliferation of prostate cancer even at the advanced hormone refractory phase. This dual reporter system offers a reliable and sensitive screening platform for the development of novel, more potent androgen antagonists and androgen synthesis inhibitors. It also permits individualized analysis of patient's response towards treatment options. Furthermore, we performed exploratory experiments to apply a PSES-driven infra-red fluorescent protein-expressing vector to detect circulating prostate cancer cells and have obtained encouraging preliminary results that intrigued us to further substantiate the applicability of this system. Last but not least, we explored two possible means to facilitate the clinical translation of adenoviral vectors for imaging and gene therapy in immunocompetent hosts and especially in hosts with pre-existing anti-Ad immunities. We first investigated the incorporation of an immunosuppressant, rapamycin, into gene therapy protocols to suppress the innate immune

responses and acute inflammation elicited by Ad infection in order to protect the host from detrimental cytokine storm and potentially lethal tissue damages. We also demonstrated that rapamycin was able to enhance Ad-mediated transgene expression by inhibiting the activation of humoral and cellular adaptive immune responses against viral particles and viral transgene-expressing cells. The second approach entailed the generation of polymer coatings that protected Ad particles from interacting with neutralizing antibodies and coagulation factors in the blood, and therefore improved cancer-targeted transduction efficiency of Ad vectors in the presence of these challenging factors. The coating can also shield the virus from triggering humoral immune responses in immunocompetent hosts, and thus reducing the antigenicity of Ad vectors. Taken together, this thesis presents substantial evidence for the pre-clinical and clinical applications of gene-based imaging and therapeutic vectors to assist the management of advanced, treatment-refractory prostate cancer.

BIBLIOGRAPHY

1. Jemal, A., et al., *Cancer statistics, 2009.* CA Cancer J Clin, 2009. **59**(4): p. 225-49.
2. Vasaitis, T.S., R.D. Bruno, and V.C. Njar, *CYP17 inhibitors for prostate cancer therapy.* J Steroid Biochem Mol Biol, 2010.
3. Tran, C., et al., *Development of a second-generation antiandrogen for treatment of advanced prostate cancer.* Science, 2009. **324**(5928): p. 787-90.
4. Nelson, J.B., et al., *Phase 3, randomized, controlled trial of atrasentan in patients with nonmetastatic, hormone-refractory prostate cancer.* Cancer, 2008. **113**(9): p. 2478-87.
5. Sadar, M.D., *Advances in small molecule inhibitors of androgen receptor for the treatment of advanced prostate cancer.* World J Urol, 2011.
6. Attar, R.M., et al., *Discovery of BMS-641988, a novel and potent inhibitor of androgen receptor signaling for the treatment of prostate cancer.* Cancer Res, 2009. **69**(16): p. 6522-30.
7. Attar, R.M., C.H. Takimoto, and M.M. Gottardis, *Castration-resistant prostate cancer: locking up the molecular escape routes.* Clin Cancer Res, 2009. **15**(10): p. 3251-5.
8. Attard, G., et al., *Antitumor activity with CYP17 blockade indicates that castration-resistant prostate cancer frequently remains hormone driven.* Cancer Res, 2009. **69**(12): p. 4937-40.
9. Scher, H.I., et al., *Targeting the androgen receptor: improving outcomes for castration-resistant prostate cancer.* Endocr Relat Cancer, 2004. **11**(3): p. 459-76.
10. Vis, A.N. and F.H. Schroder, *Key targets of hormonal treatment of prostate cancer. Part 1: the androgen receptor and steroidogenic pathways.* BJU Int, 2009. **104**(4): p. 438-48.
11. Mulholland, D.J., et al., *Cell autonomous role of PTEN in regulating castration-resistant prostate cancer growth.* Cancer Cell, 2011. **19**(6): p. 792-804.
12. Li, Y., et al., *Intragenic rearrangement and altered RNA splicing of the androgen receptor in a cell-based model of prostate cancer progression.* Cancer Res, 2011. **71**(6): p. 2108-17.
13. Li, Y., et al., *AR intragenic deletions linked to androgen receptor splice variant expression and activity in models of prostate cancer progression.* Oncogene, 2012.
14. Garcia, J.A. and B.I. Rini, *Castration-resistant prostate cancer: Many treatments, many options, many challenges ahead.* Cancer, 2011.
15. Chang, K.H., et al., *Dihydrotestosterone synthesis bypasses testosterone to drive castration-resistant prostate cancer.* Proc Natl Acad Sci U S A, 2011. **108**(33): p. 13728-33.
16. Dehm, S.M., et al., *Splicing of a novel androgen receptor exon generates a constitutively active androgen receptor that mediates prostate cancer therapy resistance.* Cancer Res, 2008. **68**(13): p. 5469-77.
17. Guo, Z., et al., *A novel androgen receptor splice variant is up-regulated during prostate cancer progression and promotes androgen depletion-resistant growth.* Cancer Res, 2009. **69**(6): p. 2305-13.
18. Hu, R., et al., *Ligand-independent androgen receptor variants derived from splicing of cryptic exons signify hormone-refractory prostate cancer.* Cancer Res, 2009. **69**(1): p. 16-22.
19. Sun, S., et al., *Castration resistance in human prostate cancer is conferred by a frequently occurring androgen receptor splice variant.* J Clin Invest, 2010. **120**(8): p. 2715-30.
20. Watson, P.A., et al., *Constitutively active androgen receptor splice variants expressed in castration-resistant prostate cancer require full-length androgen receptor.* Proc Natl Acad Sci U S A, 2010. **107**(39): p. 16759-65.
21. Hu, R., W.B. Isaacs, and J. Luo, *A snapshot of the expression signature of androgen receptor splicing variants and their distinctive transcriptional activities.* Prostate, 2011. **71**(15): p. 1656-67.

22. Lee, S.J., et al., *Novel prostate-specific promoter derived from PSA and PSMA enhancers.* Mol Ther, 2002. **6**(3): p. 415-21.
23. Dzojic, H., W.S. Cheng, and M. Essand, *Two-step amplification of the human PPT sequence provides specific gene expression in an immunocompetent murine prostate cancer model.* Cancer Gene Ther, 2007. **14**(3): p. 233-40.
24. Shashkova, E.V., et al., *Macrophage depletion combined with anticoagulant therapy increases therapeutic window of systemic treatment with oncolytic adenovirus.* Cancer Res, 2008. **68**(14): p. 5896-904.
25. Liu, Q., et al., *The role of capsid-endothelial interactions in the innate immune response to adenovirus vectors.* Hum Gene Ther, 2003. **14**(7): p. 627-43.
26. Shayakhmetov, D.M., et al., *Adenovirus binding to blood factors results in liver cell infection and hepatotoxicity.* J Virol, 2005. **79**(12): p. 7478-91.
27. Shayakhmetov, D.M., et al., *Analysis of adenovirus sequestration in the liver, transduction of hepatic cells, and innate toxicity after injection of fiber-modified vectors.* J Virol, 2004. **78**(10): p. 5368-81.
28. Shayakhmetov, D.M., et al., *Interference with the IL-1-signaling pathway improves the toxicity profile of systemically applied adenovirus vectors.* J Immunol, 2005. **174**(11): p. 7310-9.
29. Venteclef, N. and P. Delerive, *Interleukin-1 receptor antagonist induction as an additional mechanism for liver receptor homolog-1 to negatively regulate the hepatic acute phase response.* J Biol Chem, 2007. **282**(7): p. 4393-9.
30. Zirger, J.M., et al., *Immune regulation of transgene expression in the brain: B cells regulate an early phase of elimination of transgene expression from adenoviral vectors.* Viral Immunol, 2006. **19**(3): p. 508-17.
31. Homicsko, K., A. Lukashev, and R.D. Iggo, *RAD001 (everolimus) improves the efficacy of replicating adenoviruses that target colon cancer.* Cancer Res, 2005. **65**(15): p. 6882-90.
32. Barcia, C., et al., *One-year expression from high-capacity adenoviral vectors in the brains of animals with pre-existing anti-adenoviral immunity: clinical implications.* Mol Ther, 2007. **15**(12): p. 2154-63.
33. Sehgal, S.N., *Rapamune (RAPA, rapamycin, sirolimus): mechanism of action immunosuppressive effect results from blockade of signal transduction and inhibition of cell cycle progression.* Clin Biochem, 1998. **31**(5): p. 335-40.
34. Lassi, K. and N.A. Dawson, *Update on castrate-resistant prostate cancer: 2010.* Curr Opin Oncol.
35. Wang, H.Q., et al., *Differential phosphoprotein levels and pathway analysis identify the transition mechanism of LNCaP cells into androgen-independent cells.* Prostate, 2010. **70**(5): p. 508-17.
36. Figueiredo, M.L., C. Kao, and L. Wu, *Advances in preclinical investigation of prostate cancer gene therapy.* Mol Ther, 2007. **15**(6): p. 1053-64.
37. de Vrij, J., et al., *Adenovirus-derived vectors for prostate cancer gene therapy.* Hum Gene Ther, 2010. **21**(7): p. 795-805.
38. Li, Y., et al., *Intragenic Rearrangement and Altered RNA Splicing of the Androgen Receptor in a Cell-Based Model of Prostate Cancer Progression.* Cancer Res, 2011. **15**(71(6)): p. 2108-17.
39. Niu, Y., et al., *Differential androgen receptor signals in different cells explain why androgen-deprivation therapy of prostate cancer fails.* Oncogene, 2010. **29**(25): p. 3593-604.
40. Shah, R.B., et al., *Androgen-independent prostate cancer is a heterogeneous group of diseases: lessons from a rapid autopsy program.* Cancer Res, 2004. **64**(24): p. 9209-16.
41. Israeli, R.S., et al., *Molecular cloning of a complementary DNA encoding a prostate-specific membrane antigen.* Cancer Res, 1993. **53**(2): p. 227-30.

42. Wright, G.L., Jr., et al., *Upregulation of prostate-specific membrane antigen after androgen-deprivation therapy.* Urology, 1996. **48**(2): p. 326-34.
43. O'Keefe, D.S., et al., *Mapping, genomic organization and promoter analysis of the human prostate-specific membrane antigen gene.* Biochim Biophys Acta, 1998. **1443**(1-2): p. 113-27.
44. Ghosh, A. and W.D. Heston, *Tumor target prostate specific membrane antigen (PSMA) and its regulation in prostate cancer.* J Cell Biochem, 2004. **91**(3): p. 528-39.
45. Zeng, H., et al., *Recombinant adenovirus mediated prostate-specific enzyme pro-drug gene therapy regulated by prostate-specific membrane antigen (PSMA) enhancer/promoter.* J Androl, 2007. **28**(6): p. 827-35.
46. Zhang, P., et al., *Improved effects of a double suicide gene system on prostate cancer cells by targeted regulation of prostate-specific membrane antigen promoter and enhancer.* Int J Urol, 2008. **15**(5): p. 442-8.
47. Sato, M., et al., *Optimization of adenoviral vectors to direct highly amplified prostate-specific expression for imaging and gene therapy.* Mol Ther, 2003. **8**(5): p. 726-37.
48. Johnson, M., et al., *Micro-PET/CT monitoring of herpes thymidine kinase suicide gene therapy in a prostate cancer xenograft: the advantage of a cell-specific transcriptional targeting approach.* Mol Imaging, 2005. **4**(4): p. 463-72.
49. Klein, K.A., et al., *Progression of metastatic human prostate cancer to androgen independence in immunodeficient SCID mice.* Nat Med, 1997. **3**(4): p. 402-8.
50. Tao, N., et al., *Sequestration of adenoviral vector by Kupffer cells leads to a nonlinear dose response of transduction in liver.* Mol Ther, 2001. **3**(1): p. 28-35.
51. Ray, S., et al., *Noninvasive imaging of therapeutic gene expression using a bidirectional transcriptional amplification strategy.* Mol Ther, 2008. **16**(11): p. 1848-56.
52. Wei, L.H., et al., *Engineered antibody fragments with infinite affinity as reporter genes for PET imaging.* J Nucl Med, 2008. **49**(11): p. 1828-35.
53. Johnson, M., et al., *Differential biodistribution of adenoviral vector in vivo as monitored by bioluminescence imaging and quantitative polymerase chain reaction.* Hum Gene Ther, 2006. **17**(12): p. 1262-9.
54. Ara, T. and Y.A. Declerck, *Interleukin-6 in bone metastasis and cancer progression.* Eur J Cancer, 2010. **46**(7): p. 1223-31.
55. Lu, Y., et al., *Activation of MCP-1/CCR2 axis promotes prostate cancer growth in bone.* Clin Exp Metastasis, 2009. **26**(2): p. 161-9.
56. Hsu, W.K., et al., *Characterization of osteolytic, osteoblastic, and mixed lesions in a prostate cancer mouse model using 18F-FDG and 18F-fluoride PET/CT.* J Nucl Med, 2008. **49**(3): p. 414-21.
57. Withofs, N., et al., *18F-fluoride PET/CT for assessing bone involvement in prostate and breast cancers.* Nucl Med Commun, 2010. **32(3)**: p. 168-76.
58. Yu, E.Y., et al., *C11-Acetate and F-18 FDG PET for Men With Prostate Cancer Bone Metastases: Relative Findings and Response to Therapy.* Clin Nucl Med, 2011. **36**(3): p. 192-8.
59. Bhang, H.E., et al., *Tumor-specific imaging through progression elevated gene-3 promoter-driven gene expression.* Nat Med, 2011. **17**(1): p. 123-9.
60. Sato, M., et al., *Functionality of androgen receptor-based gene expression imaging in hormone refractory prostate cancer.* Clin Cancer Res, 2005. **11**(10): p. 3743-9.
61. Scher, H.I., et al., *Antitumour activity of MDV3100 in castration-resistant prostate cancer: a phase 1-2 study.* Lancet, 2010. **375**(9724): p. 1437-46.
62. Zhang, L., et al., *Interrogating androgen receptor function in recurrent prostate cancer.* Cancer Res, 2003. **63**(15): p. 4552-60.

63. Burton, J.B., et al., *Adenovirus-mediated gene expression imaging to directly detect sentinel lymph node metastasis of prostate cancer.* Nat Med, 2008. **14**(8): p. 882-8.
64. Adams, J.Y., et al., *Visualization of advanced human prostate cancer lesions in living mice by a targeted gene transfer vector and optical imaging.* Nat Med, 2002. **8**(8): p. 891-7.
65. Cooper, C.R., et al., *Stromal factors involved in prostate carcinoma metastasis to bone.* Cancer, 2003. **97**(3 Suppl): p. 739-47.
66. Logothetis, C.J., N.M. Navone, and S.H. Lin, *Understanding the biology of bone metastases: key to the effective treatment of prostate cancer.* Clin Cancer Res, 2008. **14**(6): p. 1599-602.
67. Lee, Y.C., et al., *Androgen depletion up-regulates cadherin-11 expression in prostate cancer.* J Pathol, 2010. **221**(1): p. 68-76.
68. Even-Sapir, E., et al., *The detection of bone metastases in patients with high-risk prostate cancer: 99mTc-MDP Planar bone scintigraphy, single- and multi-field-of-view SPECT, 18F-fluoride PET, and 18F-fluoride PET/CT.* J Nucl Med, 2006. **47**(2): p. 287-97.
69. Toegel, S., et al., *Uptake of bone-seekers is solely associated with mineralisation! A study with 99mTc-MDP, 153Sm-EDTMP and 18F-fluoride on osteoblasts.* Eur J Nucl Med Mol Imaging, 2006. **33**(4): p. 491-4.
70. Liu, I.J., et al., *Fluorodeoxyglucose positron emission tomography studies in diagnosis and staging of clinically organ-confined prostate cancer.* Urology, 2001. **57**(1): p. 108-11.
71. Oyama, N., et al., *Prognostic value of 2-deoxy-2-[F-18]fluoro-D-glucose positron emission tomography imaging for patients with prostate cancer.* Mol Imaging Biol, 2002. **4**(1): p. 99-104.
72. Greig, J.A., et al., *Influence of coagulation factor x on in vitro and in vivo gene delivery by adenovirus (Ad) 5, Ad35, and chimeric Ad5/Ad35 vectors.* Mol Ther, 2009. **17**(10): p. 1683-91.
73. Carlisle, R.C., et al., *Human erythrocytes bind and inactivate type 5 adenovirus by presenting Coxsackie virus-adenovirus receptor and complement receptor 1.* Blood, 2009. **113**(9): p. 1909-18.
74. Liu, H., et al., *Atomic structure of human adenovirus by cryo-EM reveals interactions among protein networks.* Science, 2010. **329**(5995): p. 1038-43.
75. Li, H.J., et al., *Combined transductional untargeting/retargeting and transcriptional restriction enhances adenovirus gene targeting and therapy for hepatic colorectal cancer tumors.* Cancer Res, 2009. **69**(2): p. 554-64.
76. Yan, M., et al., *A novel intracellular protein delivery platform based on single-protein nanocapsules.* Nat Nanotechnol, 2010. **5**(1): p. 48-53.
77. Jiang, Z.K., et al., *Androgen-independent molecular imaging vectors to detect castration-resistant and metastatic prostate cancer.* Cancer Res, 2011. **71**(19): p. 6250-60.
78. Kawakami, M. and J. Nakayama, *Enhanced expression of prostate-specific membrane antigen gene in prostate cancer as revealed by in situ hybridization.* Cancer Res, 1997. **57**(12): p. 2321-4.
79. Ananias, H.J., et al., *Expression of the gastrin-releasing peptide receptor, the prostate stem cell antigen and the prostate-specific membrane antigen in lymph node and bone metastases of prostate cancer.* Prostate, 2009. **69**(10): p. 1101-8.
80. Kuroda, K., et al., *Docetaxel down-regulates the expression of androgen receptor and prostate-specific antigen but not prostate-specific membrane antigen in prostate cancer cell lines: implications for PSA surrogacy.* Prostate, 2009. **69**(14): p. 1579-85.
81. Minner, S., et al., *High level PSMA expression is associated with early psa recurrence in surgically treated prostate cancer.* Prostate, 2010.
82. Serda, R.E., et al., *1alpha,25-Dihydroxyvitamin D3 down-regulates expression of prostate specific membrane antigen in prostate cancer cells.* Prostate, 2008. **68**(7): p. 773-83.
83. Tsui, P., M. Rubenstein, and P. Guinan, *Correlation between PSMA and VEGF expression as markers for LNCaP tumor angiogenesis.* J Biomed Biotechnol, 2005. **2005**(3): p. 287-90.

84. Watt, F., et al., *A tissue-specific enhancer of the prostate-specific membrane antigen gene, FOLH1.* Genomics, 2001. **73**(3): p. 243-54.
85. Barbazan, J., et al., *Molecular characterization of circulating tumor cells in human metastatic colorectal cancer.* PLoS One, 2012. **7**(7): p. e40476.
86. Clawson, G.A., et al., *Circulating tumor cells in melanoma patients.* PLoS One, 2012. **7**(7): p. e41052.
87. Delacruz, A., *Using circulating tumor cells as a prognostic indicator in metastatic castration-resistant prostate cancer.* Clin J Oncol Nurs, 2012. **16**(2): p. E44-7.
88. Kirby, B.J., et al., *Functional characterization of circulating tumor cells with a prostate-cancer-specific microfluidic device.* PLoS One, 2012. **7**(4): p. e35976.
89. Lucci, A., et al., *Circulating tumour cells in non-metastatic breast cancer: a prospective study.* Lancet Oncol, 2012. **13**(7): p. 688-95.
90. Punnoose, E.A., et al., *Evaluation of circulating tumor cells and circulating tumor DNA in non-small cell lung cancer: association with clinical endpoints in a phase II clinical trial of pertuzumab and erlotinib.* Clin Cancer Res, 2012. **18**(8): p. 2391-401.
91. Schmetzer, O., et al., *Detection of circulating tumor-associated antigen depends on the domains recognized by the monoclonal antibodies used: N-terminal trimmed EpCAM-levels are much higher than untrimmed forms.* Immunol Lett, 2012. **143**(2): p. 184-92.
92. Perets, R., et al., *Genome-wide analysis of androgen receptor targets reveals COUP-TF1 as a novel player in human prostate cancer.* PLoS One, 2012. **7**(10): p. e46467.
93. Evans, M.J., et al., *Noninvasive measurement of androgen receptor signaling with a positron-emitting radiopharmaceutical that targets prostate-specific membrane antigen.* Proc Natl Acad Sci U S A, 2011. **108**(23): p. 9578-82.
94. Ruggiero, A., et al., *Targeting the internal epitope of prostate-specific membrane antigen with 89Zr-7E11 immuno-PET.* J Nucl Med, 2011. **52**(10): p. 1608-15.
95. Ulmert, D., et al., *Imaging androgen receptor signaling with a radiotracer targeting free prostate-specific antigen.* Cancer Discov, 2012. **2**(4): p. 320-7.
96. Gorges, T.M. and K. Pantel, *Circulating tumor cells as therapy-related biomarkers in cancer patients.* Cancer Immunol Immunother, 2013.
97. Miyamoto, D.T., et al., *Androgen receptor signaling in circulating tumor cells as a marker of hormonally responsive prostate cancer.* Cancer Discov, 2012. **2**(11): p. 995-1003.
98. Kishimoto, H., et al., *In vivo imaging of lymph node metastasis with telomerase-specific replication-selective adenovirus.* Nat Med, 2006. **12**(10): p. 1213-9.
99. Bangari, D.S. and S.K. Mittal, *Current strategies and future directions for eluding adenoviral vector immunity.* Curr Gene Ther, 2006. **6**(2): p. 215-26.
100. Driesse, M.J., et al., *Intra-CSF administered recombinant adenovirus causes an immune response-mediated toxicity.* Gene Ther, 2000. **7**(16): p. 1401-9.
101. Sakurai, H., et al., *Adenoviral expression of suppressor of cytokine signaling-1 reduces adenovirus vector-induced innate immune responses.* J Immunol, 2008. **180**(7): p. 4931-8.
102. Varnavski, A.N., et al., *Evaluation of toxicity from high-dose systemic administration of recombinant adenovirus vector in vector-naive and pre-immunized mice.* Gene Ther, 2005. **12**(5): p. 427-36.
103. Koizumi, N., et al., *Fiber-modified adenovirus vectors decrease liver toxicity through reduced IL-6 production.* J Immunol, 2007. **178**(3): p. 1767-73.
104. Seregin, S.S., et al., *Transient pretreatment with glucocorticoid ablates innate toxicity of systemically delivered adenoviral vectors without reducing efficacy.* Mol Ther, 2009. **17**(4): p. 685-96.

105. Gregory, S.M., S.A. Nazir, and J.P. Metcalf, *Implications of the innate immune response to adenovirus and adenoviral vectors.* Future Virol, 2011. **6**(3): p. 357-374.
106. Brunetti-Pierri, N., et al., *Acute toxicity after high-dose systemic injection of helper-dependent adenoviral vectors into nonhuman primates.* Hum Gene Ther, 2004. **15**(1): p. 35-46.
107. Liu, Z.X., et al., *NK cells cause liver injury and facilitate the induction of T cell-mediated immunity to a viral liver infection.* J Immunol, 2000. **164**(12): p. 6480-6.
108. Muruve, D.A., et al., *Adenoviral gene therapy leads to rapid induction of multiple chemokines and acute neutrophil-dependent hepatic injury in vivo.* Hum Gene Ther, 1999. **10**(6): p. 965-76.
109. Muruve, D.A., et al., *Helper-dependent adenovirus vectors elicit intact innate but attenuated adaptive host immune responses in vivo.* J Virol, 2004. **78**(11): p. 5966-72.
110. Nazir, S.A. and J.P. Metcalf, *Innate immune response to adenovirus.* J Investig Med, 2005. **53**(6): p. 292-304.
111. Minagawa, M., et al., *Suppression of adenoviral gene expression in the liver: role of innate vs adaptive immunity and their cell lysis mechanisms.* Liver Int, 2005. **25**(3): p. 622-32.
112. Rawle, F.C., et al., *Mouse anti-adenovirus cytotoxic T lymphocytes. Inhibition of lysis by E3 gp19K but not E3 14.7K.* J Immunol, 1989. **143**(6): p. 2031-7.
113. Trevejo, J.M., et al., *TNF-alpha -dependent maturation of local dendritic cells is critical for activating the adaptive immune response to virus infection.* Proc Natl Acad Sci U S A, 2001. **98**(21): p. 12162-7.
114. Sehgal, S.N., *Sirolimus: its discovery, biological properties, and mechanism of action.* Transplant Proc, 2003. **35**(3 Suppl): p. 7S-14S.
115. Thomson, A.W., H.R. Turnquist, and G. Raimondi, *Immunoregulatory functions of mTOR inhibition.* Nat Rev Immunol, 2009. **9**(5): p. 324-37.
116. Aagaard-Tillery, K.M. and D.F. Jelinek, *Inhibition of human B lymphocyte cell cycle progression and differentiation by rapamycin.* Cell Immunol, 1994. **156**(2): p. 493-507.
117. Hleb, M., et al., *Evidence for cyclin D3 as a novel target of rapamycin in human T lymphocytes.* J Biol Chem, 2004. **279**(30): p. 31948-55.
118. Nourse, J., et al., *Interleukin-2-mediated elimination of the p27Kip1 cyclin-dependent kinase inhibitor prevented by rapamycin.* Nature, 1994. **372**(6506): p. 570-3.
119. Zhang, S., et al., *Constitutive reductions in mTOR alter cell size, immune cell development, and antibody production.* Blood, 2011. **117**(4): p. 1228-38.
120. Luan, F.L., et al., *Rapamycin blocks tumor progression: unlinking immunosuppression from antitumor efficacy.* Transplantation, 2002. **73**(10): p. 1565-72.
121. Blazar, B.R., et al., *Rapamycin inhibits the generation of graft-versus-host disease- and graft-versus-leukemia-causing T cells by interfering with the production of Th1 or Th1 cytotoxic cytokines.* J Immunol, 1998. **160**(11): p. 5355-65.
122. Yaghoubi, S., et al., *Human pharmacokinetic and dosimetry studies of [(18)F]FHBG: a reporter probe for imaging herpes simplex virus type-1 thymidine kinase reporter gene expression.* J Nucl Med, 2001. **42**(8): p. 1225-34.
123. Ellwood-Yen, K., et al., *Myc-driven murine prostate cancer shares molecular features with human prostate tumors.* Cancer Cell, 2003. **4**(3): p. 223-38.
124. Zhu, J., X. Huang, and Y. Yang, *Type I IFN signaling on both B and CD4 T cells is required for protective antibody response to adenovirus.* J Immunol, 2007. **178**(6): p. 3505-10.
125. Hume, D.A. and K.P. MacDonald, *Therapeutic applications of macrophage colony-stimulating factor-1 (CSF-1) and antagonists of CSF-1 receptor (CSF-1R) signaling.* Blood, 2012. **119**(8): p. 1810-20.

126. Bradley, R.R., et al., *Adenovirus serotype 5-specific neutralizing antibodies target multiple hexon hypervariable regions.* J Virol, 2012. **86**(2): p. 1267-72.
127. Rogee, S., et al., *Influence of chimeric human-bovine fibers on adenoviral uptake by liver cells and the antiviral immune response.* Gene Ther, 2010. **17**(7): p. 880-91.
128. Zhang, Z., et al., *Systemic delivery of a novel liver-detargeted oncolytic adenovirus causes reduced liver toxicity but maintains the antitumor response in a breast cancer bone metastasis model.* Hum Gene Ther, 2011. **22**(9): p. 1137-42.
129. Haisma, H.J. and A.R. Bellu, *Pharmacological interventions for improving adenovirus usage in gene therapy.* Mol Pharm, 2011. **8**(1): p. 50-5.
130. Khare, R., et al., *Generation of a Kupffer cell-evading adenovirus for systemic and liver-directed gene transfer.* Mol Ther, 2011. **19**(7): p. 1254-62.
131. Parker, A.L., et al., *Multiple vitamin K-dependent coagulation zymogens promote adenovirus-mediated gene delivery to hepatocytes.* Blood, 2006. **108**(8): p. 2554-61.
132. Alba, R., et al., *Coagulation factor X mediates adenovirus type 5 liver gene transfer in non-human primates (Microcebus murinus).* Gene Ther, 2012. **19**(1): p. 109-13.
133. Lieber, A., et al., *The role of Kupffer cell activation and viral gene expression in early liver toxicity after infusion of recombinant adenovirus vectors.* J Virol, 1997. **71**(11): p. 8798-807.
134. Iimuro, Y., et al., *Blockade of liver macrophages by gadolinium chloride reduces lethality in endotoxemic rats--analysis of mechanisms of lethality in endotoxemia.* J Leukoc Biol, 1994. **55**(6): p. 723-8.
135. Danielsson, A., et al., *An ex vivo loop system models the toxicity and efficacy of PEGylated and unmodified adenovirus serotype 5 in whole human blood.* Gene Ther, 2010. **17**(6): p. 752-62.
136. Yoshihara, C., K. Hamada, and Y. Koyama, *Preparation of a novel adenovirus formulation with artificial envelope of multilayer polymer-coatings: therapeutic effect on metastatic ovarian cancer.* Oncol Rep, 2010. **23**(3): p. 733-8.
137. Lanciotti, J., et al., *Targeting adenoviral vectors using heterofunctional polyethylene glycol FGF2 conjugates.* Mol Ther, 2003. **8**(1): p. 99-107.
138. Inada, Y., et al., *Biomedical and biotechnological applications of PEG- and PM-modified proteins.* Trends Biotechnol, 1995. **13**(3): p. 86-91.
139. Croyle, M.A., et al., *"Stealth" adenoviruses blunt cell-mediated and humoral immune responses against the virus and allow for significant gene expression upon readministration in the lung.* J Virol, 2001. **75**(10): p. 4792-801.
140. Kreppel, F. and S. Kochanek, *Modification of Adenovirus Gene Transfer Vectors With Synthetic Polymers: A Scientific Review and Technical Guide.* Mol Ther, 2007. **16**(1): p. 16-29.
141. Fasbender, A., et al., *Complexes of adenovirus with polycationic polymers and cationic lipids increase the efficiency of gene transfer in vitro and in vivo.* J Biol Chem, 1997. **272**(10): p. 6479-89.
142. Clark, P.R., et al., *Polycations and cationic lipids enhance adenovirus transduction and transgene expression in tumor cells.* Cancer Gene Ther, 1999. **6**(5): p. 437-46.
143. Arcasoy, S.M., et al., *Polycations increase the efficiency of adenovirus-mediated gene transfer to epithelial and endothelial cells in vitro.* Gene Ther, 1997. **4**(1): p. 32-8.
144. Toyoda, K., H. Nakane, and D.D. Heistad, *Cationic polymer and lipids augment adenovirus-mediated gene transfer to cerebral arteries in vivo.* J Cereb Blood Flow Metab, 2001. **21**(9): p. 1125-31.
145. Dodds, E., et al., *Cationic lipids and polymers are able to enhance adenoviral infection of cultured mouse myotubes.* J Neurochem, 1999. **72**(5): p. 2105-12.

146. Deming, T.J., *Facile synthesis of block copolypeptides of defined architecture.* Nature, 1997. **390**(6658): p. 386-389.
147. Deming, T.J., *Cobalt and iron initiators for the controlled polymerization of alpha-amino acid-N-carboxyanhydrides.* Macromolecules, 1999. **32**(13): p. 4500-4502.
148. Ziyue Karen Jiang a, S.B.S.K., Makoto Sato, Ivo C. Atanasov, Mai Johnson, Z. Hong Zhou, Timothy J. Deming, Lily Wu, *Engineering Polypeptide Coatings to Augment Gene Transduction and in vivo Stability of Adenoviruses.* Journal of Controlled Release, 2013.
149. Waddington, S.N., et al., *Adenovirus serotype 5 hexon mediates liver gene transfer.* Cell, 2008. **132**(3): p. 397-409.
150. Maybodi, M., M.L. Guler, and H.J. Kaplan, *Chapter 34* Immunology of Uveitis.